Modelling of Chemical Kinetics of Methane/Nitrogen Dioxide/Oxygen Flames

by

Rashid Waheed Khalid Ahmed

A Thesis Presented to the

FACULTY OF THE COLLEGE OF GRADUATE STUDIES

KING FAHD UNIVERSITY OF PETROLEUM & MINERALS

DHAHRAN, SAUDI ARABIA

In Partial Fulfillment of the
Requirements for the Degree of

MASTER OF SCIENCE

In

MECHANICAL ENGINEERING

November, 1990

INFORMATION TO USERS

This manuscript has been reproduced from the microfilm master. UMI films the text directly from the original or copy submitted. Thus, some thesis and dissertation copies are in typewriter face, while others may be from any type of computer printer.

The quality of this reproduction is dependent upon the quality of the copy submitted. Broken or indistinct print, colored or poor quality illustrations and photographs, print bleedthrough, substandard margins, and improper alignment can adversely affect reproduction.

In the unlikely event that the author did not send UMI a complete manuscript and there are missing pages, these will be noted. Also, if unauthorized copyright material had to be removed, a note will indicate the deletion.

Oversize materials (e.g., maps, drawings, charts) are reproduced by sectioning the original, beginning at the upper left-hand corner and continuing from left to right in equal sections with small overlaps. Each original is also photographed in one exposure and is included in reduced form at the back of the book.

Photographs included in the original manuscript have been reproduced xerographically in this copy. Higher quality 6" x 9" black and white photographic prints are available for any photographs or illustrations appearing in this copy for an additional charge. Contact UMI directly to order.

UMI

A Bell & Howell Information Company
300 North Zeeb Road, Ann Arbor MI 48106-1346 USA
313/761-4700 800/521-0600

MODELLING OF CHEMICAL KINETICS OF METHANE / NITROGEN DIOXIDE /OXYGEN FLAMES

BY

RASHID WAHEED KHALID AHMED

A Thesis Presented to the

FACULTY OF THE COLLEGE OF GRADUATE STUDIES

KING FAHD UNIVERSITY OF PETROLEUM & MINERALS

DHAHRAN, SAUDI ARABIA

In Partial Fulfillment of the
Requirements for the Degree of

MASTER OF SCIENCE

In

MECHANICAL ENGINEERING

NOVEMBER 1990

KING FAHD UNIVERSITY OF PETROLEUM & MINERALS

DHAHRAN, SAUDI ARABIA

This thesis, written by

RASHID WAHEED KHALID AHMED

under the direction of his thesis committee, and approved by all the members, has been presented to and accepted by the Dean, College of Graduate Studies, in partial fulfillment of the requirements for the degree of

MASTER OF SCIENCE IN MECHANICAL ENGINEERING

Thesis Committee

Chairman (Dr. A.A. Al-Farayedhi)

Member (Dr. H.I. Abualhamayel)

Member (Dr. M.A. Habib)

Dr. H.I. Abualhamayel
Department Chairman

Dr. Ala H. Rabeh
Dean College of Graduate Studies

Date : 26-12-90

This thesis is dedicated to

my family, friends

and

alma maters

ACKNOWLEDGEMENT

Praise and gratitude be to Allah Almighty, with whose gracious help it was possible to accomplish this work. Acknowledgement is due to King Fahd University of Petroleum and Minerals for extending all facilities and providing financial support.

I would like to offer my indebtedness and sincere appreciation to my advisor and committee chairman, Dr. Abdulghani Al-Farayedhi, who has been a constant source of help and encouragement during this work. I also greatly appreciate the invaluable co-operation and support extended by Dr. Habib I. Abualhamayel, Chairman of Mechanical Engineering Department, for creating and upgrading research facilities in the department, and for acting as one of the committee members. Thanks are due to Dr. Mohamad A. Habib, who also served as a member of thesis committee.

I wish to acknowledge the assistance given by Mr. Hamed Mostafa Kadrey and Mr. Mohammed Siddiq for their help in debugging and running the computer programs. I also express my thanks to all of my friends for their moral support.

I owe my family an expression of gratitude for their patience, understanding and encouragement.

Lastly, but not the least, I am thankful to all faculty, staff, colleagues and friends who made my stay at K.F.U.P.M. a memorable experience.

TABLE OF CONTENTS

LIST OF TABLES

LIST OF FIGURES

THESIS ABSTRACT

NAME OF STUDENT : *RASHID WAHEED KHALID AHMED*

TITLE OF STUDY : *Modelling of Chemical Kinetics of CH_4 / NO_2 / O_2 Flames*

MAJOR FIELD : *Mechanical Engineering*

DATE OF DEGREE : *November, 1990*

A chemical kinetic model is developed to describe mechanism of different laminar, one-dimensional, premixed, sub-atmospheric pressure, flat CH_4 / NO_2 / O_2 flames. All the flames considered are lean with equivalence ratios ranging from 0.20 to 0.92.

The developed chemical kinetic mechanism consists of 101 elementary reactions among 30 different species. The developed chemical mechanism computes the concentration of stable species CH_4, CO_2, CO, H_2, O_2, H_2O, N_2, NO, NO_2, and N_2O and radical species CH_3, CH_2, CH, CH_3O, CH_2O, HCO, H, O, OH, HO_2, H_2O_2, NH, CN, HCN, HNO_2, HNO, NCO, $HNCO$, N_2H and NH_2 as a function of distance above the surface of the burner. The comparison between the calculated and experimental concentration profiles shows good quantitative and qualitative agreement for the stable species H_2O, NO_2, NO, N_2, CO, CO_2 and for the radical species OH, CH, CN, NH and NH_2. Concentration values of CO_2, CO, H_2O, N_2, NO and NO_2 and peak concentrations of CH, NH and CN are plotted against the equivalence ratio and compared with the experimental data. The results of these plots support the validity of the developed chemical mechanism for accurate prediction of the behaviour of CH_4 / NO_2 / O_2 flames.

The formulation of this mechanism is useful in understanding the nitrogen chemistry controlling the combustion of gas phase in solid rocket propellants and in reducing pollutant formation in the atmosphere.

MASTER OF SCIENCE DEGREE

KING FAHD UNIVERSITY OF PETROLEUM AND MINERALS

Dhahran , Saudi Arabia

November 1990

خلاصـــة الرسالة

اسم الطالب الكامل : راشد وحيد خالد أحمد

عنوان الدراســـــــة : تشكيل الحركية الكيميائية للهب $CH_4/NO_2/O_2$

التخـــــــــصص : الهندسة الميكانيكية .

تاريخ الشهـــــــادة : نوفمبر ١٩٩٠م

لقد تم في هذا البحث تطوير نموذج للحركية الكيميائية لوصف عدة انواع من اللهب المكون من $CH_4/NO_2/O_2$. ولقد كان اللهب مسطحاً ، احادي البعد ، ذو مزيج مخلوط ، انسيابي الطبقات وتحت ضغط أقل من الضغط الجوي . كما كان اللهب مكوناً من مزيج شحيح الاكسجين ذو نسبة تكافؤ تتراوح من ٠ر٢٠ الى ٠ر٩٢ .

ويتألف النموذج المطور للحركية الكيميائية لهذه التركيبة من ١٠١ تفاعل أولى ضمن ٣٠ مركباً متميزاً . كما أن هذه التركيبـــة الكيميائيـــة المطـــورة تحسب التركيز للمركبات المستقـــرة :

$CH_4, CO_2, CO, H_2, O_2, H_2O, N_2, NO, NO_2, N_2O$

وللمركبات الجذريـــــــــــــــــــة : $CH_3, CH_2, CH, CH_3O, CH_2O, HCO, H, O, OH, HO_2,$

$H_2O_2, NH, CN, HCN, HNO_2, HNO, HCO, HNCO, N_2H, NH_2$

كدالة للمسافة فوق سطح الموقد . إن المقارنة بين القيم المحسوبة والقيم المعملية لمنحنيات التركيز تشير الى توافق جيد من حيث الكم والشكل للمركبـــــــــــات المستقرة : $H_2O, NO_2, NO, N_2, CO, CO_2$ وللمركبات الجذرية : OH, CH, CN, NH, NH_2 .

كما رسمت بيانياً قيم التركيز لكل من CO_2, CO, H_2O, NO, NO_2 وذروة التركيز لكل من CH, NH, CN مقابل نسبة التكافؤ . ولقد قورنت هذه البيانات بالقيم المعملية . وهذه النتائج دعمت صحة هذه التركيبة الكيميائية المطورة للتخمين الدقيق لعمل اللهب $CH_4/NO_2/O_2$.

إن صياغة هذه التركيبة مفيدة في فهم كيمياء النيتروجين والتي تتحكم في اشتعال الوقود الصلب للصواريخ وفي تقليل التلوث الحادث في الهواء .

درجة الماجستير في العلوم
جامعة الملك فهد للبترول والمعادن
الظهران ، المملكة العربية السعودية
التاريخ نوفمبر ١٩٩٠م

CHAPTER 1

INTRODUCTION

Reactions of nitrogen oxides (NO_x) with hydrocarbon fuels are of great importance, not only because nitrogen oxides are considered as major atmospheric pollutants, but also because nitrogen oxides are the major oxidizer in many solid rocket propellants and commercial explosives. Characteristics of hydrocarbon fuels supported by nitrogen oxides are observed in some of these systems, but few detailed studies which describe the structure of these flames are available.

Nitramine based solid rocket propellants have the advantage of high specific impulse due to low molecular weight combustion products and reduced infrared emission due to relatively low CO_2 and H_2O concentrations in the products. There remains considerable uncertainty, however, about the basic chemical and physical processes which control the combustion of these propellants. This is particularly true of the gas phase reactions above the surface of the solid propellant during combustion. Hydrocarbon/nitrogen dioxide flames simulate the gas phase reaction in the combustion of nitramine solid propellants [10].

The results of the present study can also describe the decomposition reactions of liquid fuels which contain nitrogen in its structure such as nitrate and nitrite esters, and can give a general understanding of combustion systems

where NO_x are the major oxidizer in comparison to the more conventional combustion systems where O_2 is the oxidizer.

1.1 Oxides of Nitrogen in the Atmosphere

Nitrogen oxides NO_x are considered as important atmospheric pollutants. These oxides consist of nitric oxide (NO), nitrogen dioxide (NO_2) and nitrous oxide (N_2O). Nitric oxide is the dominant and most stable of these oxides. Oxides of nitrogen directly effect the environment through smog formation, which is the result of the photochemical reactions between hydrocarbons and NO_x in the presence of sunlight, or through the formation of acid rain, which is the result of reactions between NO_x and moisture. The major source of atmospheric NO_x is electric utility plants and automobiles. The focus of many investigators has been on the development of methods by which to control NO_x.

From the pollution standpoint, progress in formulating the chemical mechanism which can describe the formation and destruction of NO_x is advanced. The major source of NO_x formation is the use of air as the oxidizer in combustion processes. Air consists of molecular nitrogen and oxygen in a molar ratio of (3.76:1). The chemical mechanism for this type of NO formation is initiated by

$$O_2 = 2O \tag{1.1}$$

then, according to Zeldovich's free radical chain mechanism,

$$O + N_2 = NO + N \tag{1.2}$$

$$N + O_2 = NO + O \tag{1.3}$$

$$N + OH = NO + H \tag{1.4}$$

The above reactions are found to be the most important in NO formation in flames, and reaction (1.2) is rate controlling since breaking the N_2 bond is the most difficult step in the Zeldovich mechanism.

A reduction in the amount of NO_x which is emitted into the atmosphere can be achieved by two methods. The primary method is to control over the reactions which produce the pollutants. The second possibility is the removal of NO_x after its formation.

The other major source of NO_x formation is from nitrogen compounds in the structure of many types of fuels, such as coal, oil and natural gas. The bonds between nitrogen atoms and the rest of the molecule are considerably weaker than the N-N bond in molecular nitrogen. Hence it is not surprising that fuel nitrogen can contribute large amounts of NO_x during combustion.

1.2 Photo-oxidation by Nitrogen Dioxide

Nitrogen dioxide is a toxic compound formed in the atmosphere by reaction between the ozone and NO. Nitrogen dioxide is a part of the discoloring atmospheric pollution that is known as smog. The reactions that lead to smog

formation are called photo-oxidation and the important reactions in this process are

$$O_2 + h\nu = 2O \tag{1.5}$$

$$O + O_2 + M = O_3 + M \tag{1.6}$$

$$O_3 + h\nu = O_2 + O \tag{1.7}$$

Reaction (1.5) occurs in the upper atmosphere (50 miles) since high energy photons (wavelength $=0.2\mu m$) are necessary to initiate the reaction. The monatomic oxygen which is produced is recombined with molecular O_2 to form the ozone layer. This layer is generated in the region between 10 and 20 miles above the earth. The conversion of NO emitted by combustion systems to NO_2 is by the reaction

$$2NO + O_2 = 2NO_2 \tag{1.8}$$

This reaction requires a high concentration of NO , up to 1000 ppm, which is significantly higher than the actual concentration in the atmosphere. If ozone (O_3) is present, however, then the conversion is extremely fast even at low NO concentration. Ozone will not form in the lower atmosphere via reactions (1.5) and (1.6) because these reactions require solar energy of the order of 580 kJ/g-mole. Thus O_3 must be generated by other means. Nitrogen dioxide is very sensitive photochemically as shown by the reaction

$$NO_2 + h\nu = NO + O \tag{1.9}$$

This reaction is one of the most important photochemical reactions in the lower atmosphere since it provides the highly reactive monatomic oxygen responsible for the formation of ozone via reaction (1.6). Thus O_3 reacts with NO in the lower atmosphere to produce NO_2 by the reaction

$$NO + O_3 = NO_2 + O_2 \tag{1.10}$$

which is much faster than reaction (1.8). From the above section we can see that NO and NO_2 play an important role in ozone depletion in the upper atmosphere and smog formation in the lower atmosphere.

1.3 Solid Propellants

The use of solid nitramine propellants has the advantage of high specific impulse due to low molecular weight products, reduced infrared radiation emissions in the exhaust plume due to relatively low CO_2 and H_2O in the products, reduced smoke and less corrosive products [37]. However, the basic chemical and physical processes which control the combustion of these propellants are not rigorously known, particularly those which occur in the gas phase near the surface of the propellants during combustion. The decomposition of the nitramine RDX (1,3,5 trinitro hexahydro 1,3,5 trizine) and HMX (1,3,5,7 tetranitro 1,3,5,7 tetracyclooctane) has been considered by several investigators.

When heated the solid RDX or HMX first undergoes solid-solid then solid-

liquid phase changes before gaseous products are formed. The major gaseous nitrogen species found are NO_2, N_2O, N_2 and NH_3 and the gaseous carbon species formed are primarily CH_2O, HCN, CO and CO_2. The relative yields of the products has been found to be a function of the pressure and heating rate. Low pressure and high heating rates were found to favor the formation of CH_2O and NO_2. High pressure and low heating rates, on the other hand, were found to favor the formation of HCN and NO_2.

Under actual combustion conditions of high pressure and high heating rate, it is likely that CH_2, HCN and NO_2 are all important. Reactions of these decomposition products support the gas phase flame reactions near the propellant surface and thereby influence the burning rate. A schematic representation of the reaction zone near the surface of a burning nitramine propellant is illustrated in Figure 1.1.

Several distinct luminous flame zones are observed in the combustion of nitramine propellant which have also been seen in hydrocarbon flames with NO_2 as an oxidizer. A very rapid, luminous reaction zone is found adjacent to the surface of the propellant followed by a dark, nonluminous zone at greater distances from the surface. Finally, an additional visible flame zone appears after the dark zone. The detailed chemistry of this flame structure is not known at this time [11].

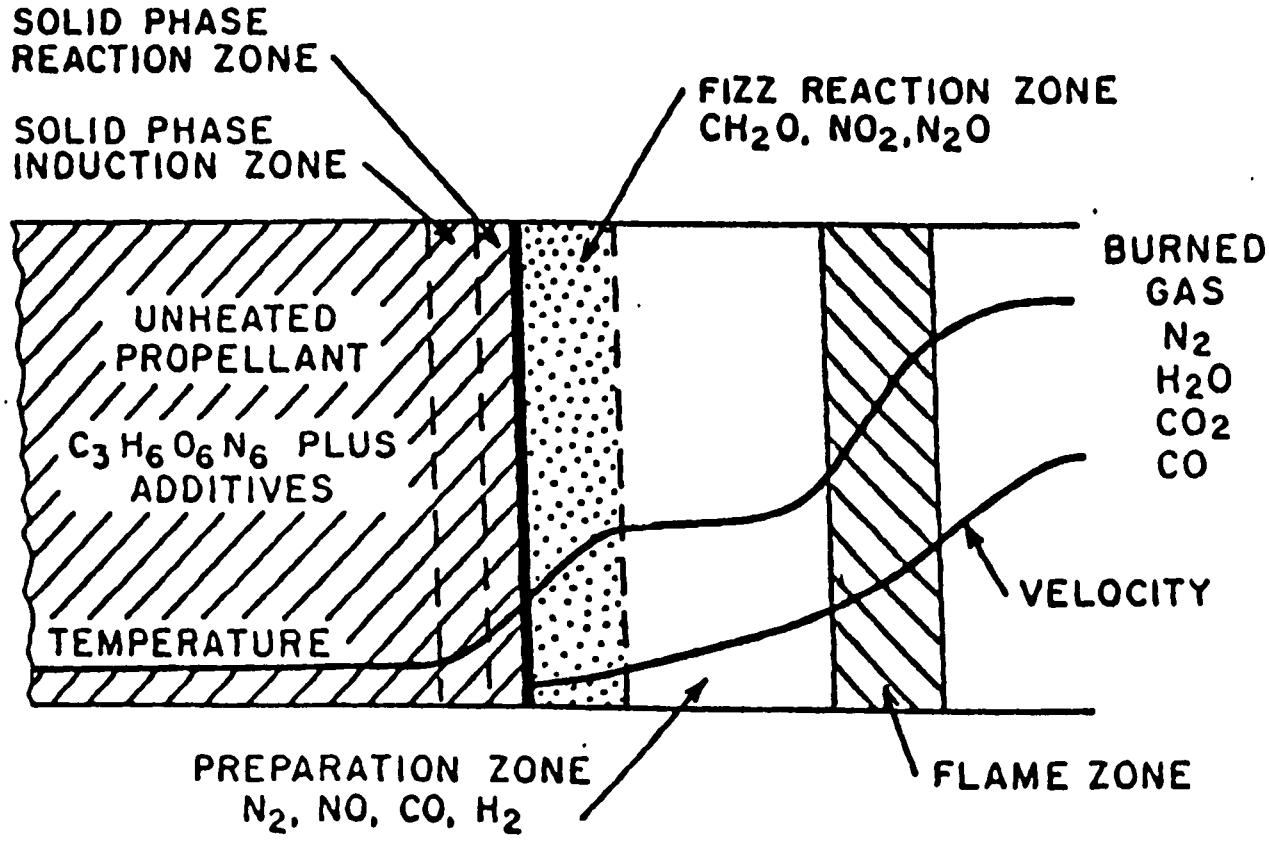

Figure 1.1 : A Schematic Representation of the Reaction Zone near the surface of a burning nitramine propellant

1.4 Nitrogenous Hydrocarbon Flames

Investigating hydrocarbon flames supported by nitrogen oxides such as nitric oxide, NO , nitrous oxide, N_2O and nitrogen dioxide, NO_2 is of great importance particularly for understanding solid propellant combustion and reduction of nitric oxide which is one of the major air pollutants produced by combustion sources.

Hydrocarbon flames supported by NO and NO_2 are characterized by two visible luminous zones in the combustion regions. Qualitative spectroscopic studies indicate that formation of more than one reaction zone in a flame can be explained by the process in which different reactions begin at different temperature levels in the combustion region [46].

1.5 Control of NO_x Emissions

Control of NO_x emissions depends on the source of NO_x formation. For thermal- NO_x formation, lowering the combustion temperature reduces the nitric oxide formation. In internal combustion engines, several procedures have been used to reduce nitric oxide formation by reducing the combustion chamber temperature. These procedures include exhaust gas recirculation (EGR), injection of moisture to the combustion chamber, engine operation biased towards lean fuel-air ratios and two-stage combustion chamber. For Fuel- NO_x

formation, the control processes are based on aftertreatment of combustor exhaust products. This strategy includes selective catalystic reduction (SCR), Thermal De- NO_x and RAPRENOx.

In the thermal De- NO_x process ammonia is injected into the combustion effluents of a stationary combustion system to initiate a series of reactions to convert nitric oxide to molecular nitrogen. The reaction proceeds as follows [43].

$$NH_3 + OH = NH_2 + H_2O \tag{1.11}$$

$$NH_2 + NO = N_2H + OH \tag{1.12}$$

$$N_2H + O = N_2 + OH \tag{1.13}$$

The technique works only over a narrow temperature window ($1100-1400K$) below which reaction (1.11) is too slow to initiate the path and above which more nitric oxide will be formed through thermal- NO_x formation. The process is also effective under excess-oxygen conditions and the ammonia needed is almost double the amount of nitric oxide to be removed.

Another promising NO_x removal technique from exhaust gas is the RAPRENOx process [48]. The method involves cyanuric acid [$(HOCN)_3$] injection into an exhaust stream containing NO. Cyanuric acid is a commercially available chemical which when heated sublimes and decomposes to form iso-cyanic acid ($HOCN$). At high temperature ($\sim$ 1000 K), the iso-cyanic acid will decompose and initiate a sequence of reactions leading to NO removal. This sequence involves the following reactions [43]

$$(HOCN)_3 = 3HNCO \quad (1.14)$$

$$HNCO + H = NH_2 + CO \quad (1.15)$$

$$NH_2 + NO = N_2H + OH \quad (1.16)$$

$$N_2H + O = N_2 + OH \quad (1.17)$$

The RAPRENOx technique has a working temperature window and the effectiveness of the process depends on the composition of the exhaust [51]. There is not as much known about the reaction kinetics controlling the RAPRENOx method as there is about those underlying the thermal De- NO_x process.

1.6 Nitrogen Chemistry in Ozone Depletion

The ozone layer is defined as a layer of relatively high concentration of ozone (O_3) located in the stratosphere. This layer is important for human life primarily for two reasons. The first is that ozone absorbs solar ultraviolet radiation at 280-320 nm wavelengths thus warming the stratosphere. This affects the vertical motion of clouds in the troposphere and therefore contributes to the control of weather and climate. A reduction in the ozone layer would cause more ultraviolet and visible radiation to reach the ground, leading to warming of the lower atmosphere and the earth's surface. At the same time

reducing ultraviolet radiation absorption in the stratosphere would reduce heating there. This situation would lead to surface cooling since less thermal radiation would be emitted from the stratosphere to the ground. These opposite effects, one of cooling and one of warming, would be complicated by the changed distribution in the ozone layer and thus the net effect of ozone depletion would be hard to predict [23].

The second reason for the importance of ozone layer is that by absorbing ultraviolet radiation it controls the amount of this UV radiation reaching the ground. Ultraviolet radiation has both beneficial and harmful effects on living organisms. On the beneficial side, the whole population gains from the action of UV-radiation in converting steroids in the skin to vitamine D. On the harmful side, it is known to affect adversely the growth composition of a wide variety of plant species and marine organisms. In animal studies, UV-radiation has been shown not only to be carcinogenic, but also to alter the response of the immunological system. In humans, UV-radiation is known to cause aging of the skin and UV-radiation is directly linked to skin cancer.

In recent years it has been suggested that nitric oxide produced from supersonic air crafts in the stratosphere, nitric oxide produced by the explosion of nuclear devices and halogens from freon could have the capability to destroy the ozone layer. Nitric oxide, because of its high residence time, participates in photochemical reactions leading to a reduction in ozone concentration through the following reactions

$$NO + O_3 = NO_2^+ + O_2 \qquad (1.18)$$

$$NO_2^+ = NO_2 + h\nu \qquad (1.19)$$

1.7 Objective of this Study

Detailed chemical analysis of $CH_4 / NO_2 / O_2$ flames with multiple luminous zones which are observed in nitrogen containing energetic fuels, nitramine solid propellants or nitrogen esters is scarce.

The present study is concerned with the structure of laminar, premixed, low pressure $CH_4 / NO_2 / O_2$ flames. These flames simulate the gas phase processes in the combustion of fuel bound nitrogen such as nitramine solid propellants and nitrogen esters. $CH_4 / NO_2 / O_2$ flames were investigated using the flame code [35] and experimental data.

Al-Farayedhi [1] measured the concentration of intermediate species and temperature profiles of $CH_4 / NO_2 / O_2$ flames by developing a new laser-induced fluorescence spectroscopy system. Sadeqi [50] in a companion study measured the concentrations of stable species by gas chromatography. These experimentally measured values will form a basis for comparison with those obtained by the proposed reaction mechanism. The main objectives of this study are depicted below :

1- Understanding the chemistry controlling the combustion of $CH_4 / NO_2 / O_2$

flames.

2- Developing a chemical kinetic model describing the reactions of these flames.

3- Comparing the experimental and computational results.

4- Discussing and interpreting the results.

The reaction mechanism is selected on the basis of reasonable agreement between calculated and measured values. Comparison are made and discussed between measured and calculated values for the concentration profiles in the $CH_4 / NO_2 / O_2$ flames.

CHAPTER 2

LITERATURE REVIEW

Nitric oxide is one of the products of most combustion processes in air and it is considered a major air pollutant. Electric utilities account for a total of 40% of the emissions of nitrogen oxides (NO_x) and the rest come from mobile sources, industrial boilers and chemical industry. The formation of NO_x is due to oxidation of nitrogen impurities in the fuel or atmospheric nitrogen when air is used as an oxidizer.

Nitrogen oxides are also involved in the decomposition of nitrite and nitrate esters. The decomposition of these species generates alcohols, hydrocarbons and formaldehyde fuels along with NO_x as oxidizers. The flames of these species show multiple luminous reaction zones, indicating complex reaction mechanisms.

The objective of the study described here is to use the available data to model $CH_4 / NO_2 / O_2$ flames and subsequently come up with a tested reaction mechanism to help clarify the chemistry of systems like those above.

2.1 Hydrocarbons / NO_2 Flames

Early studies of hydrocarbon / NO_2 reactions were presented by Thomas [59]. The study involved the gas phase reaction between acetylene (C_2H_2) and

NO_2 over a temperature range of 420 to 470 K. A chemical mechanism was proposed which started with the formation of glyoxal ($C_2H_2O_2$). The glyoxal then reacted with NO_2 in a manner presented by Thomas in another study [60]. The final products of the reactions were NO, CO, CO_2, H_2O, N_2, $C_2H_2O_2$ (a yellow deposit) and residual NO_2. The rate constant for the reaction (C_2H_2 + NO_2) was calculated and it was reported to be

$$k = 10^9 \, exp(-15{,}000/RT) \quad \text{liter/mole-sec}$$

Parker et al. [46] also reported on hydrocarbon/ NO_2 flames. Two distinct reaction zones were observed. The first zone resembled the yellow zone in H_2 / NO_2 flames. The second reaction zone was violet and consisted of strong CN bands and weaker OH, NH, NO, CH and C_2 bands. Temperature measurements were made for the yellow zone and readings of 970-1070 °K were recorded. The final product of the reaction was reported to consist of large amounts of water, CO_2, CO and NO.

Wolfhard and Parker [67] investigated hydrocarbon / NO_2 reactions spectroscopically and reported that hydrocarbon / NO_2 flames contained two reaction zones. The first zone had a spectrum extending from the red to the blue and gives off yellow light. The second reaction zone resembled the reaction zone of the same hydrocarbon and NO flames which emitted violet radiation. An after glow was seen just like the glow over the lean NO flame. The OH bands were lean in the second reaction zone but intensified in the after glow region. It

was suggested that the hydrocarbon was broken down to a simpler form in the first reaction zone and then free radicals were formed establishing the second reaction zone which consisted of the spectrum of C_2, CH, CN, and NH.

Propane (C_3H_8) / NO_2 was studied by Myerson et al. [44]. They described the reaction as a multiple stage ignition which consisted of a cool flame with a pale orange color followed by the hot flame which was bluish-white in color. The intensity of the cool flame increased with an increase in the percentage of NO_2 added. They used an infrared spectroscopic technique for concentration measurements and Pt/Pt-13%Rh thermocouples for temperature measurements. A mechanism was proposed for the reaction suggesting that the reaction is initiated by forming the complex intermediate [$CH_3CH_2(NO_2)CH_3$] and not by hydrogen abstraction. Further reaction between the intermediate and NO_2 resulted in the formation of nitroethane, which decomposes thermally at 700-755 K forming ethylene, NO, CH_4, CO, CH_2O and H_2O. The hot flame consisted of the reaction between ethylene and NO_2. When this reaction intensifies and the flame increases in temperature other reactions take place including the reaction between methane and NO.

Wharton et al. [65] used a spectroscopic method to analyze n-butane / NO_2 flames. The flat flame which was constructed on an Egerton type burner had two distinct reaction zones. The result of the analytical values of the concentration showed that CN, CH and NH have maximum values at the region close to the surface of the burner. The intensity of OH increased in the region past the primary reaction zone. It was reported that the OH radical increased

where the NO concentration was decreasing. This was an indication that OH was formed from the reaction between the O_2 released by NO decomposition and the hydrocarbon fragments. In the study no detection of C_2 was made and this was reported to be the result of the following reaction

$$C_2 + OH = CO + CH \tag{2.1}$$

This reaction was reported to occur in the outer region of the primary reaction zone and it is responsible for C_2 removal.

Miller et al. [42] reported on n-butane / NO_2 reactions in air using a shadowgraph and direct photography. The analysis of the results of the direct photograph showed that the maximum velocity of the laminar flame was 19.8 cm/sec at 16 percent Butane and from the shadowgraph was 18.3 cm/sec at 14.6 percent Butane. The flame was described to consist of two distinct reaction zones. The inner zone is violet in color and was reported to be due to reaction between the partially oxidized fuel and NO.

Ashmore and Preston [3] determined ignition boundaries in mixtures of $CH_4 / O_2 / NO_2 / NO$. At temperatures around 770 K they monitored the formation of intermediates and products and the changes in the NO_2 concentration, and suggested a tentative reaction mechanism. Ashmore and Preston also summarized earlier electric furnace investigations that were carried out by Norwich and Wallace [45] and Ashmore [2]. They concluded that the reaction scheme for ignition of $CH_4 / O_2 / NO_2$ is very complex.

A mechanism for the sensitization by $\dot{NO}_2$ at high temperatures was suggested by Dorko et al. [22]. The key step of this mechanism is the decomposition of NO_2 to form NO and O, followed by the chain branching of O and CH_4. Burcat [12] incorporated this mechanism into a 38-reaction model to compute $CH_4 / O_2 / NO_2$ ignition. The validity of this mechanism has been questioned and its limitations have been discussed in a comment by Slack [54]. He pointed out that Burcat's mechanism appears incomplete and was predicted upon untenably low rate coefficients for the following two reactions.

$$NO_2 + O = NO + O_2 \tag{2.2}$$

$$CH_3 + NO_2 = CH_3O + NO \tag{2.3}$$

Slack and Grillo [55] presented induction time measurements and photometeric measurements in mixtures of $CH_4 / O_2 / NO_2 / Ar$, with NO_2 mole fraction ranging from 0 to 0.05, temperatures ranging from 1310 to 1790 K and pressures ranging from 1.8 to 3.6 atmospheres. Comparisons were made with the previous literature on CH_4 / O_2 and $CH_4 / O_2 / NO_2$ induction times. Theoretical induction times were predicted with the NASA General Chemical Kinetics Computer Program developed by Bittker and Scullin [8]. Observed NO_2 decay rates during induction were independent of O_2 concentration, were very much faster than NO_2 dissociation, and suggest a rapid chain reaction involving NO_2 and CH_4 as the sensitization mechanism. A rate coefficient was derived for the hydrogen abstraction reaction :

$$CH_4 + NO_2 = CH_3 + HNO_2 \tag{2.4}$$

Computer modelling of observations adequately predicted the majority of observations but failed to predict the inhibiting role of argon.

Fifer [25] investigated the kinetics of NO_2 / CH_2O mixtures, and suggested a linear chain mechanism initiated by the H -abstraction reaction

$$CH_2O + NO_2 = CH + HNO_2 \qquad (2.5)$$

and followed by

$$CHO + NO_2 = CO + HNO_2 \qquad (2.6)$$

$$CHO + M = H + CO + M \qquad (2.7)$$

$$H + NO_2 = OH + NO \qquad (2.8)$$

$$OH + CH_2O = H_2O + CHO \qquad (2.9)$$

$$OH + HNO_2 = H_2O + NO_2 \qquad (2.10)$$

$$HNO_2 + M = OH + NO + M \qquad (2.11)$$

Because of the importance of CH_2O in the $CH_4 - O_2$ chain, Fifer's mechanism should be included in the $CH_4 / NO_2 / O_2$ mechanism.

Thorne et al. [61] studied a low pressure (25 torr, 1 torr = 1 mm Hg), rich (φ = 1.5), $H_2 / O_2 - Ar$ flame and added to it various combinations of C_2H_2, HCN, and NO. Details of NO interactions with hydrocarbon free radicals under combustion conditions were investigated. The kinetic model indicates that the NO removal occurs primarily by the reaction with C and CH ;

reaction with CH_2 is less important in these flames.

Smith and Thorne [57] investigated low-pressure (25 torr), premixed, flat flames of cyanogen-nitrogen dioxide in an attempt to understand the chemistry of gas phase combustion of solid propellant nitramine. These flames were characterized by three distinct luminous zones. The first zone with a yellow emission and a thickness of about 1.5 mm started 3 mm above the burner surface. Directly above the yellow zone, a blue zone 3 mm thick occured, followed by a very intense pink zone extending downstream to the second pink zone which was much less intense. Smith and Thorne reported for the rich flame that the dominant reactions in order of importance are thermal decomposition of NO_2, followed by reactions of NO_2 with CN and O:

$$NO_2 + M = NO + O + M \tag{2.12}$$

$$NO_2 + CN = NO + NCO \tag{2.13}$$

$$NO_2 + O = NO + O_2 \tag{2.14}$$

followed by a net creation of reactive intermediates CN and NCO:

$$C_2N_2 + O = NCO + CN \tag{2.15}$$

$$C_2N_2 + M = 2CN + M \qquad (2.16)$$

For the less rich flames, reaction of atomic oxygen with NO_2 is the dominant path, followed by thermal decomposition of NO_2. This mechanism yields a net consumption of reactive intermediates.

Branch [10] carried out a detailed kinetics modelling of the gas phase reactions involved in the combustion of the nitramine solid propellant (RDX) at a pressure of 40 atmospheres. The calculations showed there was a two zone structure. In the fizz zone near the surface there was a rapid reaction between H_2CO and NO_2 to form NO and CO . The global decomposition reaction of RDX was represented by

$$\text{RDX} = 3CH_2O + NO_2 + N_2O + \frac{3}{2}N_2 = \text{Products} \qquad (2.17)$$

The model contained 45 reactions involving 19 species and utilized the CHEMKIN code developed at Sandia by Kee et al [33]. The results of the model predicted a rapid exothermic reaction in the fizz zone accompanied by complete CH_2O consumption followed by a slower exothermic reaction in the flame zone.

Parr and Hanson-Parr [47] very recently presented an investigation on the combustion of solid propellant (HMX) at an atmospheric pressure, using the

imaging planer laser induced fluorescence technique. A Nd:YAG laser pumped-dye laser with a 0.5 cm^{-1} bandwidth was employed to measure species and rotational temperature profiles and obtain time resolved images of NO_2, NO, CN, NH, H_2CO, and OH during ignition of HMX.

The identification of NO_2 in the flame from its fluorescence spectra was not confirmed due to the broadness of absorbsion and emission curves of NO_2, but from time delay measurements of the fluorescence signal and emission spectra, the fluorescence signal was believed to be for NO_2. However the fluorescence detection of NO indicated that NO_2 and NO were the major oxidizers in the HMX flame. The search for formaldehyde fluorescence spectra indicated that formaldehyde was not the major fuel component in the HMX combustion. Measurements of fluorescence profiles of CN from $B^2\Sigma - X^2\Sigma$ (0,0) band, NH from $A^3\Pi - X^3\Sigma^-$ (1,0), and OH $A^2\Sigma - X^2\Sigma$ (1,0) band showed that NH was generated slightly before CN and both formed a thin flame sheet just after the depletion of NO_2, while OH peaked after CN and NH peaks. An OH rotational temperature profile was reported with a value of 2772 ± 35 K just beyond the CN / NH flame sheet.

The first concentration profile measurements of the intermediates CH, CN, NH, OH and NH_2 in CH_4 / NO_2 / O_2 flames along with the stable species measurements were performed by Al-Farayedhi [1] with a laser-induced fluorescence spectroscopy system.

Sadeqi [50] presented the concentration profiles of the stable species (CH_4, CH_2O, O_2, CO_2, CO, H_2O, NO_2, NO, and N_2) for CH_4 / NO_2 / O_2 and

CH_2O / NO_2 / O_2 flames as well as the temperature profiles. The concentration profiles were measured by gas chromatography. The temperature profiles were measured by a silica coated 0.0076 cm diameter Pt/Pt-13 % Rh thermocouple.

Miller and Bowman [43] illustrated the knowledge of the mechanisms and rate parameters for the gas-phase reactions of nitrogen compounds that are relevant to combustion-generated air pollution by kinetic results with experimental data. Available information on the rate parameters for these important elementary reactions was surveyed, and recommendations for the rate coefficients for these reactions were provided. The principle areas of uncertainty in nitrogen reaction mechanisms were also outlined.

CHAPTER 3

PREMIXED FLAME EQUATIONS

The equations governing steady, isobaric, quasi-one-dimensional flame propagation [35] may be written as follows:

$$M = \rho u A \tag{3.1}$$

$$M\frac{dT}{dx} - \frac{1}{c_p}\frac{d}{dx}\left(\lambda A\frac{dT}{dx}\right) + \frac{A}{c_p}\sum_{k=1}^{K}(\rho Y_k V_k)c_{pk}\frac{dT}{dx} + \frac{A}{c_p}\sum_{k=1}^{K}\dot{\omega}_k h_k W_k = 0 \tag{3.2}$$

$$M\frac{dY_k}{dx} + \frac{d}{dx}(\rho A Y_k V_k) - A\dot{\omega}_k W_k = 0 \qquad (k = 1,\ldots,K) \tag{3.3}$$

$$P = \frac{\rho R T}{W} \tag{3.4}$$

The net chemical production rate $\dot{\omega}_k$ of each species results from a competition between all the chemical reactions involving that species. Each reaction was presumed to proceed according to the law of mass action. The details of the chemical reaction equations and the thermochemical properties are described in the following section.

3.1 Chemical Rate Expressions

Consider I elementary reversible (or irreversible) reactions involving chemical species which can be represented in the general form given below,

$$\sum_{k=1}^{K} \nu'_{ki}\, \chi_k \rightarrow \sum_{k=1}^{K} \nu''_{ki}\, \chi_k \qquad (i=1,...,I) \tag{3.5}$$

The stoichiometric coefficients ν_{ki} are integers. Normally a reaction involves three or four species; hence the ν_{ki} matrix is quite sparse for a large set of reactions.

The production rate $\dot{\omega}_k$ of the k^{th} species can be written as a summation of the rate of progress variables for all reactions involving the k^{th} species:

$$\dot{\omega}_k = \sum_{i=1}^{I} \nu_{ki}\, q_i \qquad (k=1,...,K) \tag{3.6}$$

where

$$\nu_{ki} = (\nu''_{ki} - \nu'_{ki}) \tag{3.7}$$

The rate of progress variable, q_i, for the i^{th} reaction is given by the difference of the forward rates minus the reverse rates as

$$q_i = k_{f_i} \prod_{k=1}^{K} [X_k]^{\nu'_{ki}} - k_{r_i} \prod_{k=1}^{K} [X_k]^{\nu''_{ki}} \tag{3.8}$$

The forward rate constants for the I reactions are assumed to have the following Arrhenius temperature dependence:

$$k_{fi} = A_i T_i^{\beta} \exp\left[- \frac{E_i}{R_c T} \right] \tag{3.9}$$

where the pre-exponential factor A_i , the temperature exponent β_i , and the activation energy E_i usually come from experiment. For all reactions the parameters in Eqn. (3.9) are required input to the CHEMKIN [33] package for each reaction.

The reverse rate constants k_{ri} are related to the forward rate constants through the equilibrium constants as

$$k_{ri} = \frac{k_{fi}}{K_{ci}} \tag{3.10}$$

Although K_{ci} is given in concentration units, the equilibrium constants K_{pi} are obtained with the relationship

$$K_{ci} = K_{pi} \left(\frac{P_{atm}}{R T} \right)^{\sum_{k=1}^{K} \nu_{ki}} \tag{3.11}$$

The equilibrium constants K_{pi} are obtained with the relationship

$$K_{pi} = \exp\left(\frac{\Delta S^{\circ}_i}{R} - \frac{\Delta H^{\circ}_i}{R T} \right) \tag{3.12}$$

The Δ refers to the change that occurs in passing completely from reactants to products by the i^{th} reaction. More specifically

$$\frac{\Delta S^{\circ}_i}{R} = \sum_{k=1}^{K} \nu_{ki} \frac{S^{\circ}_k}{R} \tag{3.13}$$

$$\frac{\Delta H^{\circ}_i}{R\,T} = \sum_{k=1}^{K} \nu_{ki} \frac{H^{\circ}_k}{R\,T} \tag{3.14}$$

Thermodynamic properties are taken to be in the form of polynomial fits to the specific heat at constant pressure.

$$\frac{C^{\circ}_{pk}}{R} = \sum_{n=1}^{N} a_{nk}\, T^{(n-1)} \tag{3.15}$$

For perfect gaeses the heat capacities are independent of pressure; the standard state values are the actual values. Other thermodynamic properties are given in terms of the fits to C°_p. First, the enthalpy is given by

$$\frac{H^{\circ}_k}{R} = \int_0^{\Pi} C^{\circ}_{pk}\, dT \tag{3.16}$$

so that

$$\frac{H^{\circ}_k}{RT} = \sum_{n=1}^{N} \frac{a_{nk} T^{(n-1)}}{n} + \frac{a_{N=1,k}}{T} \tag{3.17}$$

where the constant of integration, $a_{N+1,k}$, is the standard formation enthalpy at 0 K. Additionally, the standard state entropy is written as

$$\frac{S^{\circ}_k}{R} = \int_0^{\Pi} \frac{C^{\circ}_{pk}}{T} dT \tag{3.18}$$

so that

$$\frac{S^{\circ}_k}{R} = a_{1k} \ln T + \sum_{n=2}^{N} \frac{a_{nk} T^{(n-1)}}{(n-1)} + a_{N+2,k} \tag{3.19}$$

where the constant of integration, $a_{N+2,k}$, is the standard formation entropy at 0 K. The order ,N , of the polynomial fit has been taken as five and hence seven coefficients are needed for the whole temperature range.

In addition to the chemical reaction rates, the transport properties of the species, i.e., thermal conductivities and diffusion coefficients, are also evaluated. Stockmayer potentials are used throughout in evaluating transport properties. An extended Eucken-Hirschfelder correction for polyatomic species is used in computing the single component conductivities. The gas mixture's thermal conductivity is determined from the individual component conductivities using an empirical combination averaging formula (Mathur, et al. [41]).

The diffusion velocity V_k is assumed to be composed of three parts

$$V_k = V_{od} + V_{td} + V_c \tag{3.20}$$

V_{od} is the ordinary diffusion velocity and is given in the Curtiss-Hirschfelder [19] and approximated by

$$V_{od} = -D_k \frac{1}{X_k} \frac{dX_k}{dx} \tag{3.21}$$

where X_k is the mole fraction, and where the mixture-averaged diffusion coefficient D_k is given explicitly in terms of the binary diffusion coefficients by

$$D_k = \frac{1 - Y_k}{\sum_{j \neq k}^{K} X_j / D_{kj}} \tag{3.22}$$

A non-zero thermal diffusion velocity V_{td} is included only for the low molecular weight species H, H_2, and He. The trace, light-component limit is employed in determining V_{td}, i.e.,

$$V_{td} = \frac{D_k k_{T_k}}{X_k} \frac{1}{T} \frac{dT}{dx} \tag{3.23}$$

where k_{T_k} is the thermal diffusion ratio (Chapman and Couling, [14]). The sign of k_{T_k} makes the lower molecular weight species diffuse from low to high temperature regions.

The correction velocity V_c (independent of species but a function of x) is included to ensure that the mass fractions sum to unity (or equivalently $\sum_{k=1}^{K} Y_k V_k = 0$). This formulation of the correction velocity is the one recommended by Coffee and Heimerl [16,17] in their extensive investigation of approximate transport models in hydrogen and methane flames.

3.2 Boundary conditions

The appropriate boundary conditions have been deduced from the early work of Curtiss and Hirschfelder [19]. For burner stabilized flames M is a known constant, the temperature and mass flux fractions

($\varepsilon_k = Y_k + \rho Y_k V_k A/M$) are specified at the cold boundary, and vanishing gradients are imposed at the hot boundary.

CHAPTER 4

NUMERICAL SOLUTION METHOD

The numerical solution method [35] begins by making finite difference approximations to reduce the boundary value problem to a system of algebraic equations. The initial approximations are usually on a very coarse mesh that may have as few as six points. After obtaining a solution on the coarse mesh, new mesh points are added in regions where the solution or its gradients change rapidly. An initial guess is obtained for the solution on the finer mesh by interpolating the coarse mesh solution. This procedure continues until no new mesh points are needed to resolve the solution to the required accuracy.

The solution of the system of algebraic equations is first attempted by the damped modified Newton algorithm. However, if the Newton algorithm fails to converge, the solution estimate is conditioned by a time integration. This provides a new starting point for the Newton algorithm that is closer to the solution, and thus more likely to be in the domain of convergence for Newton's method.

4.1 Finite Difference Approximations

The first task in solving the flame problem is to discretcize the governing conservation equations. Finite difference approximations have been used on a nonuniform grid with points numbered from 1 at the cold boundary to J at the hot boundary. On the convective terms, either first order windward differences or central differences may be used. Both cases are illustrated using the convective term in the energy equation. The windward difference is given as

$$\left(M\frac{dT}{dx}\right)_j \approx M_j\left(\frac{T_j - T_{j-1}}{x_j - x_{j-1}}\right) \tag{4.1}$$

where the index j refers to the mesh point. The central difference formula is

$$\left(M\frac{dT}{dx}\right)_j \approx M_j\left(\frac{h_{j-1}}{h_j(h_j+h_{j-1})}T_{j-1} + \frac{h_j - h_{j-1}}{h_j h_{j-1}}T_j - \frac{h_j}{h_{j-1}(h_j+h_{j-1})}T_{j-1}\right) \tag{4.2}$$

where $h_j = x_{j+1} - x_j$. The windward difference formulas introduce artificial diffusion on a coarse mesh; this has the effect of spreading out the solution and making the convergence of Newton's method less sensitive to the starting estimate. However, because the mesh is refined in regions of high gradient, the artificial diffusion becomes relatively unimportant after the solution has progressed to the fine meshes. Nevertheless, for a given mesh, the windward difference approximation is less accurate than the upward difference formula.

The first derivative in the summation term in the energy equation (3.2) is always approximated by an upwind difference formula,

$$\left(\frac{dT}{dx}\right)_j \approx \left(\frac{T_j - T_{j-1}}{x_j - x_{j-1}}\right) \tag{4.3}$$

and the coefficients in the summation are evaluated at j.

The second derivative term in the energy equation is approximated by the following second order central difference.

$$\frac{d}{dx}\left(\lambda A \frac{dT}{dx}\right)_j \approx \left(\frac{2}{x_{j+1} - x_{j-1}}\right)\left[\lambda A_{j+1/2}\left(\frac{T_{j+1} - T_j}{x_{j+1} - x_j}\right) - \lambda A_{j-1/2}\left(\frac{T_j - T_{j-1}}{x_j - x_{j-1}}\right)\right] \tag{4.4}$$

The coefficients in this formula (at $j \pm 1/2$) are evaluated using the averages of the dependent variables between mesh points.

The diffusive term in the species conservation equation is approximated in a similar way, but it appears to be different because it has been written using diffusion velocities. The ordinary (Eq. 3.16) and thermal (Eq. 3.18) diffusion velocities are approximated at the $j \pm 1/2$ positions as illustrated by

$$(Y_k V_{od})_{j+1/2} \approx -\left(\frac{W_k D_k}{W}\right)_{j+1/2}\left(\frac{X_{kj+1} - X_{kj}}{x_{j+1} - x_j}\right) \tag{4.5}$$

$$(Y_k V_{td})_{j+1/2} \approx -\left(\frac{W_k D_k k_{T_k}}{WT}\right)_{j+1/2}\left(\frac{T_{j+1} - T_j}{x_{j+1} - x_j}\right) \tag{4.6}$$

After the diffusion velocities are computed at all mesh midpoints, the correction velocity V_c is computed at the midpoints from

$$V_c = -\sum_{k=1}^{K} Y_k (V_{od} + V_{td}) . \tag{4.7}$$

Upon forming the full diffusion velocities $V_k = V_{od} + V_{td} + V_c$ the diffusion term is evaluated with the following difference approximation.

$$\frac{d}{dx}(\rho A Y_k V_k)_j \approx \frac{(\rho A Y_k V_k)_{j+1/2} - (\rho A Y_k V_k)_{j-1/2}}{x_{j+1/2} - x_{j-1/2}} \tag{4.8}$$

All the nondifferentiated terms, such as the chemical production rate terms, are evaluated at the mesh points j. Coefficients not appearing within derivatives are evaluated at the mesh points.

4.2 Boundary Conditions

The boundary conditions are relatively easily implemented. At the cold boundary the mass flux fractions and the temperature are specified, i.e.,

$$\varepsilon_{k,1} - Y_{k,1} - (\rho A Y_k V_k)_{j=3/2} = 0 \tag{4.9}$$

and

$$T_1 - T_b = 0 \tag{4.10}$$

where T_b is the specified burner temperature. At the hot boundary all gradients vanish, i.e.,

$$\frac{Y_{k,j} - Y_{k,j-1}}{x_j - x_{j-1}} = 0 \tag{4.11}$$

and

$$\frac{T_j - T_{j-1}}{x_j - x_{j-1}} = 0 \qquad (4.12)$$

The boundary conditions for M depend on whether the given problem is a burner stabilized or a freely propagating flame.

4.3 Starting Estimates

The program needs a starting estimate of the solution from which to begin its iteration. The general form of this estimate is shown in Figure 4.1. For this estimate it is presumed that there is a reaction zone in which the reactants change from their unreacted values (the unburned composition) to the products. The estimates for the location and thickness of the reaction zone are provided by the user. Estimated values of the product species (the fully burned composition) are also required by the program. Within the reaction zone the program uses straight lines between the initial and final values for both the reactants and products. On the cold side of the reaction zone the reactant species profiles are flat at the unburned values. On the hot side, the product species are flat at the estimated product values. Any given species can be both a reactant and a product species. For example, the nitrogen in a hydrocarbon-air flame will be both a reactant and a product. The excess fuel in a rich flame will also be both a reactant and a product. Species can also be identified as "intermediates." Intermediates, such as short-lived radical species, are assumed to have a Gaussian profile that peaks in the center of the reaction zone. The peak height is specified in the input to the program, and the Gaussian's width is

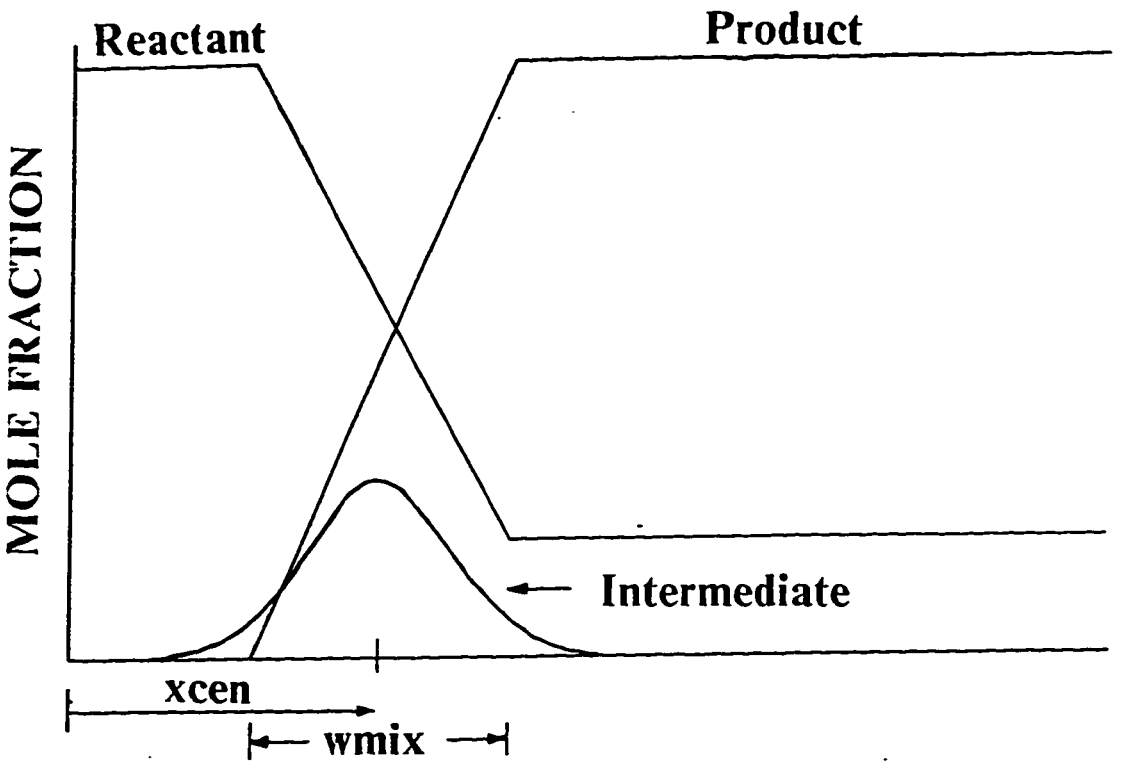

(*Note*: **wmix** is the estimated width of the reaction zone, and **xcen** is the estimated value for center of the flame).

(*Courtesy* Sandia National Laboratories, Livermore, California, U.S.A.)

Figure 4.1 : The General Form of the Starting Estimate

such that the profile is at 1/10 of its peak value at the edges of the reaction zone.

It has been found [35] that the shape of the assumed species profiles is not too important. Smoother functions, such as cubic polynomials and hyperbolic tangents for the reactant and product species, have no apparent effect on the convergence properties of the method. Since the starting profiles are typically evaluated on a very coarse mesh, it makes little difference whether the underlying function is smooth or not. Therefore, in the program linear starting profiles have been used.

4.4 Program Structure

The premix flame code [35] is written in two modules. One is a piece of software to solve boundary value problems; it is completely independent and could easily be used for problems not related to flames. The other module contains flame specific coding. It reads input from the user, defines the governing equations, makes calls to the boundary value solver, and prints solutions for the flame problem.

In addition to input directly from the user, the flame program [35] depends on data and subroutines from the CHEMKIN (Kee, et al. [33]) and transport packages (Kee, et al. [34]). Therefore, to solve a flame problem the user must be able to set up a command procedure that allows for the execution of several preprocessor programs, the access to several data bases, the loading of

subroutines from several libraries, and the passing of files from one process to another. Figure 4.2 shows the relationships between these various components.

The first step is to execute the CHEMKIN Interpreter. The CHEMKIN Interpreter first reads user-supplied information about the species and chemical reactions for a particular reaction mechanism. It then extracts further information about the species' thermodynamic properties from a data base. This information is stored on the CHEMKIN Linking File; a file that is needed by the transport property fitting program, TRANFT [34] and later by the CHEMKIN subroutine library, which will be accessed by the flame program. In addition, the CHEMKIN Interpreter requires an additional binary scratch file.

The next program to be executed is the transport property fitting program, TRANFT. It needs input from a Transport property data base and from the CHEMKIN subroutine library. Its purpose is to compute polynomial representations of the temperature-dependent parts of the individual species viscosities, thermal conductivities, and the binary diffusion coefficients. Like the CHEMKIN Interpreter, the TRANFT program produces a Linking File that is later needed in the transport property subroutine library, which will evaluate mixture properties during the course of the flame computation.

Both the CHEMKIN and the transport subroutine libraries must be initialized before use and the flame program makes the appropriate initialization calls. The purpose of the initialization is to read the Linking Files and set up the internal working and storage space required by all subroutines in the libraries.

The input that defines a particular flame and the parameters needed to

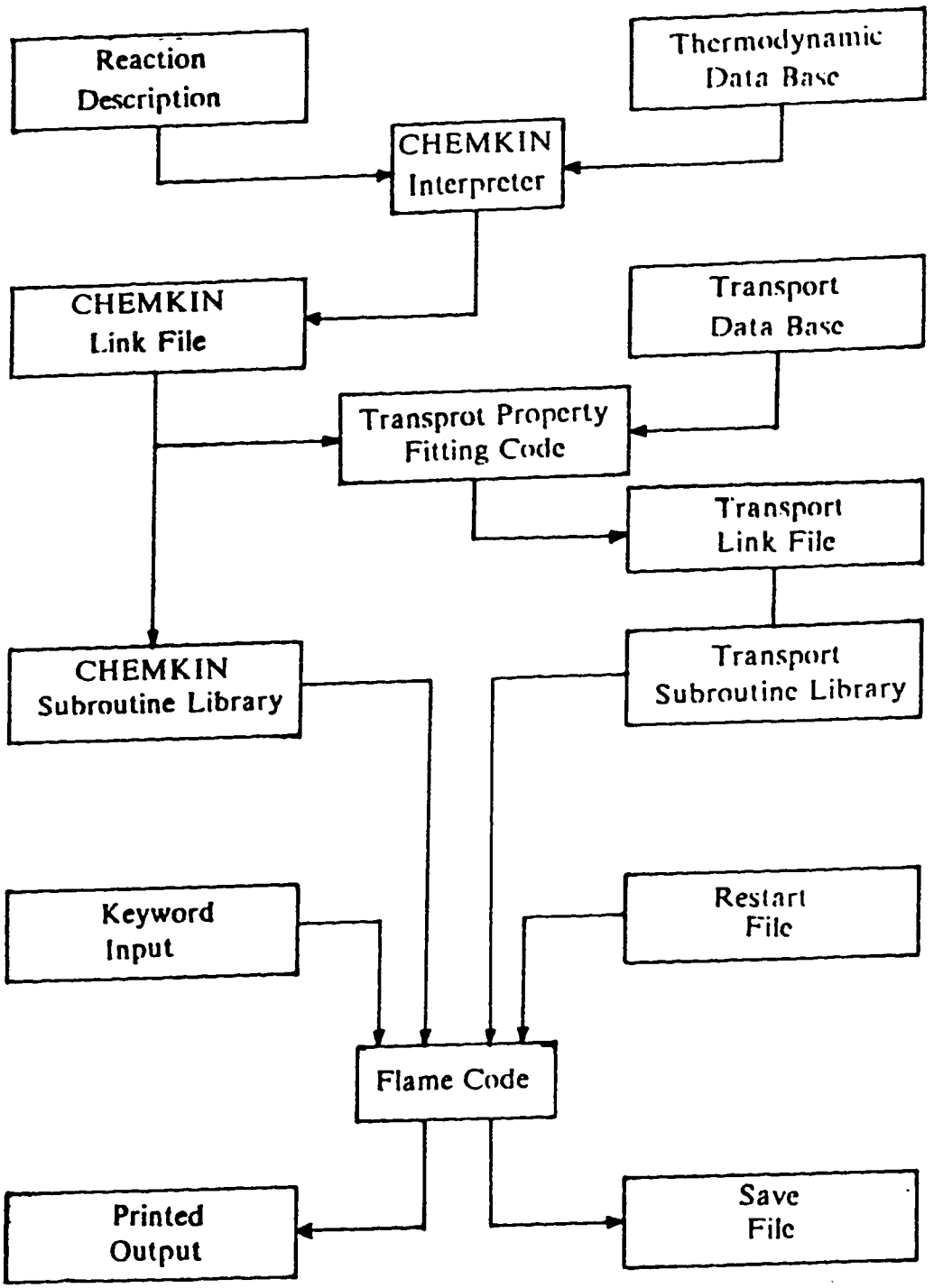

(*Courtesy* Sandia National Laboratories, Livermore, California, U.S.A.)

Figure 4.2 : Relationship of the Flame Program to the CKEMKIN and Transport Preprocessors and the associated Input and Output Files

solve it are read by the flame program [35] in a Keyword format. The flame program produces printed output and it saves the solution in a Save file.

4.5 Main Program

The flame program is written as a subroutine. A main program is written that opens all appropriate files, allocates the working storage, and calls the flame program through its subroutine interface. Changes must be made in this program every time some reactions are inserted or taken out from from the reaction mechanism. In addition, a subroutine has been provided that specifies the stream tube area for the burner-stabilized flame.

The boundary value solution program also provides information about the CPU time used in the various portions of the iterations. It does this by making a subroutine call that is specific to the particular computer on which it is running. This call is contained in a subroutine called CPUTIM. The system call was changed in this routine to accomodate the computer system in KFUPM.

4.6 CPU Time

The flame code [35] can run on any mainframe computer. The total CPU time required for the solutin of a particular flame depends on a large number of factors such as the user-specified "guess" at the solution, the absolute and relative tolerances and so on. The CPU time taken for the final solutions of

Flame 1 to Flame 5 were 69, 665, 415, 91, and 73 seconds, respectively. The CPU time decreases considerably as the user learns to use the flame code efficiently.

CHAPTER 5

CHEMICAL INTERPRETATION OF THE RESULTS

Modelling in combustion research may be defined as a procedure of deducing the mathematical description of a process, i.e., a model, from experimental observations. A strategy for modelling is usually based upon various factors involved in a particular study, such as objectives of the investigation, purpose of the modelling, experimental technique employed, quality and quantity of the experimental observations, reference data available, desired degree of reliability of the model, etc.

A model is defined as a functional relationship or relationships among various quantities involved in a physical process. The relationships may be expressed in the form of algebraic, differential, or integral equations, which need not necessarily possess an explicit analytical solution. Combustion modelling is done through dynamic models, which are models formulated in terms of differential equations.

5.1 Objectives of Combustion Modelling :

The objectives of the combustion modelling are :

1) to simulate combustion processes and to develop predictive capability for combustion behavior under various conditions.

2) to help in interpreting and understanding observed combustion phenomenon.

3) to substitute for difficult or expensive experiments.

4) to guide the design of combustion experiments.

Chemical kinetic modelling of flames is an important means of understanding the complete structure of the flames and of evaluating critical reaction paths. The chemical kinetics of combustion systems is usually not well-established. Nevertheless, it is often possible to construct plausible mechanisms including elementary reactions of various degrees of certainty and even hypothetical ones never identified in direct laboratory experiments. The corresponding model, being physico-empirical in nature, is called a mechanistic model. The adequacy of the latter, in a statistical sense, does not necessarily mean that the "true" model is derived, but rather that with a certain probability the model cannot be rejected. Such an interpretation reflects the empiricism of mechanistic modelling and suggests that future experimental discoveries may lead to modification of the model.

5.2 Applications of Combustion Modelling :

Some important applications of computer modelling are given below.

1) Combustion effects on the environment which include
   - Formation of Pollutants such as NO_x, CO, SO_x
   - Formation of particulates such as soot, coke
   - Methods of comparison and temperature control of exhaust

2) Fire prevention and safety

3) Power Production such as
   - Combustion in power stations
   - Liquid fuels for automobiles, aircrafts, ships, and so on
   - Solid and liquid propellants in rocket motors

5.3 Chemical Aspects to Keep in Mind :

1) There is a hierarchy of confidence that can be placed in rate-coefficient expressions. Some are accurate and some are only more or less educated guesses.

2) Comparisons between theory and experiment can be no more accurate than the degree to which the physical constraints adopted for the modelling equations are faithful representations of the constraints that actually pertain in the laboratory. Some experiments lend themselves, by choice of reaction conditions, better to modelling than others.

5.4 Combustion in Flames :

In pre-mixed flames (high temperature), the mechanism of combustion differs markedly from that responsible for low temperature oxidation. When true ignition occurs the majority of the enthalpy of reaction is released rapidly in a narrow reaction zone leading to the production of very high temperatures. These high temperatures produce steep temperature gradients and the transport of heat or of active centres makes the flame self propagating. The resulting combustion wave can be stabilized on a burner in the normal way.

The high temperature generated provides the key to the change in mechanism. At high temperatures, equilibrium considerations favours dissociation and typical flames in oxygen at 2000-3000 K may contain 10-50% of the fuel in the form of radicals. Furthermore, because the kinetic order of dissociation is lower than that of recombination, radical concentrations will tend to 'overshoot', that is, to exceed the local equilibrium values and will return to them relatively slowly. Although as a result of the high temperature all reactions will be correspondingly faster, because of the increased radical concentrations radical-radical reactions become progressively more significant. The nature of the dominant active intermediates is also likely to change, degenerate-branching species such as peroxides and aldehydes being replaced by simple radicals and atoms.

The effects of high temperature once established are self-perpetuating and a transition from slow combustion to true ignition can be effected, under appropriate conditions, simply by supplying a sufficiently active source of ignition, that is, a region of very high temperature or very high radical concentration.

Although the majority of reaction occurs within a very narrow spatial region, three distinct zones (a pre-heat zone, a true-reaction zone, and a recombination zone) may be distinguished. The nature of the reactions in the pre-heat zone depends very much on the fuel involved. For a very stable molecule like methane, with a first order decomposition rate constant of only $10^4\ s^{-1}$ even at 2000 K, little or no pyrolysis occurs within the short residence time in the flame.

With the majority of hydrocarbons, considerable degeneration occurs and the fuel fragments leaving this zone will comprise mainly lower hydrocarbons, alkenes and hydrogen. One major effect of this is that the composition in the reaction zone proper is always very similar, irrespective of the nature of the fuel, thus explaining why flame temperature and burning velocities vary by only a small amount for a wide range of fuels. In the pre-heat zone, the oxygen plays only a catalytic role and is itself little consumed.

5.5 Reaction Mechanism :

Reaction mechanism of a certain flame is a useful tool which can be used to serve many purposes. It provides the description of the elementary reaction steps to convert the input fuel and oxidizer to final stable products. This mechanism consists of most of the chemical species which affect the combustion process, and the elementary reactions among them.

The reaction mechanism developed for the $CH_4 / NO_2 / O_2$ flames is given in Table 5.1. It contains 101 elementary reactions involving 30 species. A literature survey was conducted to obtain the rate constants given in Table 5.1 which are based entirely on experimental measurements. References from which these rate constants have taken are also included in Table 5.1. The postulated mechanism was used as an input to the flame code [35] in order to calculate the species concentrations versus distance. The results of the flame calculations and the experiments shows a good match which emphasizes the validity of the proposed chemical kinetic mechanism.

5.5.1 Methane Oxidation Mechanisms :

Based on earlier investigations [3,22,25,50] and present observations, it is suggested that, under the conditions in which experimental observations were made [1], methane is oxidized by two parallel mechanisms which takes place consecutively in two distinct zones.

TABLE 5.1

Chemical Reaction Mechanism for $CH_4 / NO_2 / O_2$ Flames

Rate Coefficients In Form $K(T) = AT^{\beta}\exp\left(-\frac{E}{RT}\right)$.

Units are moles, cm^3, sec, K and cal/mole.

No.	REACTION	A	β	E	Ref
R1	$CH_4 + H = CH_3 + H_2$	2.24E04	3.0	8.75E03	15
R2	$CH_4 + OH = CH_3 + H_2O$	1.60E06	2.1	2.46E03	24
R3	$CH_4 + M = CH_3 + H + M$	6.32E17	0.0	8.80E04	28
R4	$CH_4 + HO_2 = CH_3 + H_2O_2$	1.80E11	0.0	1.87E04	43
R5	$CH_4 + NO_2 = CH_3 + HNO_2$	1.20E13	0.0	3.00E04	55
R6	$CH_4 + O_2 \rightarrow CH_3 + HO_2$	8.00E13	0.0	5.60E04	53
R7	$CH_3 + HO_2 \rightarrow CH_4 + O_2$	1.00E12	0.0	4.00E02	53
R8	$CH_3 + NO_2 = CH_3O + NO$	1.30E13	0.0	0.00E00	55
R9	$CH_3 + O_2 = CH_2O + OH$	5.20E13	0.0	3.46E04	61
R10	$CH_3 + O = CH_2O + H$	7.00E13	0.0	0.00E00	64
R11	$CH_3 + O_2 = CH_2O + H + O$	1.50E13	0.0	2.87E04	64
R12	$CH_3 + OH = CH_2 + H_2O$	7.50E07	2.0	5.00E03	43
R13	$CH_3 + H = CH_2 + H_2$	9.00E13	0.0	1.50E04	43
R14	$CH_3 + M = CH_2 + H + M$	1.00E16	0.0	9.06E04	64
R15	$CH_3 + OH = CH_2O + H_2$	3.98E12	0.0	0.00E00	28
R16	$CH_3 + HO_2 = CH_3O + OH$	6.00E11	0.0	0.00E00	43
R17	$CH_3 + NO = CH_2O + NH$	2.00E13	0.0	0.00E00	9

TABLE 5.1(cont.)

No.	REACTION	A	β	E	Ref
R18	$CH_3 + NO = HCN + H_2O$	1.00E11	0.0	1.50E04	43
R19	$CH_3 + O_2 = CH_3O + O$	2.05E19	-1.6	2.92E04	43
R20	$CH_2 + NO = HCN + OH$	2.00E13	0.0	0.00E00	43
R21	$CH_2 + OH = CH + H_2O$	4.50E13	0.5	3.00E03	61
R22	$CH_2 + H = CH + H_2$	4.00E13	0.00	0.00E00	64
R23	$CH_2 + O = CO + H + H$	5.00E13	0.00	0.00E00	43
R24	$CH_2 + O = CH + OH$	1.99E11	0.68	2.50E04	66
R25	$CH_2 + O_2 = CO_2 + H_2$	6.90E11	0.0	5.00E02	43
R26	$CH_2 + O_2 = CO_2 + H + H$	1.30E13	0.0	1.50E03	64
R27	$CH_2 + O_2 = CO + OH + H$	8.64E10	0.0	-5.00E02	43
R28	$CH_2 + O_2 = HCO + OH$	4.32E10	0.0	-5.00E02	43
R29	$CH_2 + O_2 = CO + H_2O$	1.87E10	0.0	-1.00E03	56
R30	$CH_2 + O_2 = CH_2O + O$	2.00E13	0.0	1.20E04	61
R31	$CH + NO = NH + CO$	1.51E14	0.0	0.00E00	40
R32	$CH + NO = HCN + O$	1.10E14	0.0	0.00E00	43
R33	$CH + NO = CN + OH$	1.00E15	0.0	0.00E00	61
R34	$CH + H_2O = CH_2O + H$	4.57E14	-.75	0.00E00	43
R35	$CH + O_2 = OH + CO$	2.00E13	0.0	0.00E00	64
R36	$CH + O = CO + H$	4.00E13	0.0	0.00E00	64
R37	$CH_2O + NO_2 = HCO + HNO_2$	1.26E10	0.0	1.51E04	25
R38	$CH_2O + M = HCO + H + M$	3.31E16	0.0	8.10E04	21

TABLE 5.1(cont.)

No.	REACTION	A	β	E	Ref
R39	$CH_2O + OH = HCO + H_2O$	7.59E12	0.0	1.70E02	4
R40	$CH_2O + H = HCO + H_2$	3.31E14	0.0	1.05E04	21
R41	$CH_2O + O = HCO + OH$	5.01E13	0.0	4.60E03	9
R42	$CH_2O + HO_2 = HCO + H_2O_2$	1.00E12	0.0	8.00E03	56
R43	$CH_2O + HO_2 \rightarrow CH_3O + O_2$	0.00E00	0.0	0.00E00	56
R44	$CH_3O + O_2 \rightarrow CH_2O + HO_2$	1.00E12	0.0	6.00E03	56
R45	$CH_3O + M = CH_2O + H + M$	5.00E13	0.0	2.10E04	56
R46	$HCO + OH = CO + H_2O$	1.00E14	0.0	0.00E00	9
R47	$HCO + H = CO + H_2$	1.99E14	0.0	0.00E00	64
R48	$HCO + NO_2 = CO + HNO_2$	1.00E14	0.0	0.00E00	25
R49	$HCO + O = CO + OH$	1.00E14	0.0	0.00E00	66
R50	$HCO + M = CO + H + M$	2.50E14	0.0	1.68E04	64
R51	$HCO + O_2 \rightarrow CO + HO_2$	1.00E14	0.0	6.80E03	27
R52	$CO + HO_2 \rightarrow HCO + O_2$	0.00E00	0.0	0.00E00	27
R53	$CO + H + H_2 = HCO + H_2$	6.90E14	0.0	1.67E03	64
R54	$CO + O + CO = CO_2 + CO$	5.30E13	0.0	-4.54E03	64
R55	$CO + OH = CO_2 + H$	4.41E06	1.5	-7.40E02	64
R56	$CO + HO_2 = CO_2 + OH$	1.50E14	0.0	2.36E04	64
R57	$CO + O_2 = CO_2 + O$	2.50E12	0.0	4.78E04	64
R58	$OH + OH = H_2O + O$	1.50E09	1.14	0.00E00	64
R59	$OH + H_2O_2 = H_2O + HO_2$	7.00E12	0.0	1.43E03	64

TABLE 5.1(cont.)

No.	REACTION	A	β	E	Ref
R60	$H_2 + O_2 \rightarrow OH + OH$	1.36E13	0.0	4.82E04	31
R61	$OH + OH \rightarrow H_2 + O_2$	4.48E11	0.0	2.98E04	31
R62	$HO_2 + NO \rightarrow NO_2 + OH$	1.00E14	0.0	0.00E00	52
R63	$NO_2 + OH \rightarrow HO_2 + NO$	0.00E00	0.0	0.00E00	52
R64	$H_2 + O = OH + H$	1.50E07	2.0	7.55E03	64
R65	$H_2 + H_2 = H + H + H_2$	8.80E14	0.0	9.61E04	64
R66	$H + O_2 = OH + O$	1.20E17	-.91	1.65E04	64
R67	$H + H_2O = OH + H_2$	4.60E08	1.60	1.86E04	64
R68	$H + HO_2 = OH + OH$	1.50E14	0.0	1.00E03	64
R69	$H + OH + H_2O = H_2O + H_2O$	1.40E23	-2.0	0.00E00	64
R70	$H + H_2O_2 = H_2O + OH$	1.00E13	0.0	3.60E03	64
R71	$H + O_2 + M = HO_2 + M$	3.61E17	-.72	0.00E00	43
R72	$HCN + O = NCO + H$	1.38E04	2.64	4.98E03	43
R73	$NO + HO_2 = HNO + O_2$	2.00E11	0.0	1.00E03	64
R74	$NO + N_2O = N_2 + NO_2$	1.00E14	0.0	2.50E04	64
R75	$2NO + O_2 = 2NO_2$	4.50E10	0.0	2.56E04	55
R76	$N_2O + M = N_2 + O + M$	1.60E18	0.0	5.16E04	43
R77	$N_2O + OH = N_2 + HO_2$	2.00E12	0.0	1.00E04	43
R78	$N_2O + H = N_2 + OH$	7.60E13	0.0	1.52E04	49
R79	$N_2O + O = N_2 + O_2$	1.00E14	0.0	2.82E04	30
R80	$N_2O + O = 2NO$	1.00E14	0.0	2.82E04	30

TABLE 5.1(cont.)

No.	REACTION	A	β	E	Ref
R81	$NCO + H = NH + CO$	5.00E13	0.0	0.00E00	43
R82	$NCO + NO = N_2O + CO$	1.00E13	0.0	-3.90E02	43
R83	$NCO + H_2 = HNCO + H$	8.58E12	0.0	9.00E03	43
R84	$HNCO + H = NH_2 + CO$	2.00E13	0.0	3.00E03	43
R85	$NH_2 + NO = NNH + OH$	2.00E13	0.0	3.00E03	61
R86	$CN + NO = N_2 + CO$	1.07E14	0.0	8.00E03	49
R87	$CN + N_2O = NCO + N_2$	1.00E13	0.0	0.00E00	43
R88	$NH + O_2 = HNO + O$	1.00E13	0.0	1.20E04	43
R89	$NH + O_2 = NO + OH$	7.60E10	0.0	1.53E03	43
R90	$NH + NO = N_2O + H$	2.40E19	-0.8	0.00E00	43
R91	$NH + NO = N_2 + OH$	2.40E15	-1.0	0.00E00	40
R92	$HNO + O = NO + OH$	5.00E11	0.5	1.00E03	30
R93	$HNO + H = NO + H_2$	1.26E13	0.0	2.00E03	64
R94	$HNO_2 + OH = H_2O + NO_2$	1.55E12	0.0	0.00E00	25
R95	$HNO_2 + M = OH + NO + M$	1.80E17	0.0	4.49E04	55
R96	$HNO + M = H + NO + M$	1.50E16	0.0	4.87E04	43
R97	$HNO + HNO = N_2O + H_2O$	3.95E12	0.0	5.00E03	43
R98	$HNO + NO = N_2O + OH$	2.00E12	0.0	2.60E04	43
R99	$NNH = N_2 + H$	1.00E04	0.0	0.00E00	43
R100	$NNH + NH = N_2 + NH_2$	5.00E13	0.0	0.00E00	43
R101	$NNH + O = N_2O + H$	1.00E14	0.0	0.00E00	43

(a) Yellow Zone :

The major propagation reactions involves radical attack on the fuel. The following reactions

$$CH_4 + NO_2 = CH_3 + HNO_2 \qquad \text{(R5)}$$

$$HNO_2 + M = OH + NO + M \qquad \text{(R95)}$$

$$CH_4 + OH = CH_3 + H_2O \qquad \text{(R2)}$$

$$CH_3 + O_2 = OH + CH_2O \qquad \text{(R9)}$$

constitute the primary mechanism whereby NO_2 accelerates the induction period kinetics of CH_4 / O_2 mixtures. Initiation occurs via the H-abstraction reaction and rapid dissociation of the HNO_2 leads to the simultaneous production of OH and NO . Reactions (2) and (9) then constitutes a fast chain with OH being regenerated as illustrated in the next page. Our observations of OH are consistent with the radical being formed early in the induction period via HNO_2 dissociation. Reaction (2) produces water.

In short, NO_2 initially sensitizes the CH_4 at low temperature which accounts for the yellow colour zone.

(b) Violet Zone :

As the temperature increases further, a second zone of violet colour is encountered. The two zones are separated by a dark line as shown in Figure (5.1). In this zone, the role of NO_2 as a hydrogen abstracter from methane comes to an end. Another set of reactions

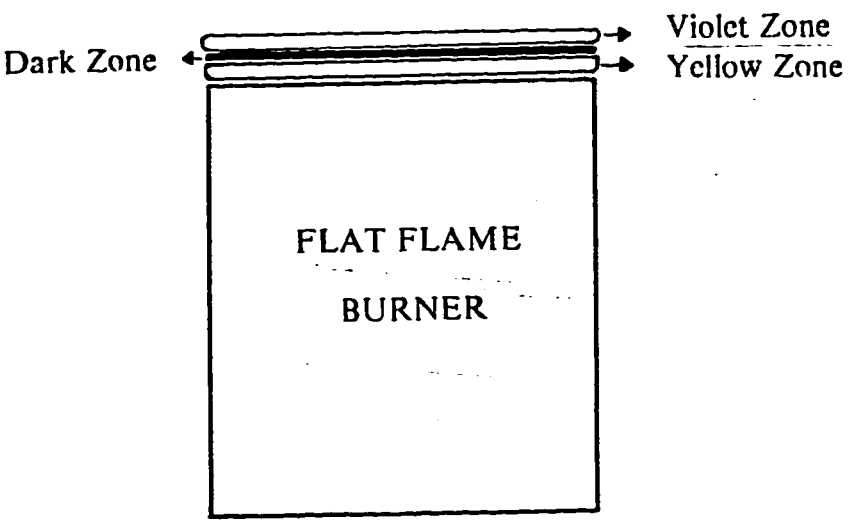

Figure 5.1 : Experimentally Observed Yellow and Violet Zones in CH_4 / NO_2 / O_2 Flames

$$CH_4 + M = CH_3 + H + M \qquad \text{(R3)}$$

$$CH_4 + H = CH_3 + H_2 \qquad \text{(R1)}$$

$$CH_3 + NO_2 = CH_3O + NO \qquad \text{(R8)}$$

$$CH_3O + M = H + CH_2O + M \qquad \text{(R45)}$$

constitutes the mechanism for the violet zone. In this zone, initiation occurs via the thermal decomposition of methane which leads to the production of H atoms. Reactions (1),(8) and (45) then constitute another fast chain with H being regenerated, as shown previously. This chain is independent of oxygen concentration. Reaction (8) accounts for the observed conversion of NO_2 to NO.

The yellow zone characterizes the low temperature decomposition of NO_2, whereas the violet zone depicts the high temperature dissociation of methane. The reactions in the two zones take place simultaneously. The dark line that separates the two zones results from the temperature difference between the two zones. Reactions are taking place in the dark zone also but the radicals that are generated by these reactions are not luminous, which accounts for the dark region between the two luminous regions.

5.6 Comparison between Experimental and Calculated Results :

The flame code has been utilized to model five different $CH_4 / NO_2 / O_2$ flames. The reactant mole fractions, flow rates, and equivalence ratios of these flames are given in Table (5.2). These values have been taken from experiments conducted by Al-Farayedhi [1] and Sadeqi [50]. All these flames are lean with equivalence ratios ranging from 0.20 to 0.92. The flames were stabilized on a flat flame burner at a pressure of 50 Torr, except for flame 1 which was stabilized at a pressure of 70 Torr.

The calculated species profiles (from flame code) are depicted in Figures (5.2a) to (5.6c).

5.6.1 Stable Species :

Comparison between the calculated and experimental profiles for CO_2 and CO for Flame 2 is shown in Figure (5.7a). It can be seen that these profiles show good agreement. The peak concentration for CO is also predicted accurately. The predicted values of the mole fractions for CO_2 are higher than their experimental counterpart, whereas for CO the situation is just the opposite.

Figure (5.7b) shows the comparison of calculated and experimental profiles for NO, N_2, NO_2, and H_2O for Flame 2. The calculated and experimental profiles show excellent agreement for NO, N_2, and H_2O. The specie NO_2 is underpredicted by the flame code compared with the experimental profile.

Figure (5.8a) shows the comparison of calculated and experimental profiles

TABLE 5.2

Reactant Mole Fractions and Pressures in Experimental Flames

Flame #	CH_4	NO_2	O_2	Ar	Flowrate (SLPM)	Pressure (Torr)	Equivalence Ratio	(O_2/NO_2) Ratio
1	0.11	0.00	0.24	0.65	2.60	70	0.92	undef
2	0.24	0.56	0.20	0.00	1.75	50	0.58	0.360
3	0.16	0.73	0.11	0.00	2.60	50	0.34	0.150
4	0.11	0.85	0.03	0.00	3.50	50	0.25	0.035
5	0.09	0.91	0.00	0.00	4.40	50	0.20	0.000

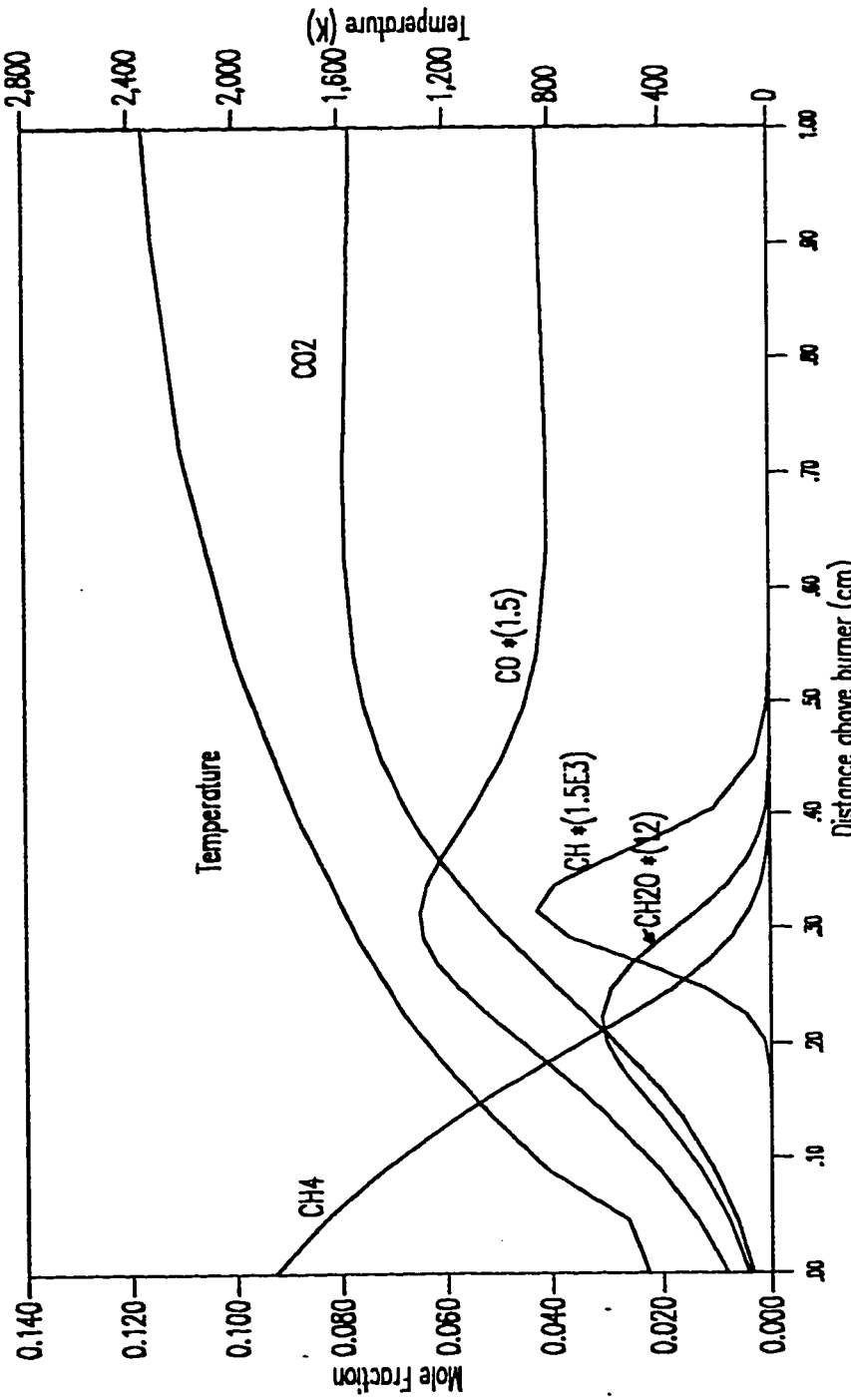

Figure 5.2a: Calculated Species Profiles for Flame 1 for CH4, CH, CO, CO2 and CH2O.

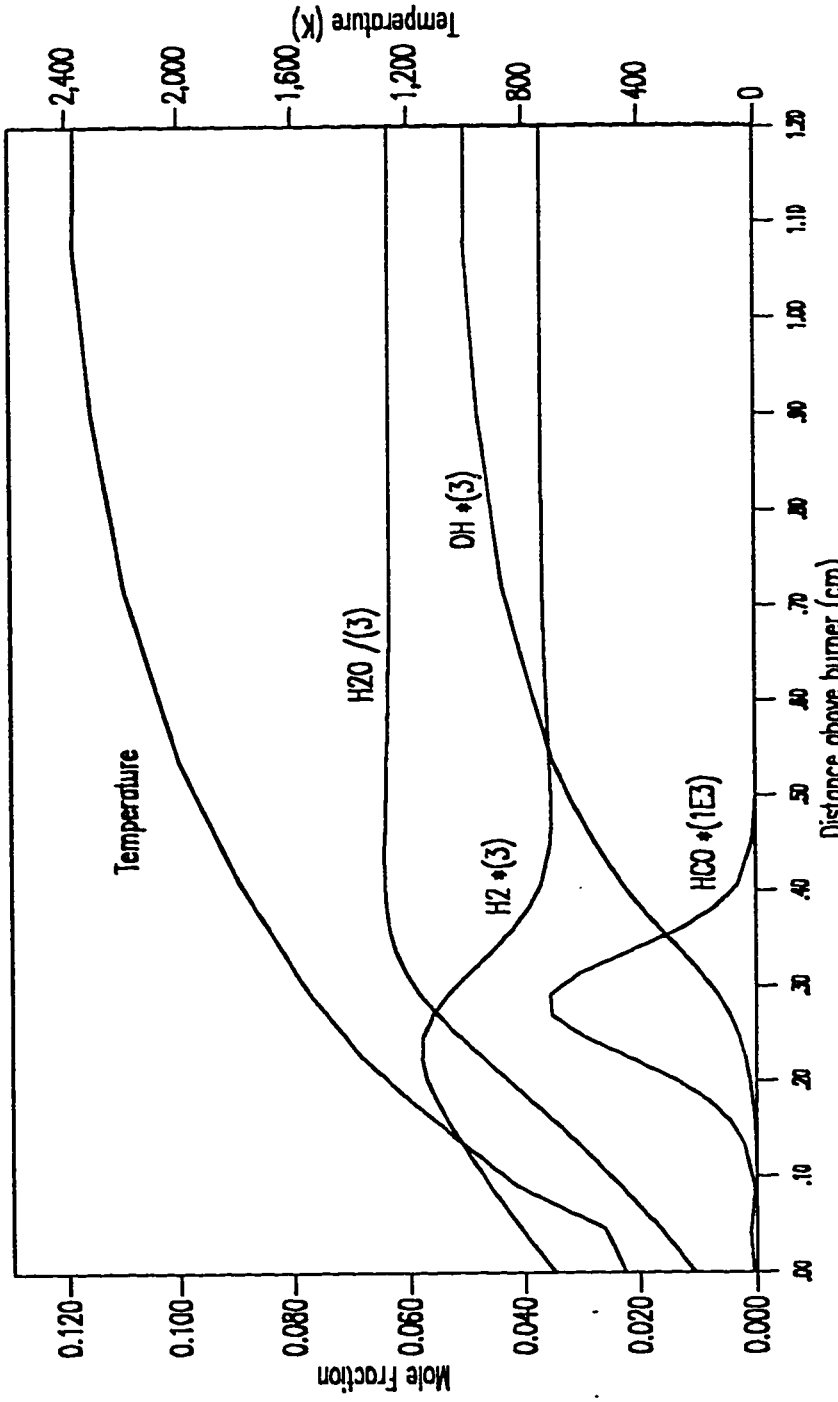

Figure 5.2b: Calculated Species Profiles for Flame 1 for H2, OH, H2O and HCO.

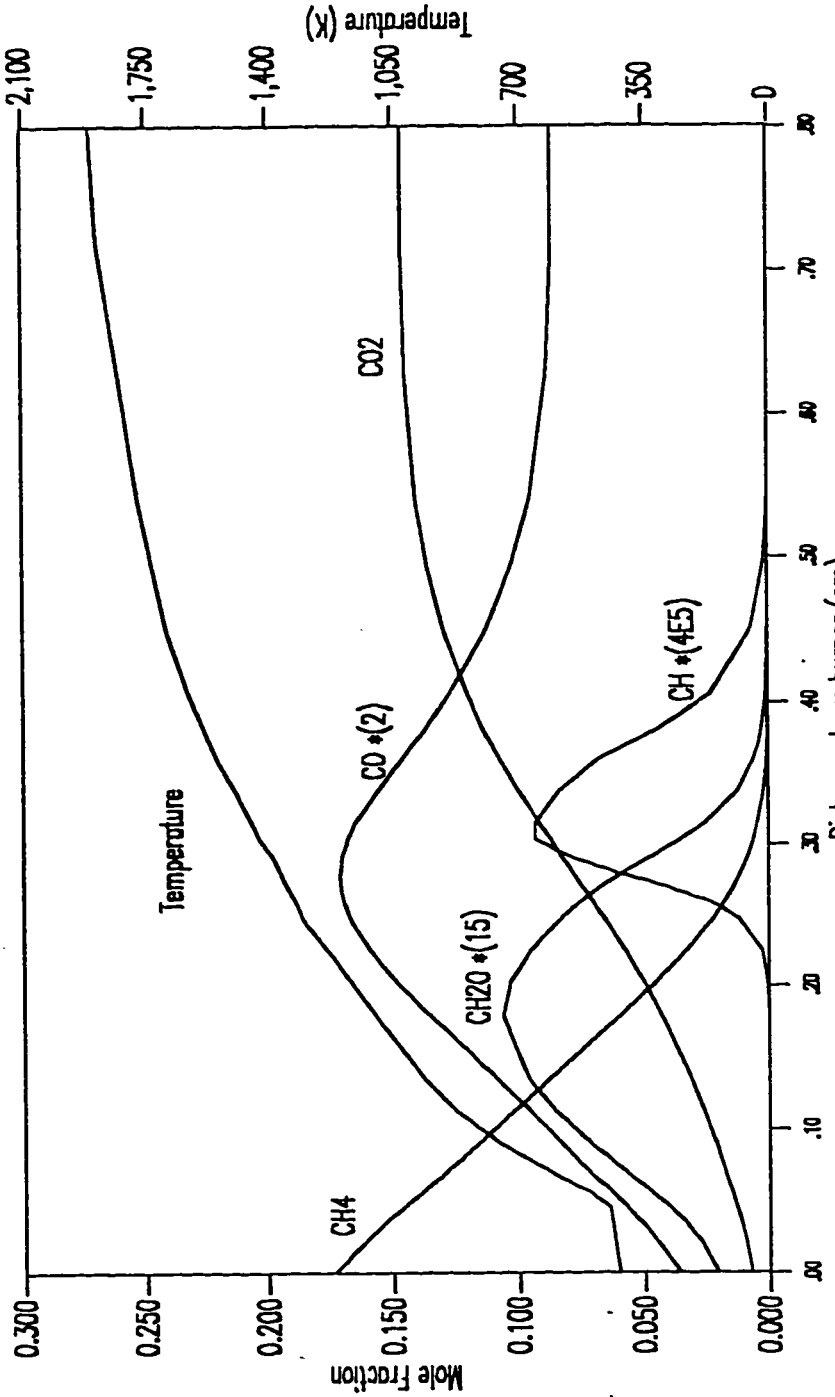

Figure 5.3a: Calculated Species Profiles for Flame 2 for CH4, CH, CO, CO2 and CH2O.

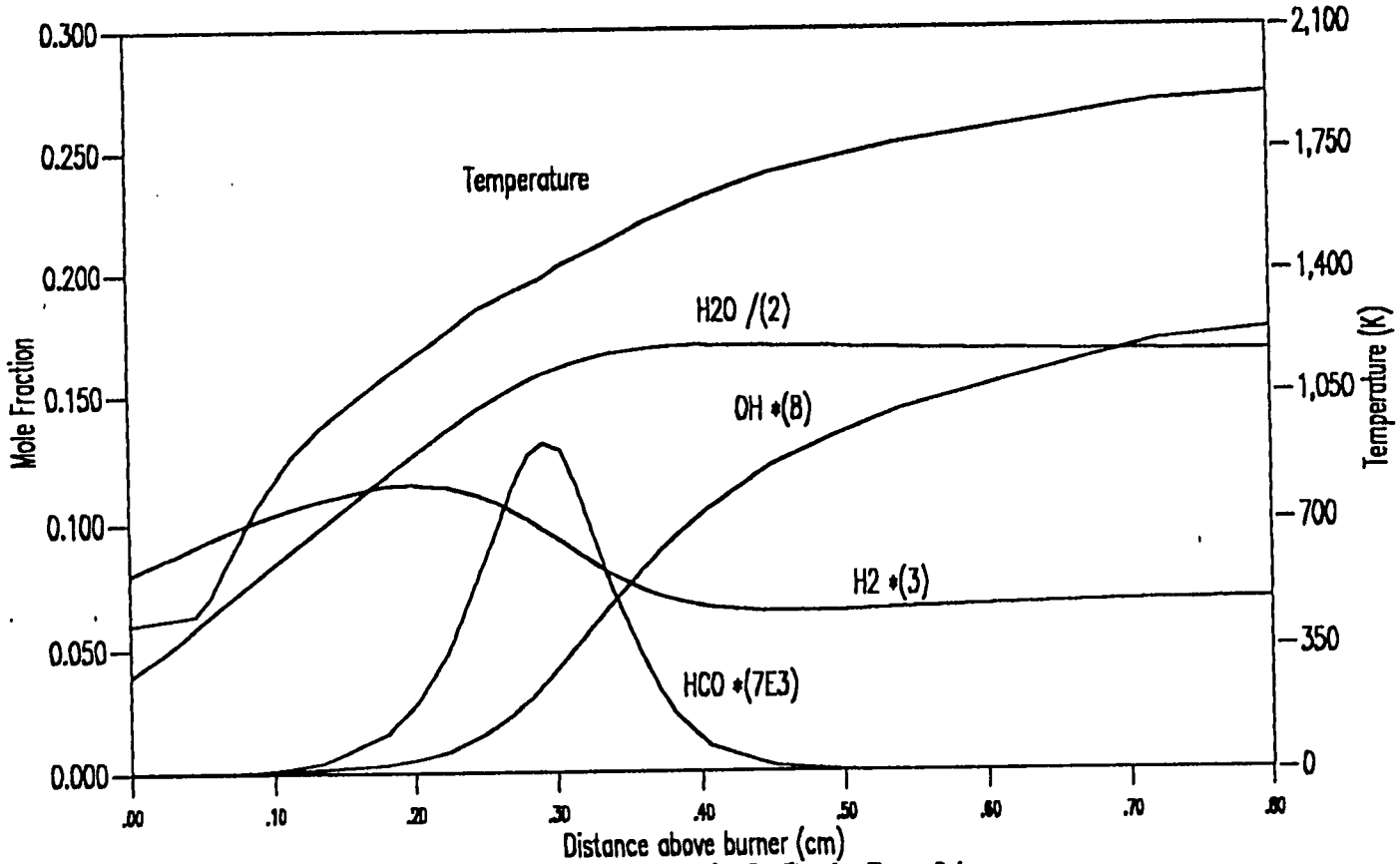

Figure 5.3b: Calculated Species Profiles for Flame 2 for H2, OH, H2O and HCO.

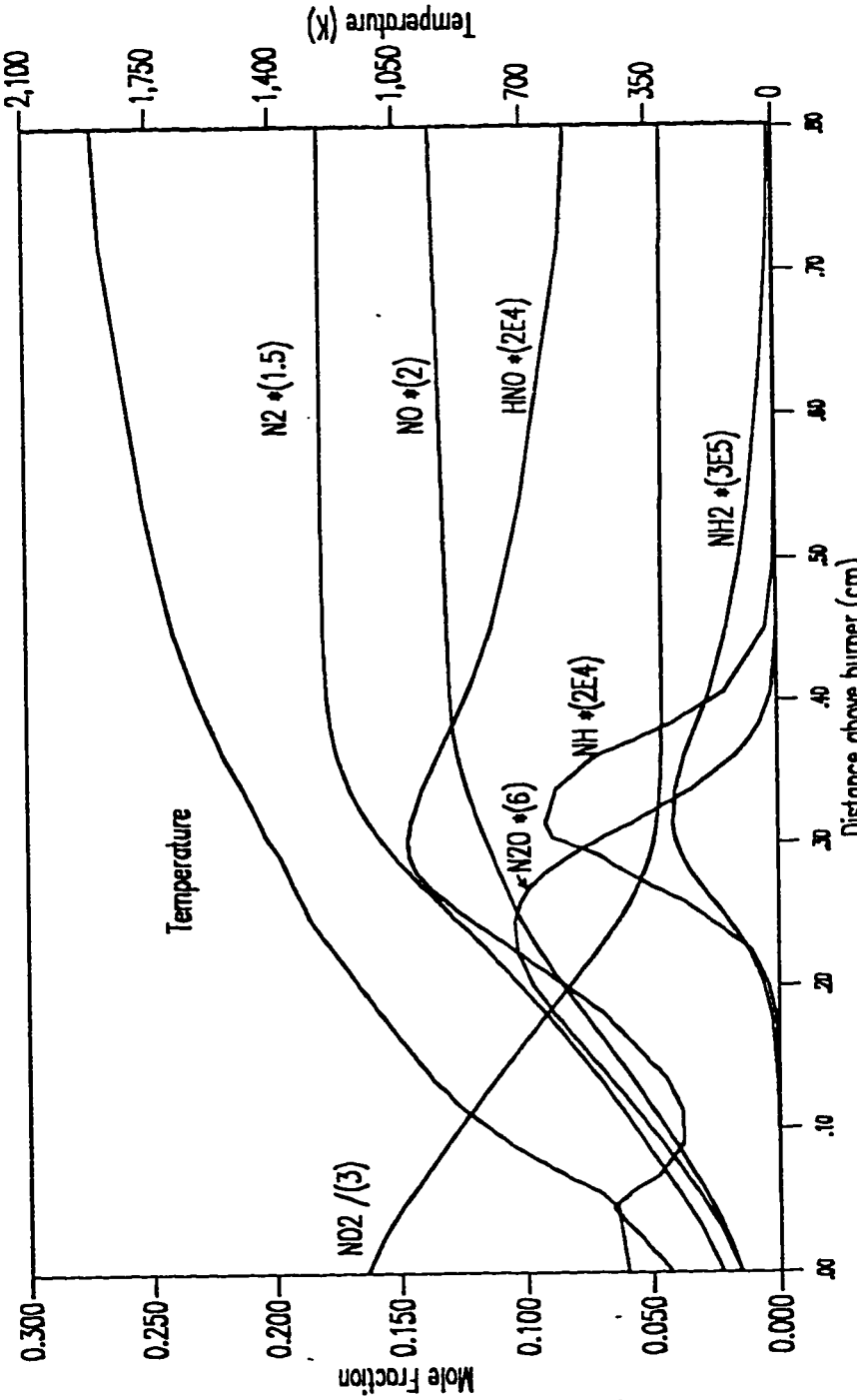

Figure 5.3c: Calculated Species Profiles for Flame 2 for N2, NO, NO2, N2O, HNO, NH and NH2.

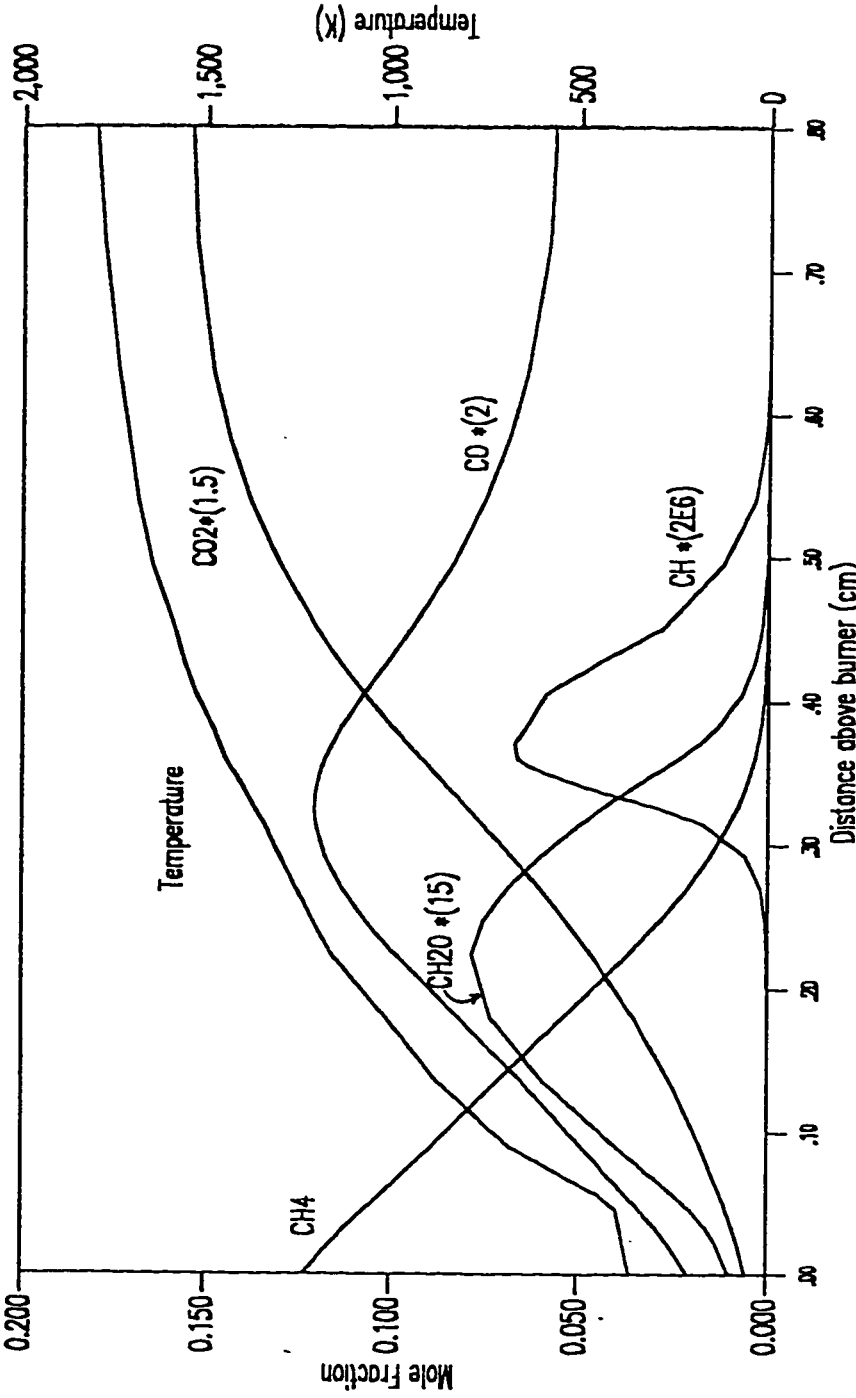

Figure 5.4a: Calculated Species Profiles for Flame 3 for CH4, CH, CO, CO2 and CH2O.

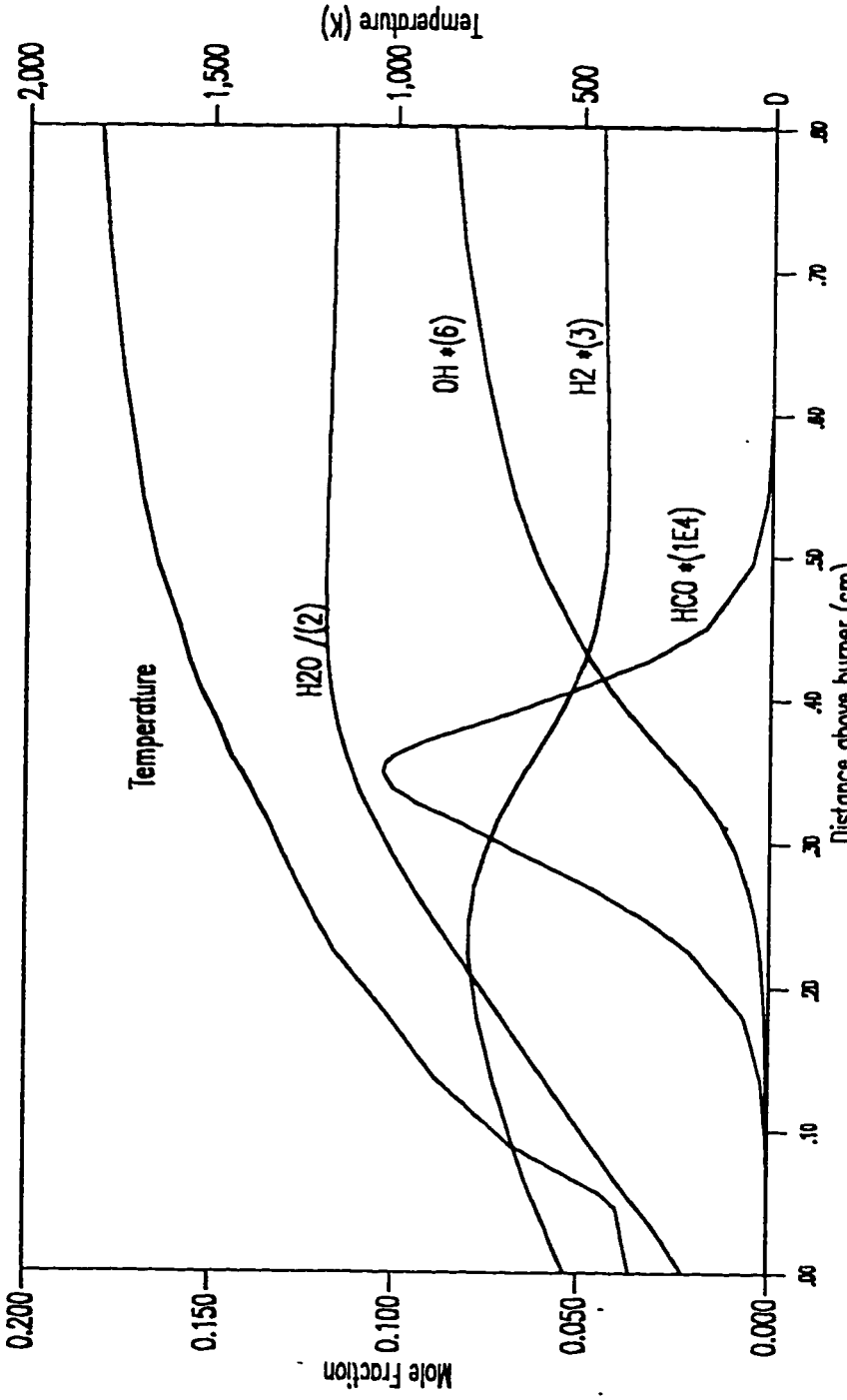

Figure 5.4b: Calculated Species Profiles for Flame 3 for H2, OH, H2O and HCO.

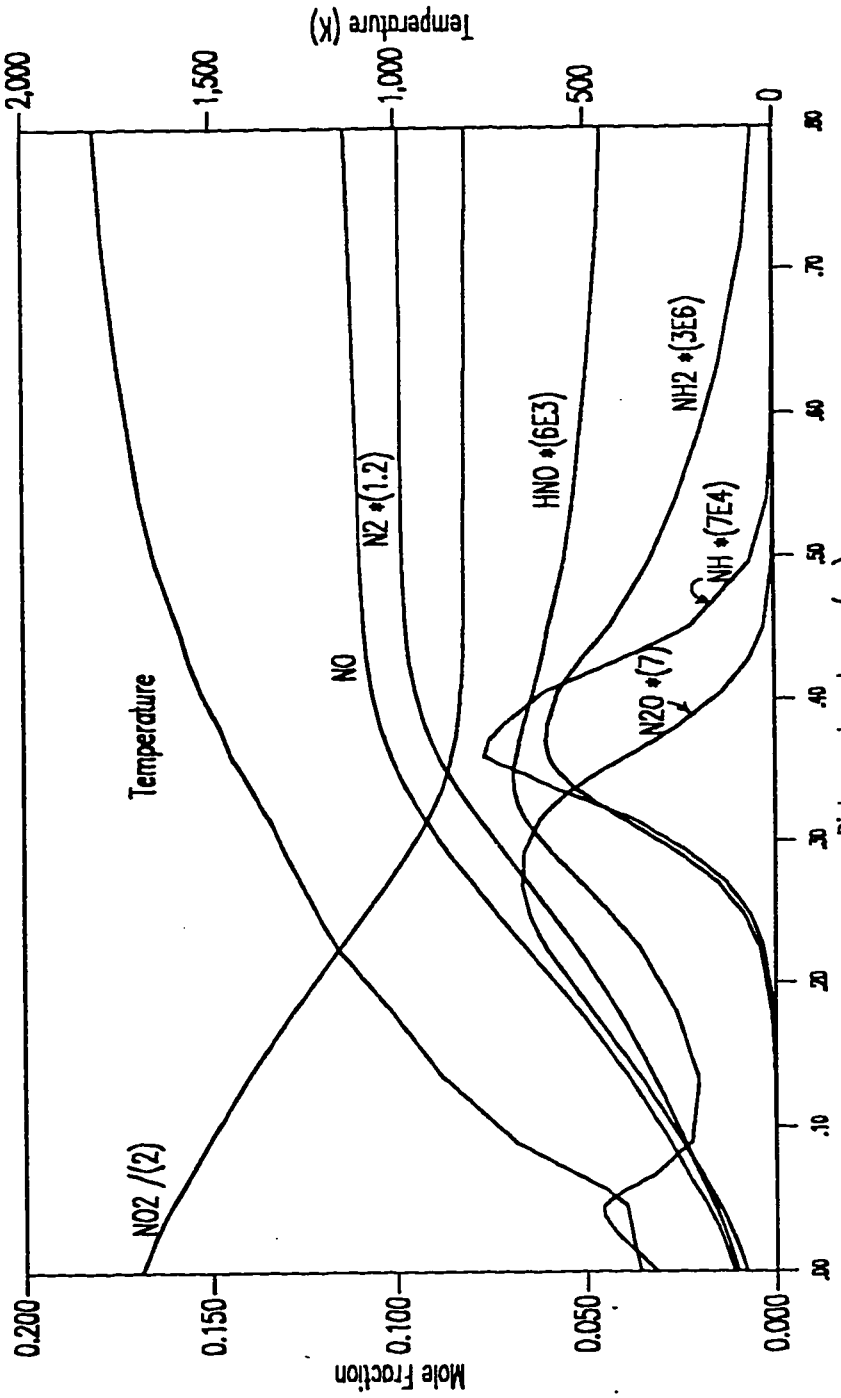

Figure 5.4c: Calculated Species Profiles for Flame 3 for N2, NO, NO2, N2O, HNO, NH and NH2.

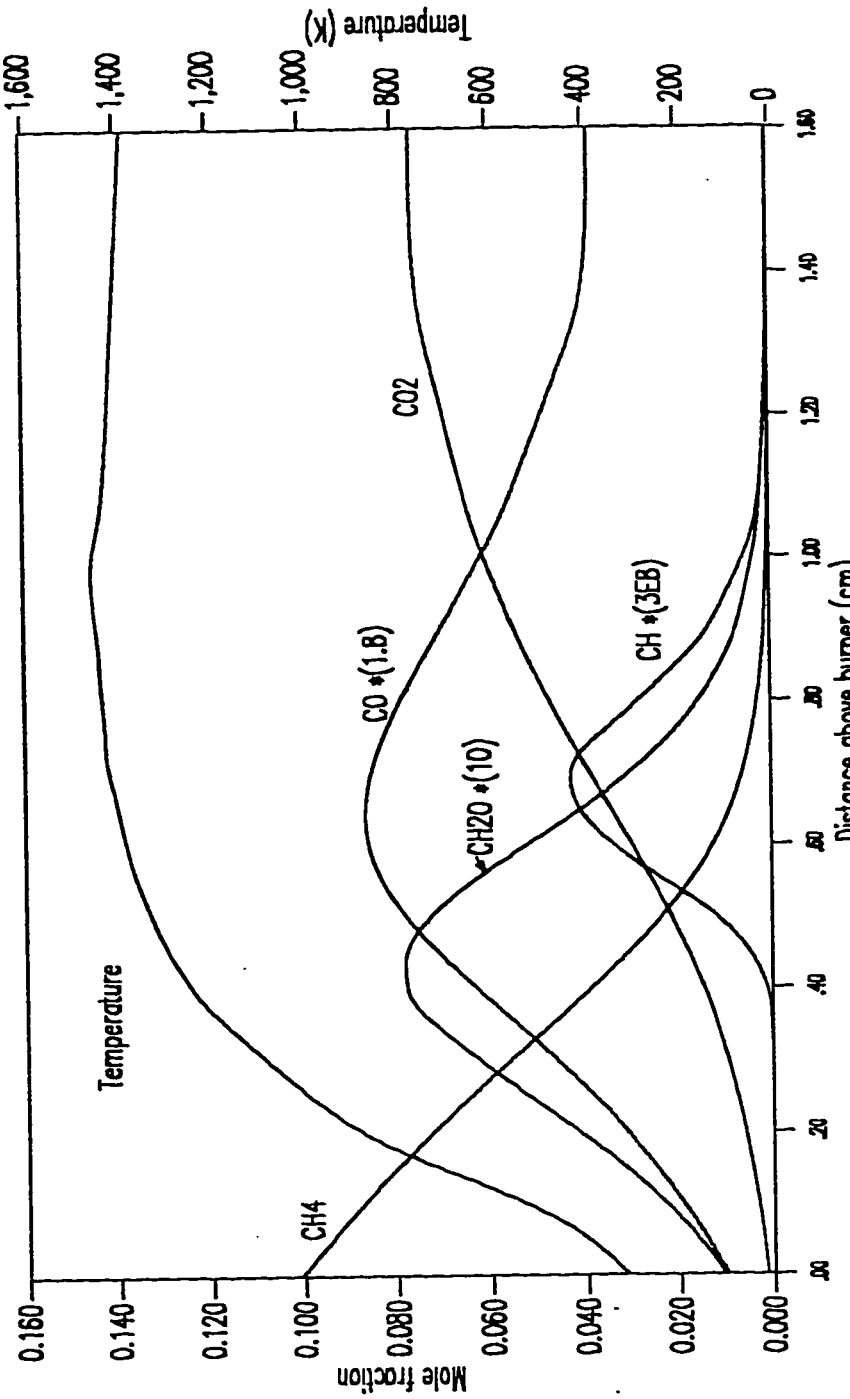

Figure 5.5a: Calculated Species Profiles for Flame 4 for CH4, CH, CO, CO2 and CH2O.

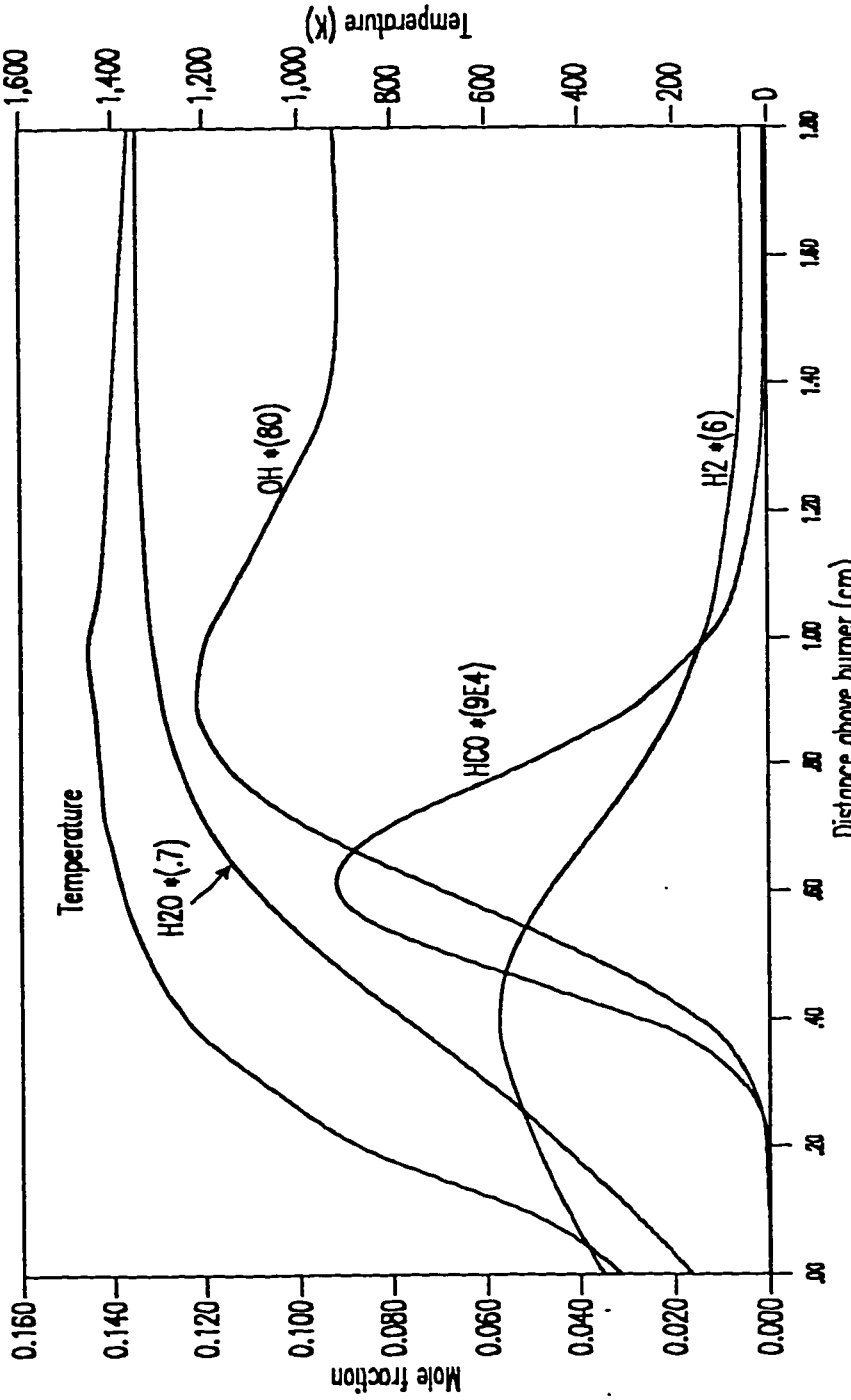

Figure 5.5b: Calculated Species Profiles for Flame 4 for H2, OH, H2O and HCO.

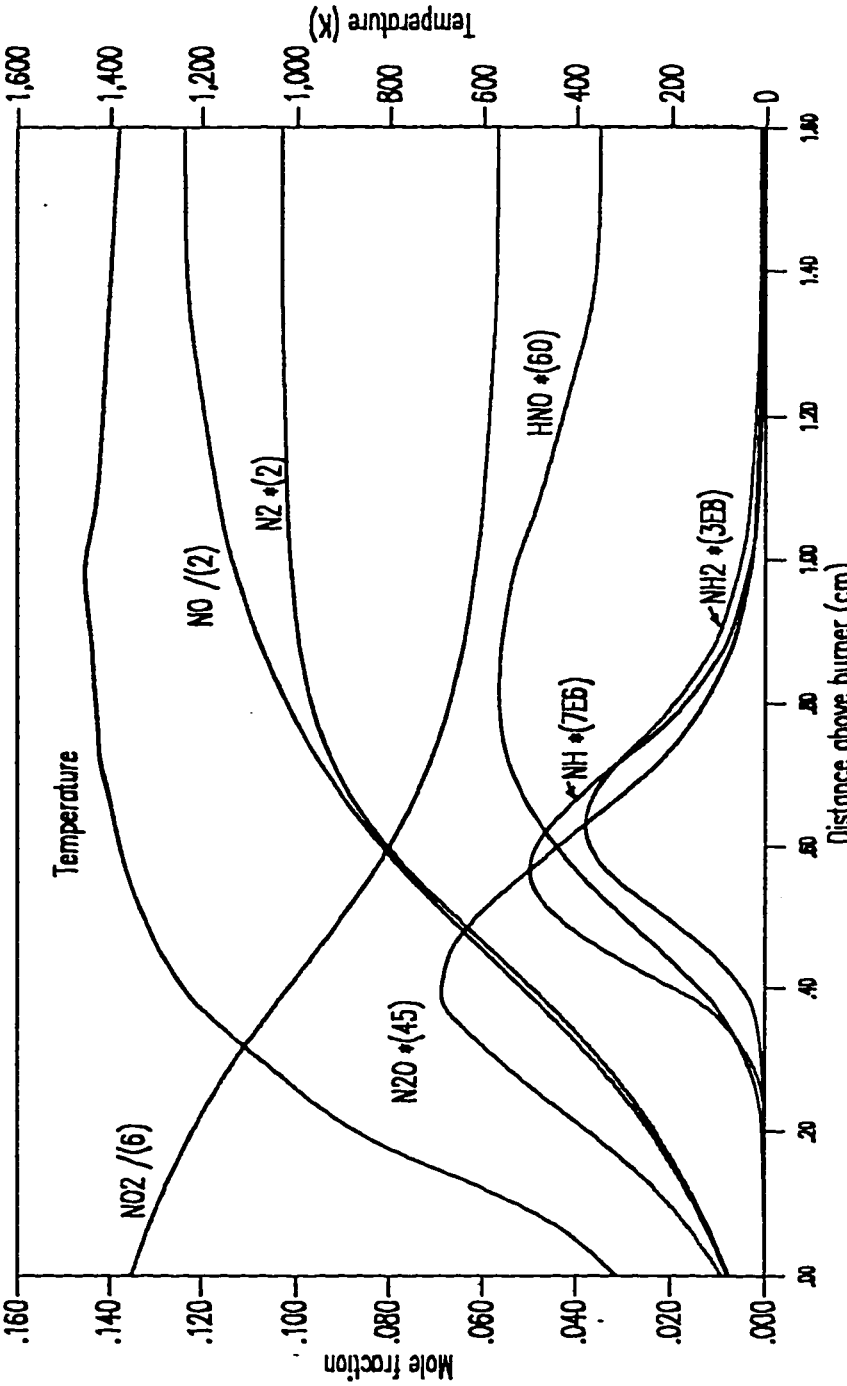

Figure 5.5c: Calculated Species Profiles for Flame 4 for N2, NO, NO2, N2O, HNO, NH and NH2.

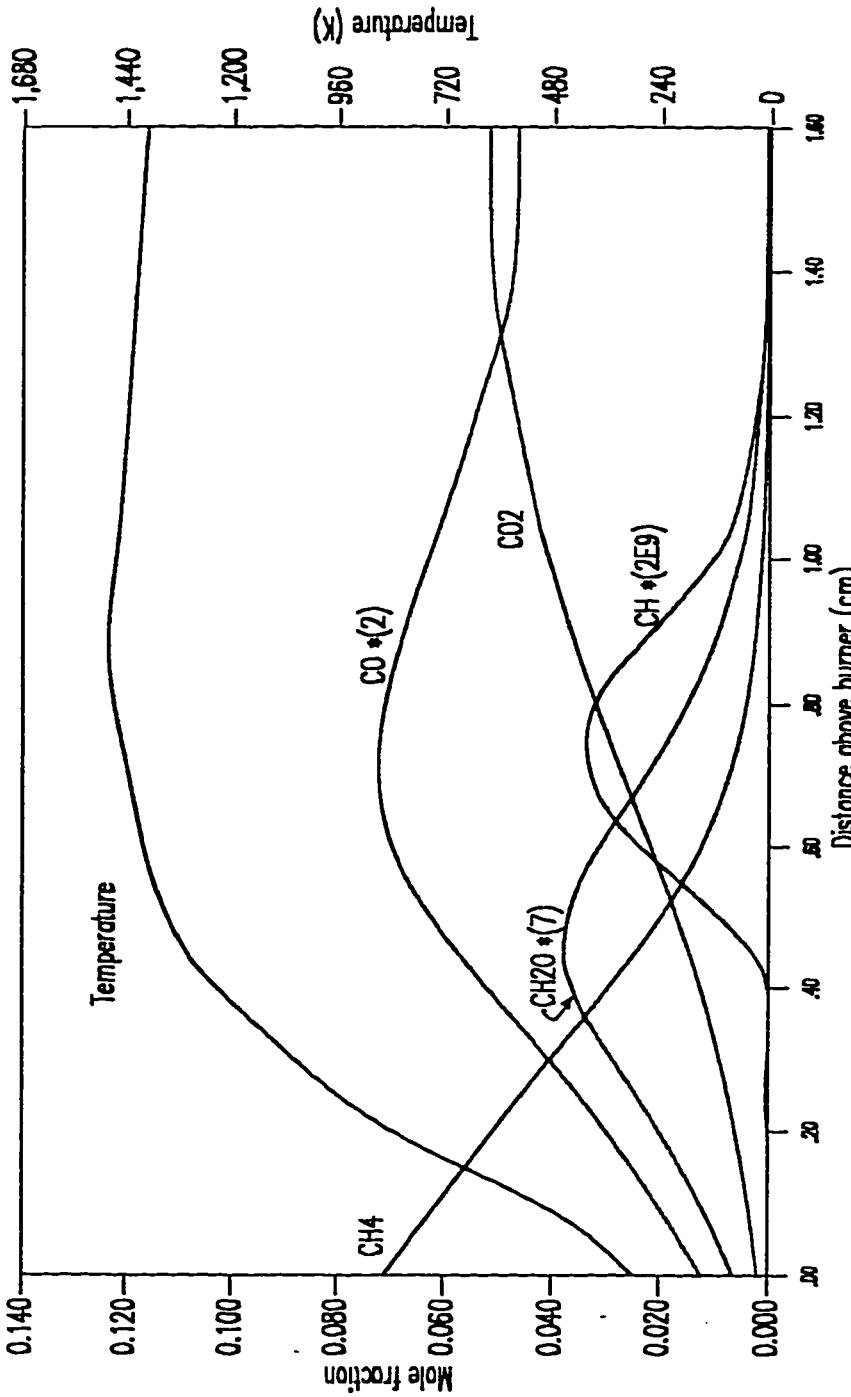

Figure 5.6a: Calculated Species Profiles for Flame 5 for CH4, CH, CO, CO2 and CH2O.

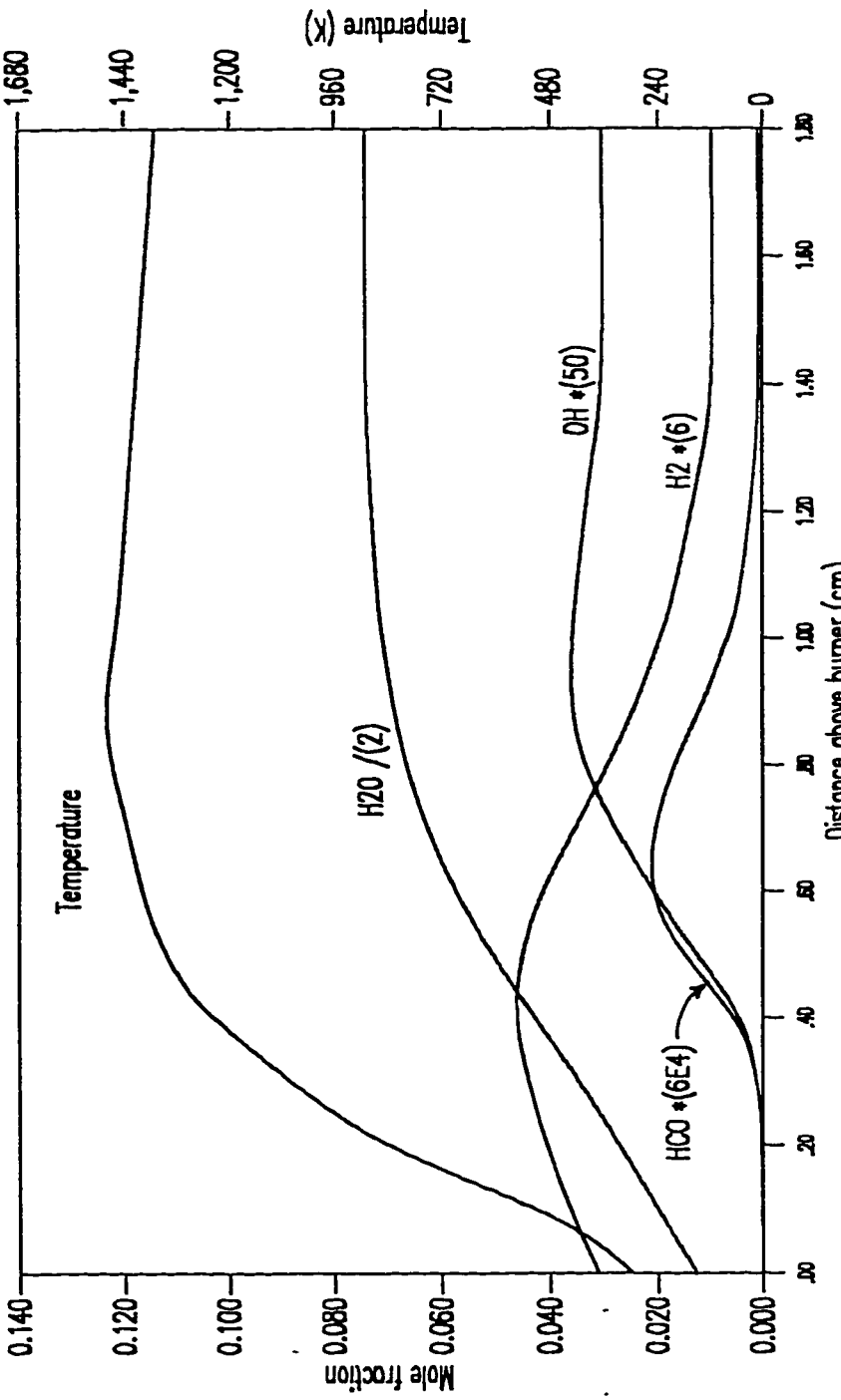

Figure 5.6b: Calculated Species Profiles for Flame 5 for H2, OH, H2O and HCO.

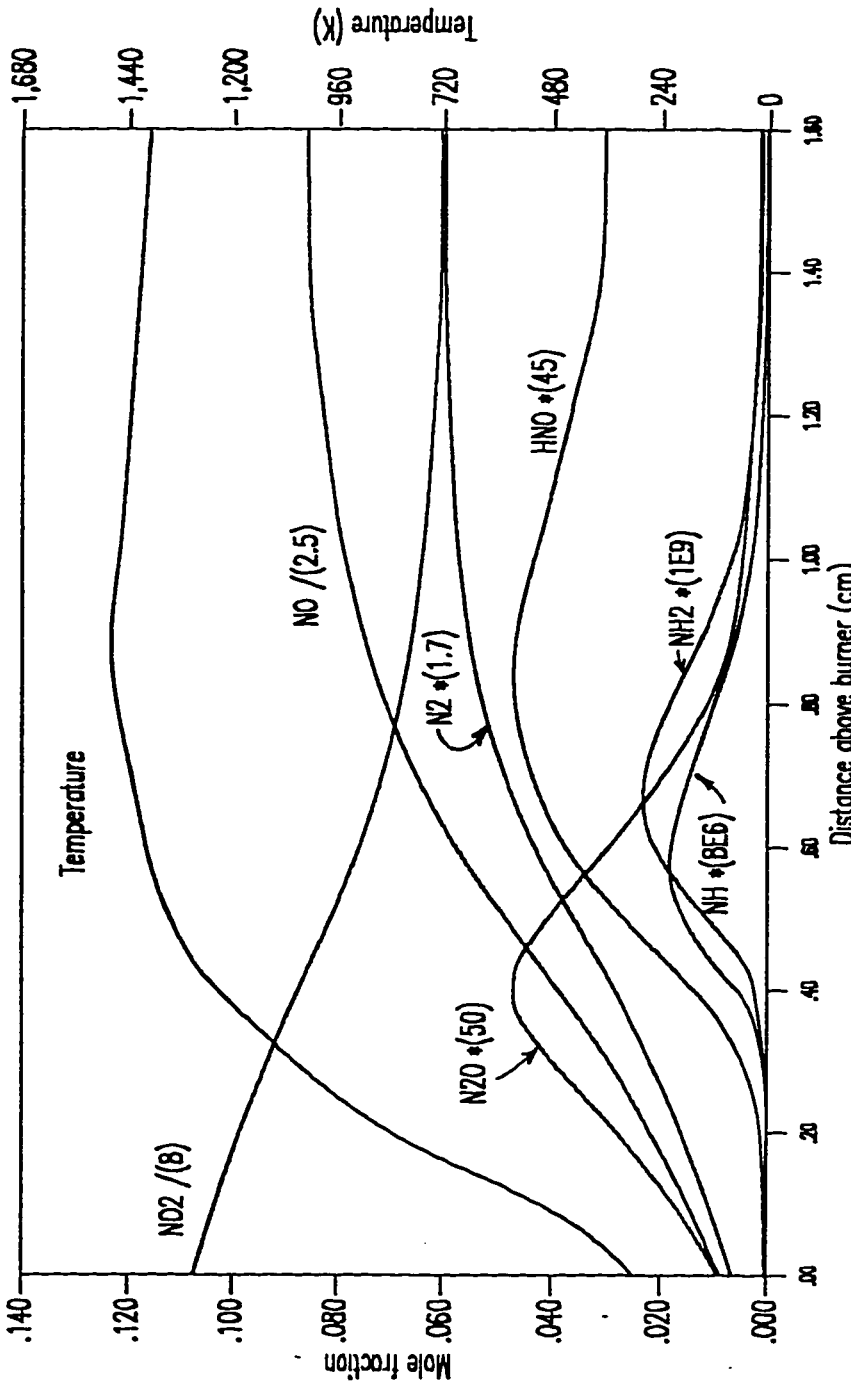

Figure 5.6c: Calculated Species Profiles for Flame 5 for N2, NO, NO2, N2O, HNO, NH and NH2.

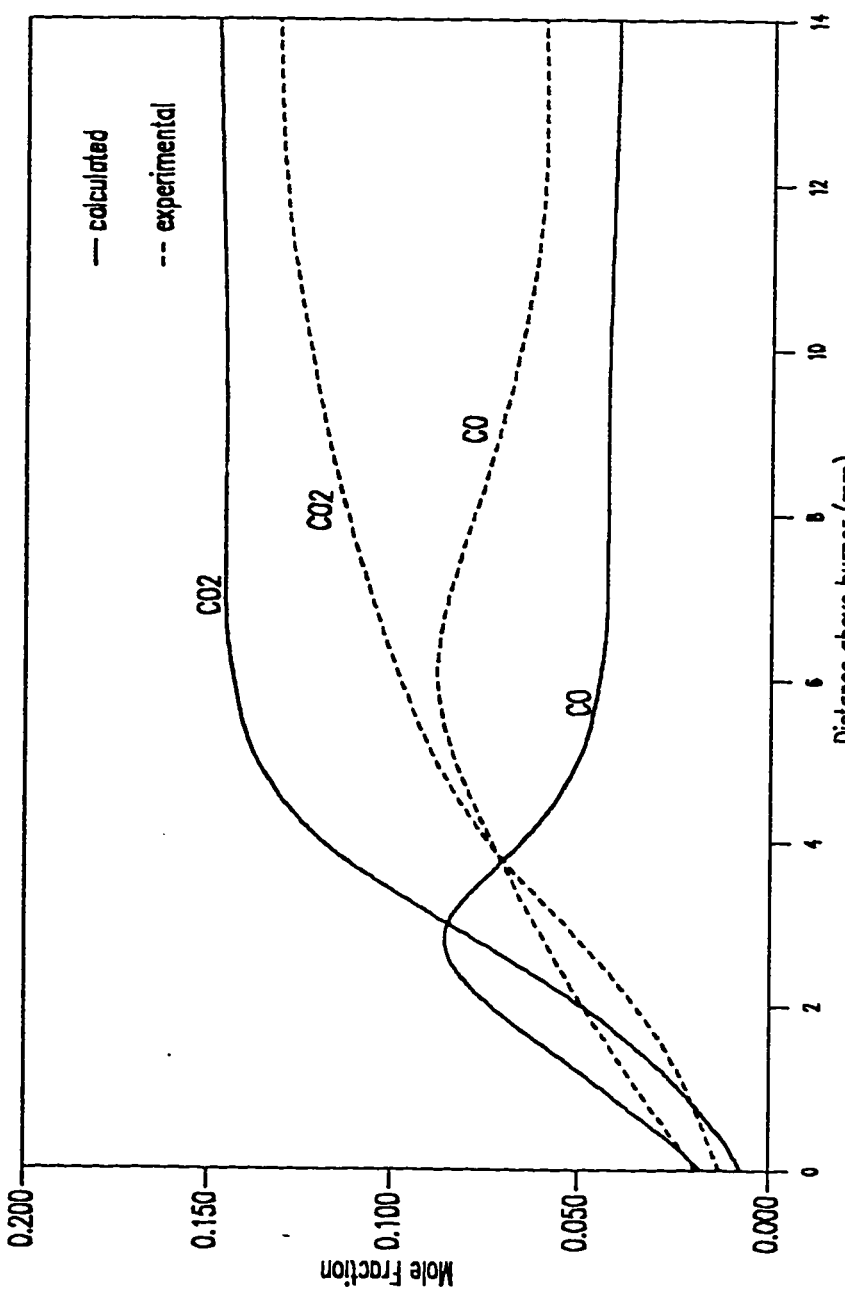

Figure 5.7a: Comparison of Calculated and Experimental Profiles for CO2 and CO for Flame 2

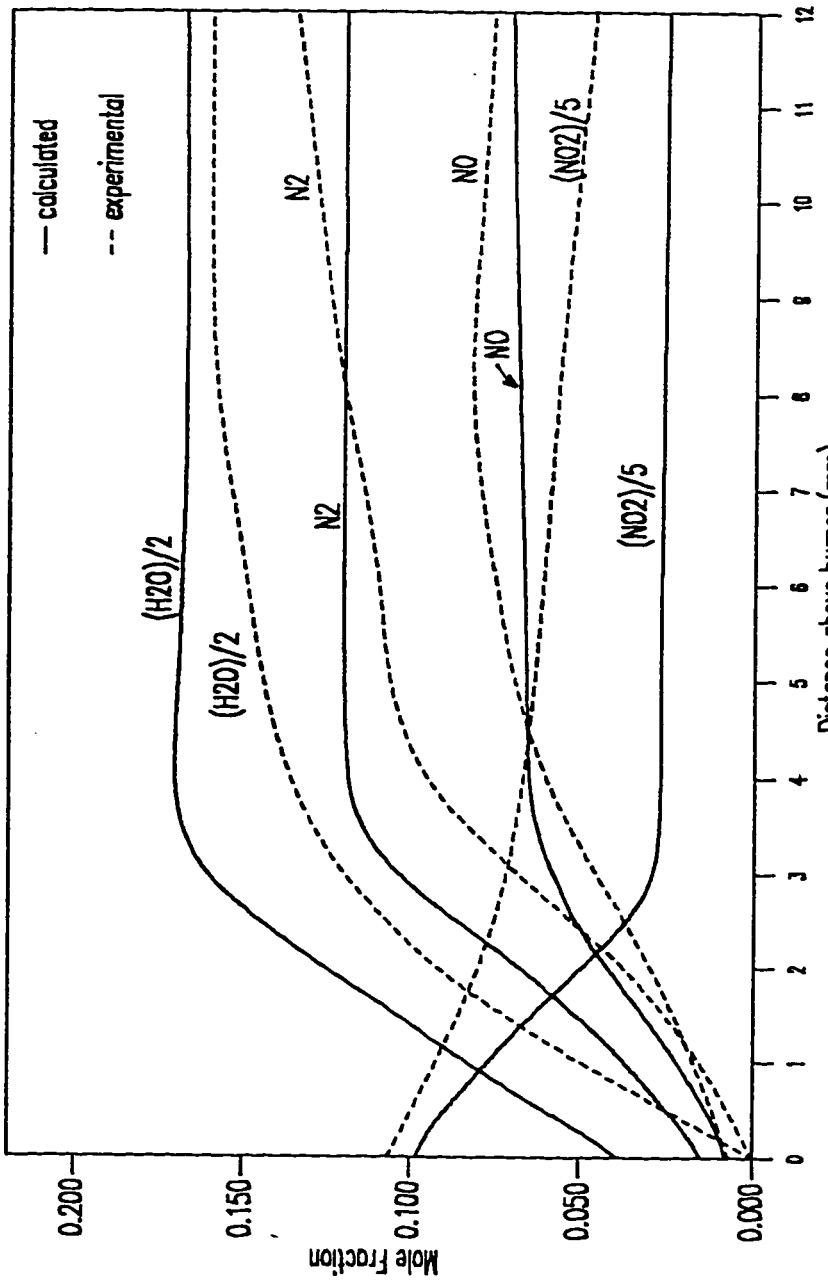

Figure 5.7b: Comparison of Calculated and Experimental Profiles for NO, N2, NO2 and H2O for Flame 2.

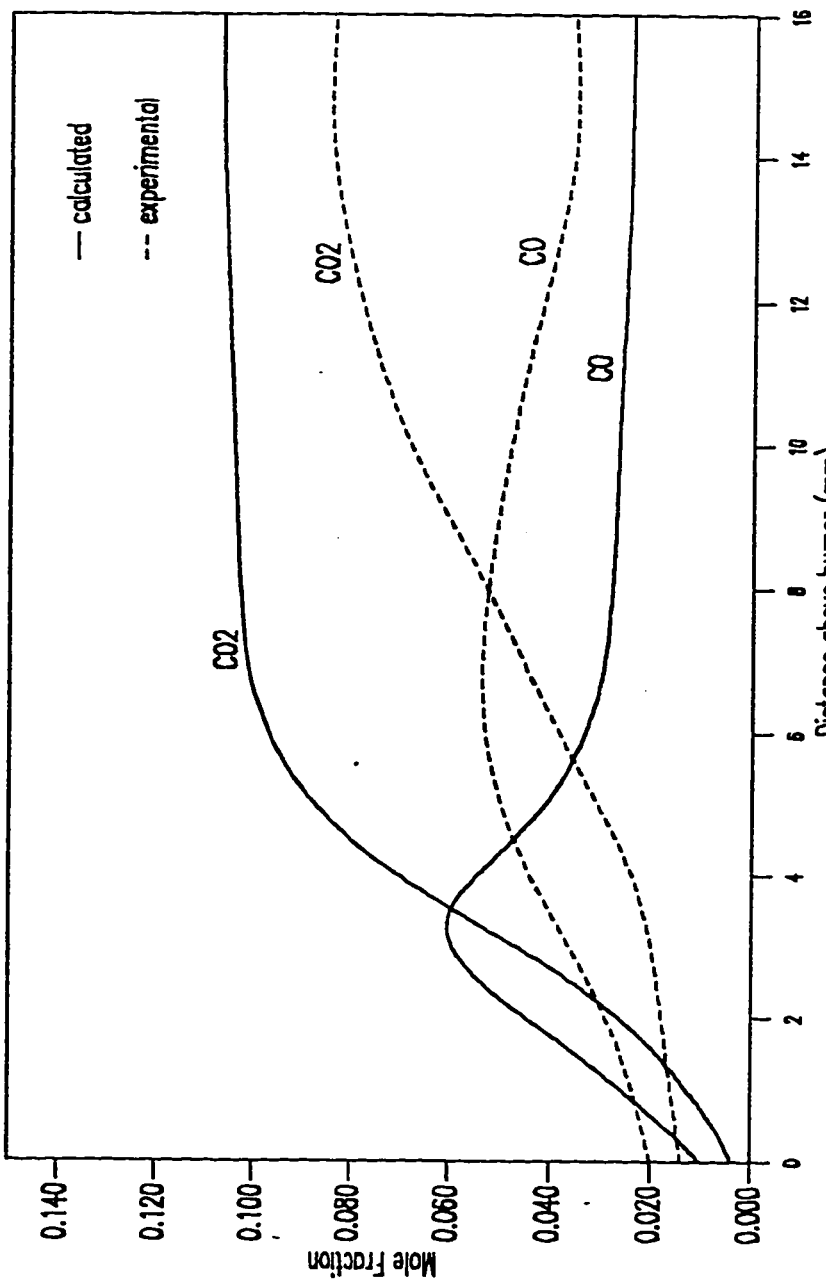

Figure 5.8a: Comparison of Calculated and Experimental Profiles of CO2 and CO for Flame 3

for CO_2 and CO for Flame 3. Here again it is observed that the predicted values for the mole fractions of CO_2 are higher and for CO lower than the corresponding experimental values. The sum of the concentrations of CO and CO_2 for both the experimental and calculated cases at any point in the flame is almost the same. This implies that the high temperature decomposition of CO_2 to CO is not as much as required to match with the experimentally observed profiles. This may be due to lower values for the reaction rates of CO_2 decomposition reactions.

Figure (5.8b) shows the comparison of calculated and experimental profiles for NO, N_2, NO_2, and H_2O for Flame 3. Once again excellent agreement between the calculated and experimental profiles of NO, N_2, and H_2O is observed, specially in the post flame region. The calculated values for NO_2 are underpredicted by the developed mechanism. The overall estimated accuracy of the experimentally determined absolute concentration profiles is $\pm$ 20% al 99% confidence [1]. The difference between the calculated and experimental NO_2 profiles therefore falls within the range of experimental accuracy.

The fuel disappears totally at the end of the luminous reaction zone. Figures (5.7b) and (5.8b) show a fast decomposition of NO_2 initially associated with a fast production of NO and N_2. Most of the CO is oxidized to CO_2 as the flames being studied are lean. High temperature decomposition of CO_2, however, is responsible for the CO that remains in the post flame region. The water concentration decreases as the equivalence ratio decreases.

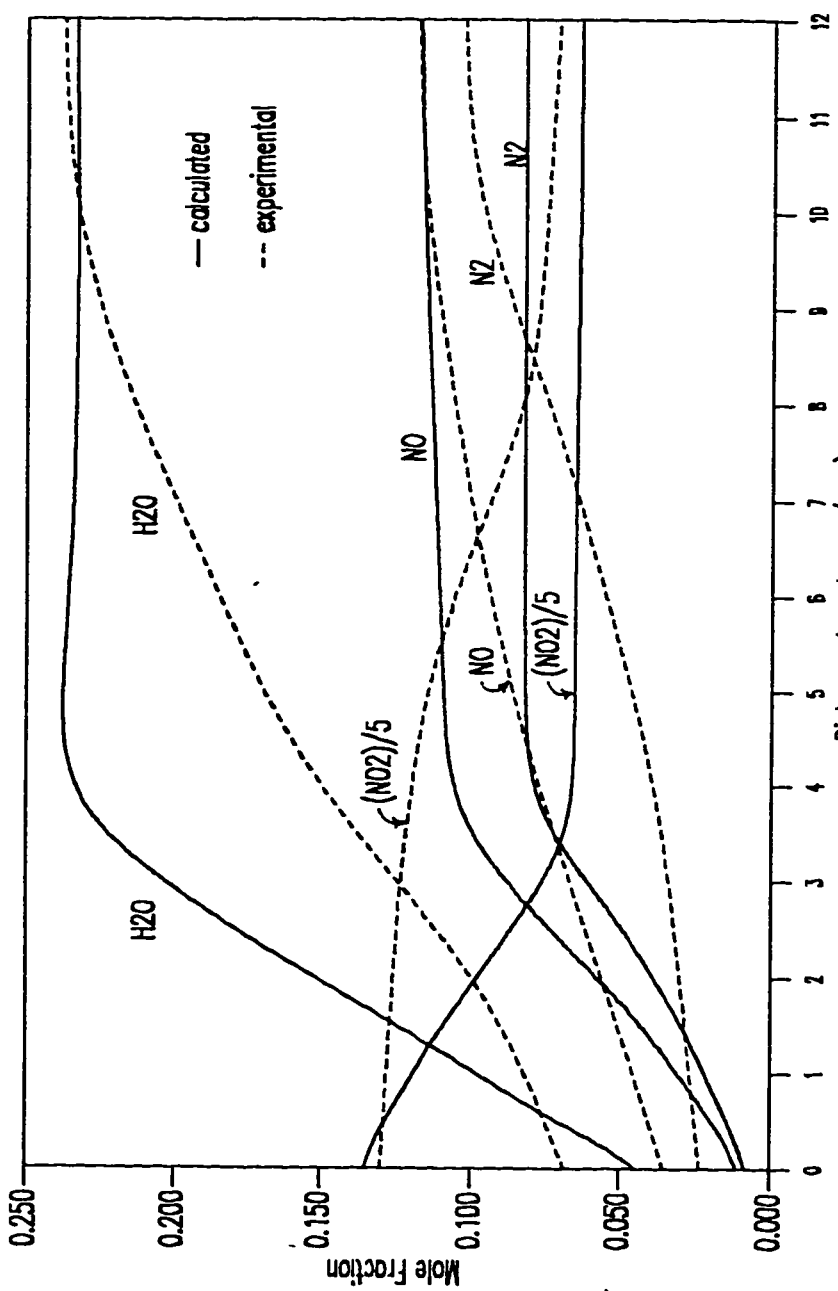

Figure 5.8b: Comparison of Calculated and Experimental Profiles of NO, N2, NO2 and H2O for Flame 3

5.6.2 Radical Species :

The concentration of radical species in the flames is very small and is therefore reported in parts per millions (ppm). Most of the radical species are "intermediate" species. These species produced in the reaction zone, reach their peak within the reaction zone, and are consumed in a very short interval before the post flame zone. The measurements of these species has been made possible only recently by virtue of the advances in technology and designing and assembling of highly sophisticated equipment by researchers. Farayedhi [1] measured the absolute concentration of the radicals CH, CN, and NH for the first time in $CH_4 / NO_2 / O_2$ and $CH_2O / NO_2 / O_2$ flames.

Due to the very low concentration of the radical species, in the order of 10 ppm, unavailability of accurate reaction rate data for reactions that generate and consume these radicals, and large number of reactions involved in the mechanism, it is very difficult to obtain precise quantitative agreement for the concentration profiles of these radicals by computer modelling.

Figure (5.9) shows the comparison of calculated and experimental profiles for CH radical for Flame 2. The predicted profile shows rapid formation and consumption of CH which indicate that the reactions responsible for the consumption of CH in the developed reaction mechanism have high reaction rates.

Figures (5.10) and (5.11) shows the comparison of calculated and experimental profiles for CN and NH radicals respectively for Flame 2. The overall shape of the profiles of both these species is the same. However, these

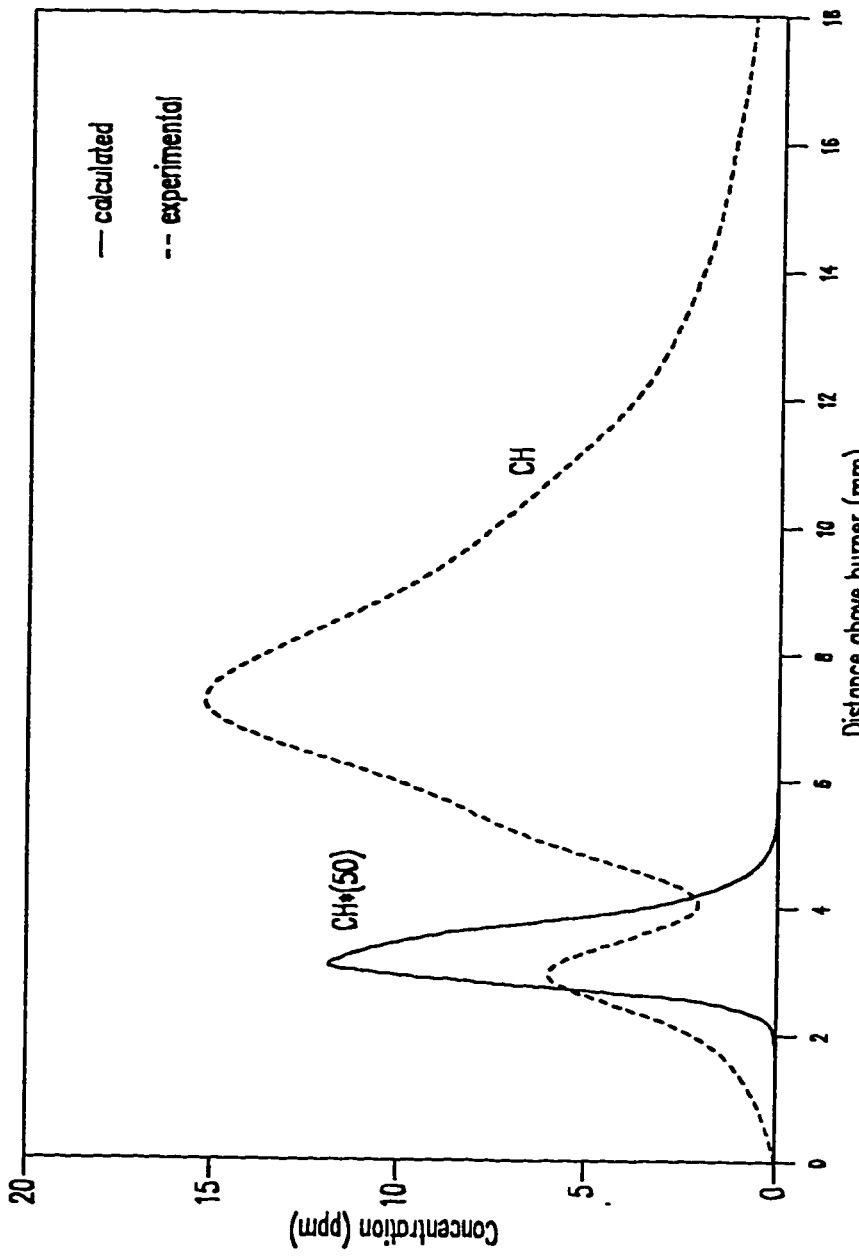

Figure 5.9 : Comparison of Calculated and Experimental Profiles for CH Radical for Flame 2

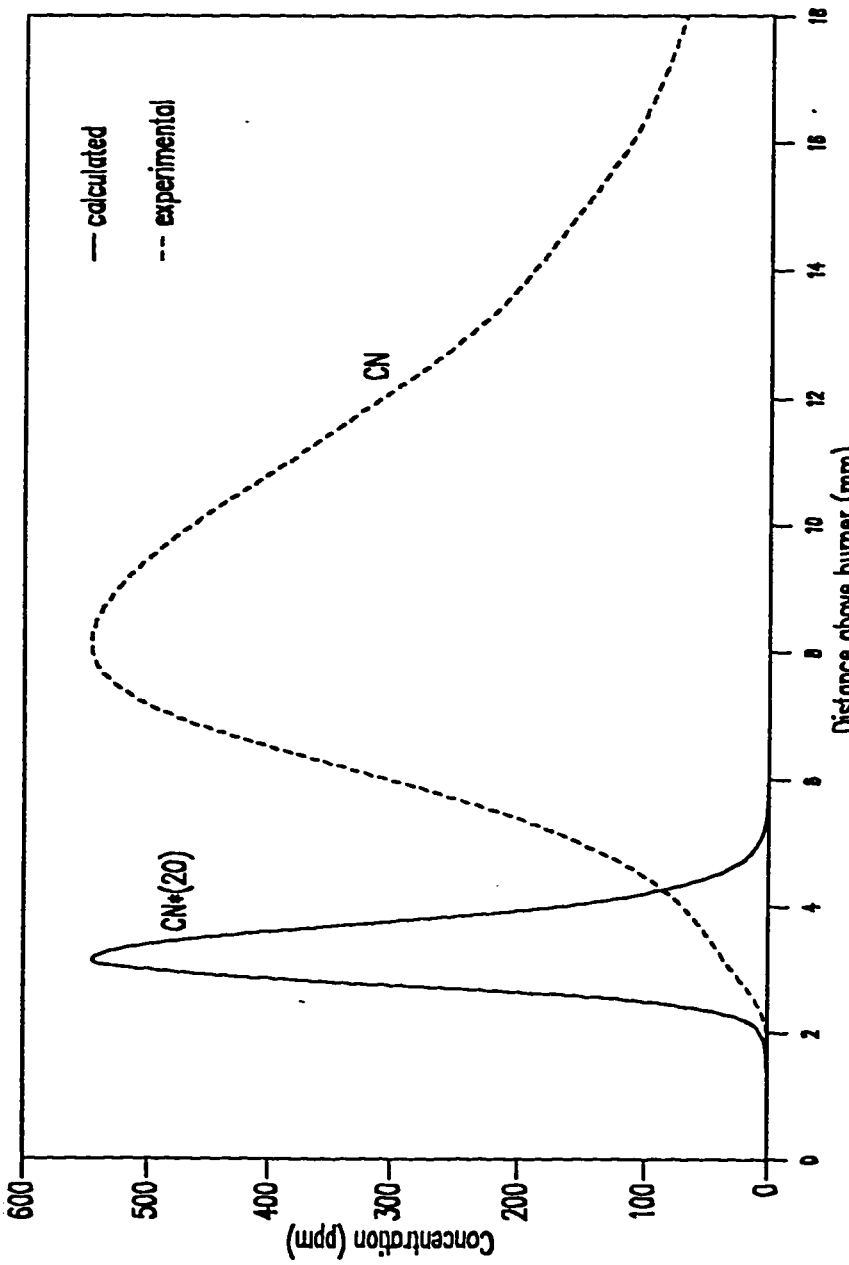

Figure 5.10: Comparison of Calculated and Experimental Profiles for CN Radical for Flame 2

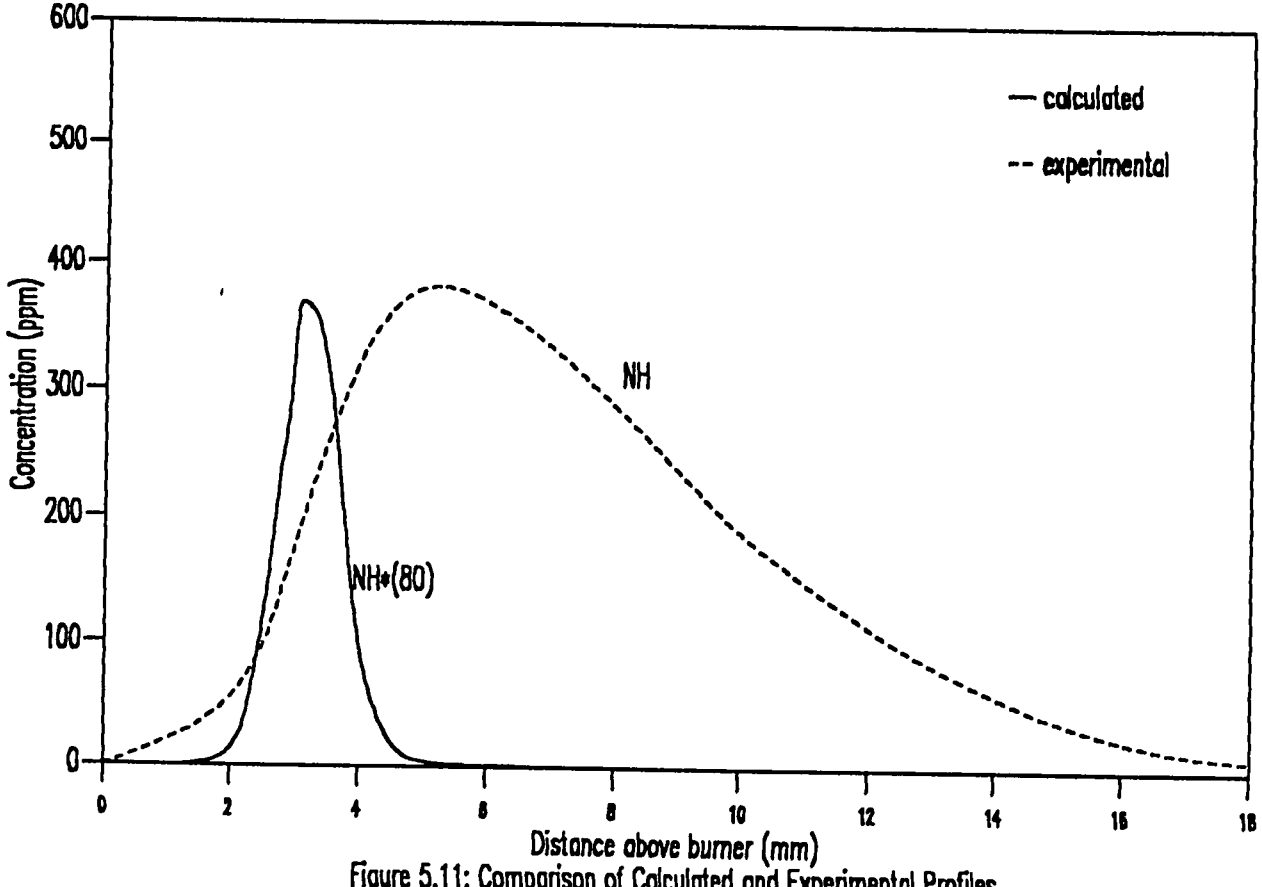

Figure 5.11: Comparison of Calculated and Experimental Profiles for NH Radical for Flame 2

radicals appear to be consumed much nearer in the flame compared with the experimental profiles.

Figures (5.12) and (5.13) shows the comparison of relative calculated and experimental profiles for NH_2 and OH radicals respectively for Flame 2. The qualitative agreement between the calculated and experimental profiles of these species is quite good.

The differences between the calculated and experimental profiles, if and when they occur, may have arisen due to the values used for the rate constants in the Arrhenius equation, the simplifying assumptions incorporated in the governing equations, the absence of some important reactions in the developed chemical kinetic mechanism, the errors associated with experimental calculations, and so on. In view of the many uncertainties in chemical kinetic data and highly nonlinear character of the equations, exact agreement is seldom, if ever, achieved in such a complex system.

5.7 The Effect of Equivalence Ratio :

Equivalence ratio is defined as the actual fuel/air ratio divided by the stoichiometric fuel/air. Figure (5.14) compares the model predictions of the mole fractions of CO and CO_2 in the post flame region at various equivalence ratios with experimental data. Both the calculated and experimental values increase with an increase in the equivalence ratio. Therefore the model predictions follow the experimentally observed trend for this case.

Figure (5.15) shows the comparison between experimental and calculated N_2

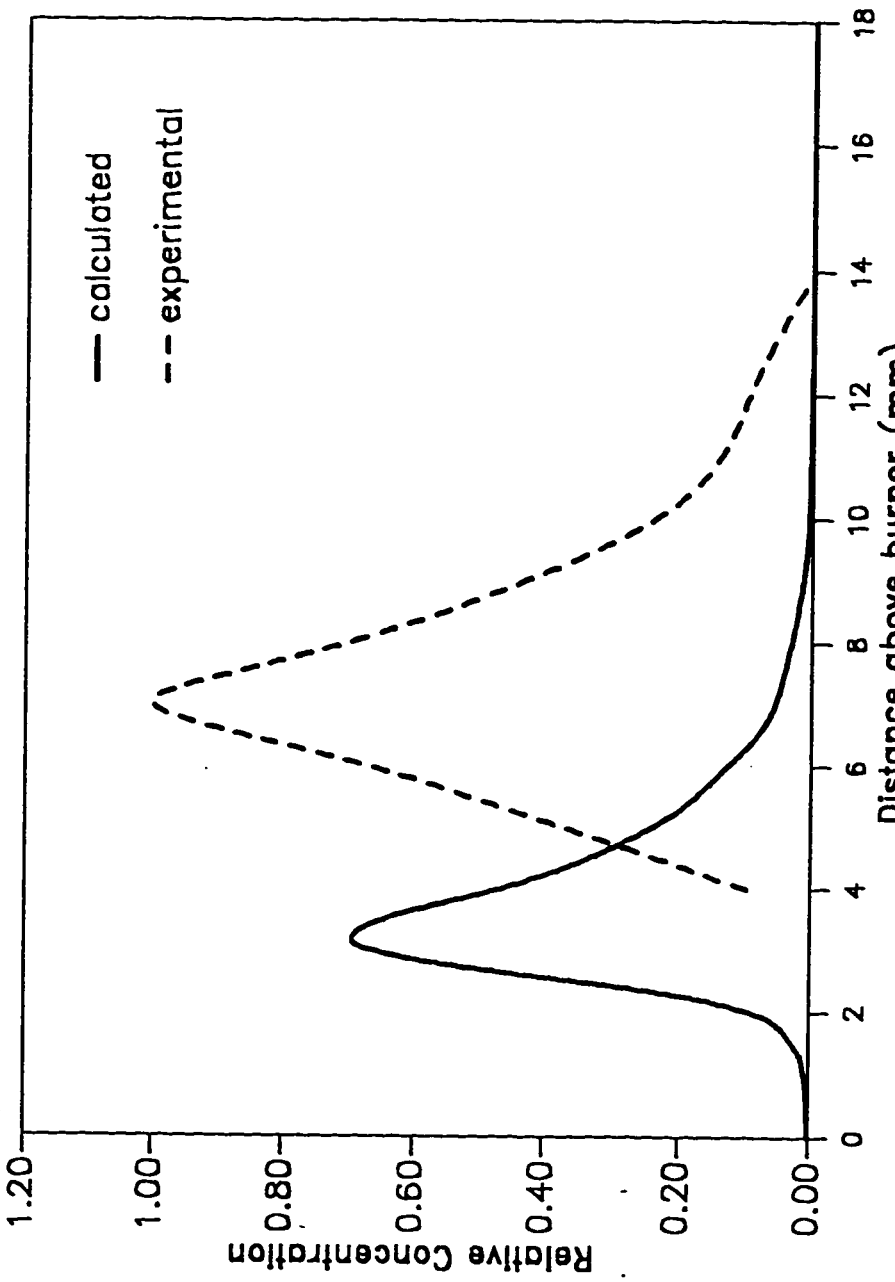

Figure 5.12: Comparison of Relative Calculated and Experimental Profiles for NH Radical for Flame 2.

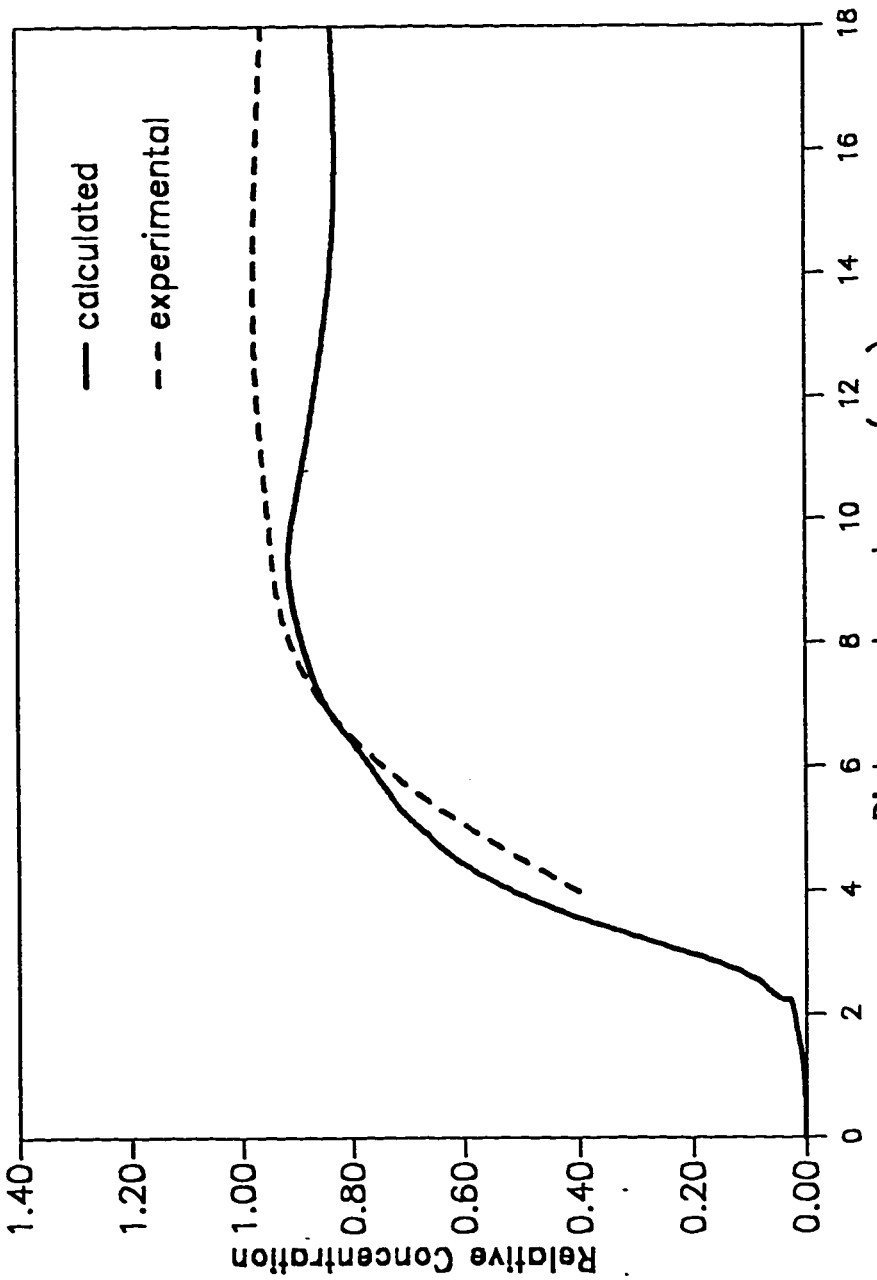

Figure 5.13: Comparison of Relative Calculated and Experimental Profiles for OH for Flame 2.

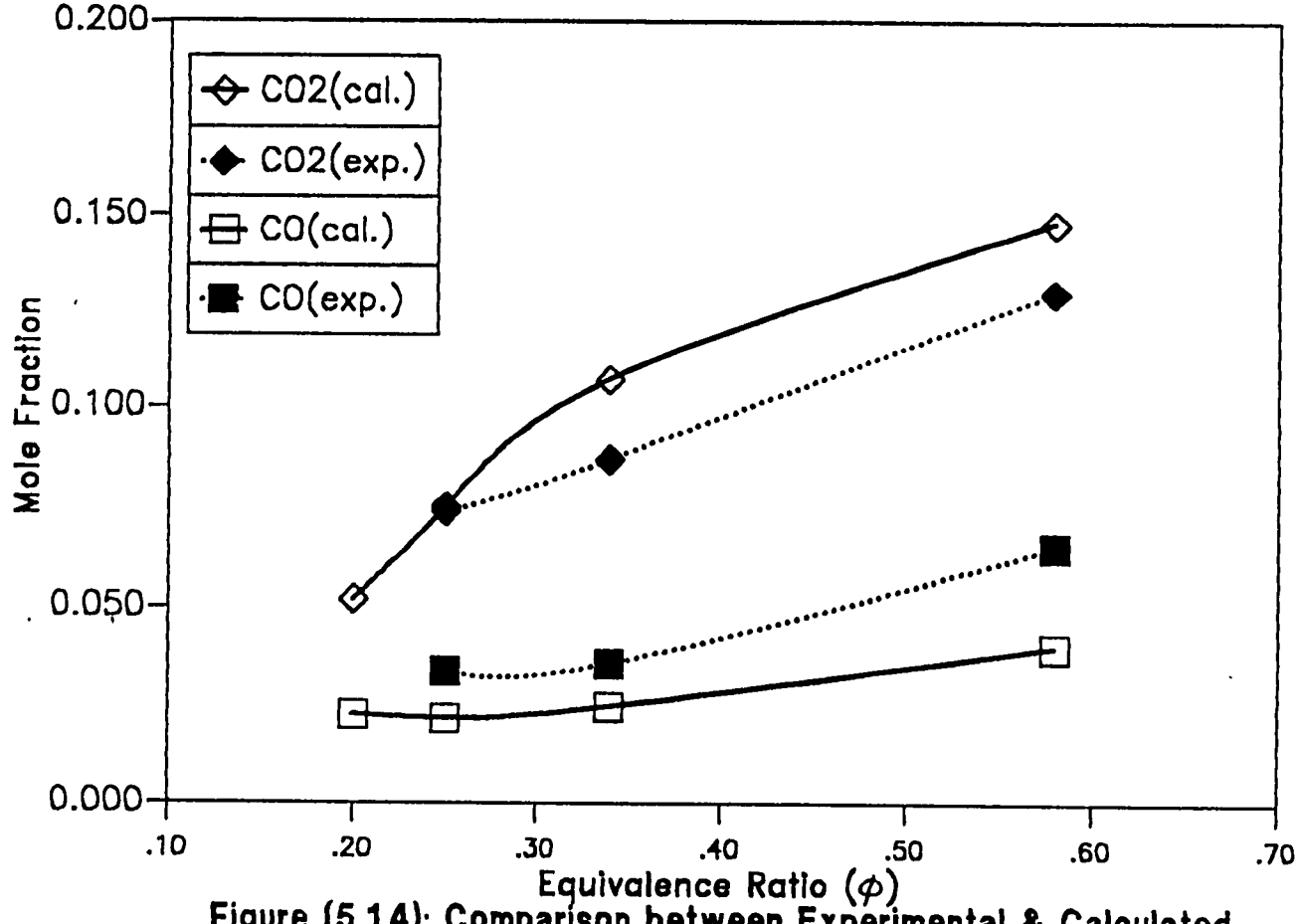

Figure (5.14): Comparison between Experimental & Calculated CO and CO2 mole fractions versus equivalence ratio.

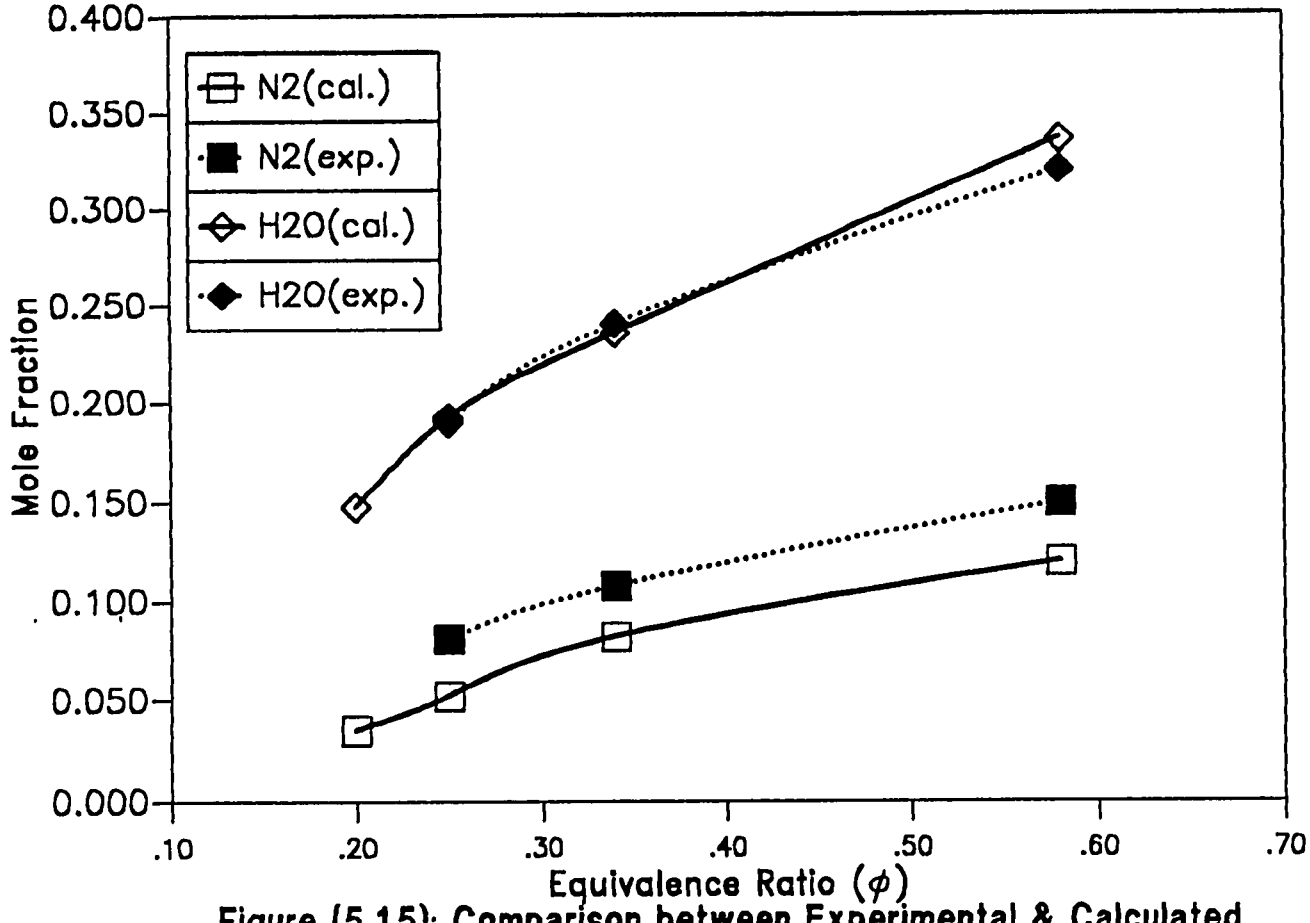

Figure (5.15): Comparison between Experimental & Calculated N2 and H2O mole fractions versus equivalence ratio.

and H_2O mole fractions versus equivalence ratio in the post flame region. This figure shows that the concentration of these species in the post flame region increases with an increase in the equivalence ratio both for the experimental and calculated cases. Therefore the model predictions follow the experimentally observed trend for this case.

Figure (5.16) shows the comparison between experimental and calculated NO and NO_2 mole fractions versus equivalence ratio in the post flame region. This figure shows that the concentration of these species in the post flame region decreases with an increase in the equivalence ratio both for the experimental and calculated cases. Therefore the model predictions follow the experimentally observed trend for this case as well.

Figure (5.17) shows the comparison between peak relative experimental and calculated OH concentrations versus equivalence ratio. This figure shows that the relative peak concentration of OH increases with an increase in the equivalence ratio both for the experimental and calculated cases. Therefore the model predictions of relative concentration profiles are in good qualitative agreement with the experimental profiles.

Figure (5.18) shows the comparison between peak relative experimental and calculated NH_2 concentrations versus equivalence ratio. This figure shows that the relative peak concentration of NH_2 increases with an increase in the equivalence ratio both for the experimental and calculated cases. Therefore, for NH_2, the model predictions of relative concentration profiles are in good qualitative agreement with the experimental profiles.

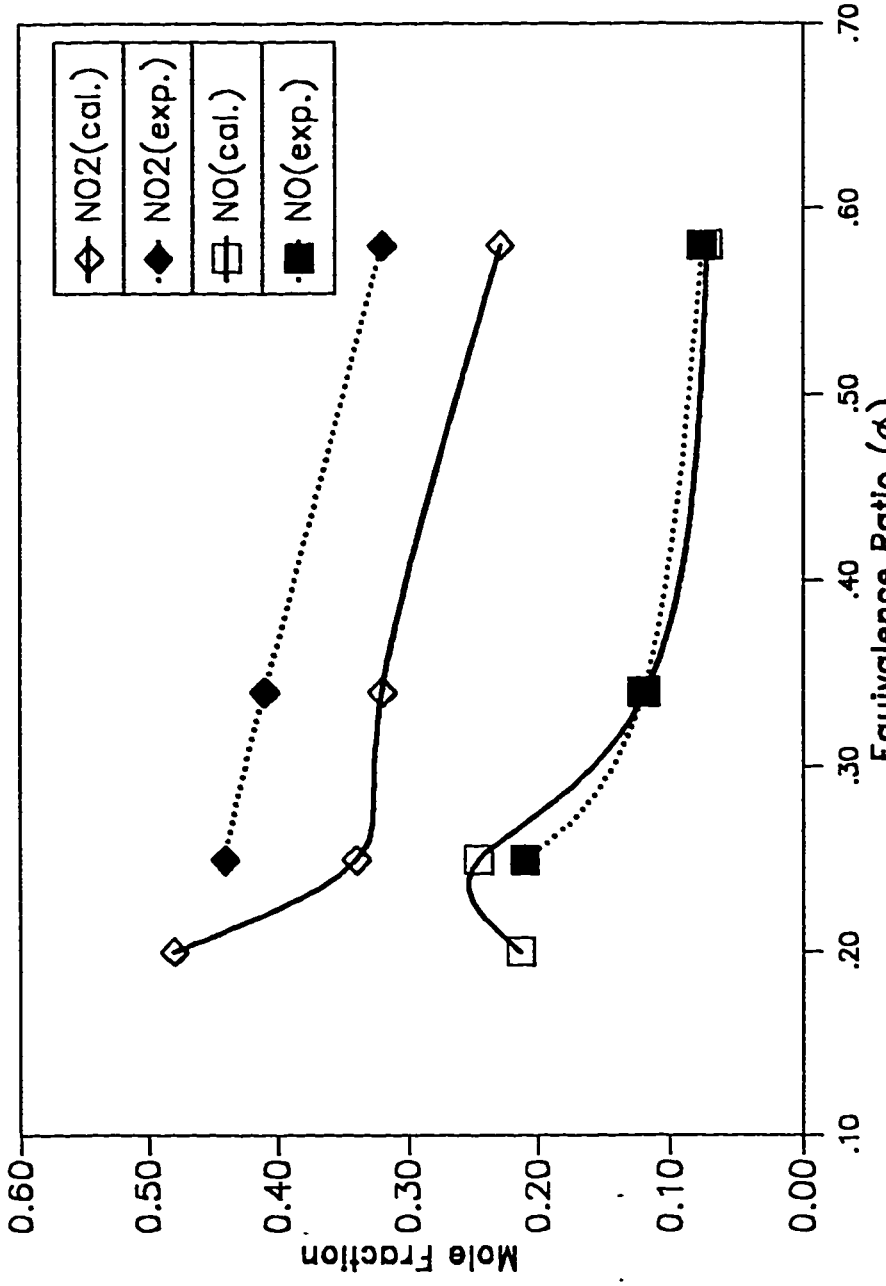

Figure (5.16): Comparison between Experimental & Calculated NO and NO2 mole fractions versus equivalence ratio.

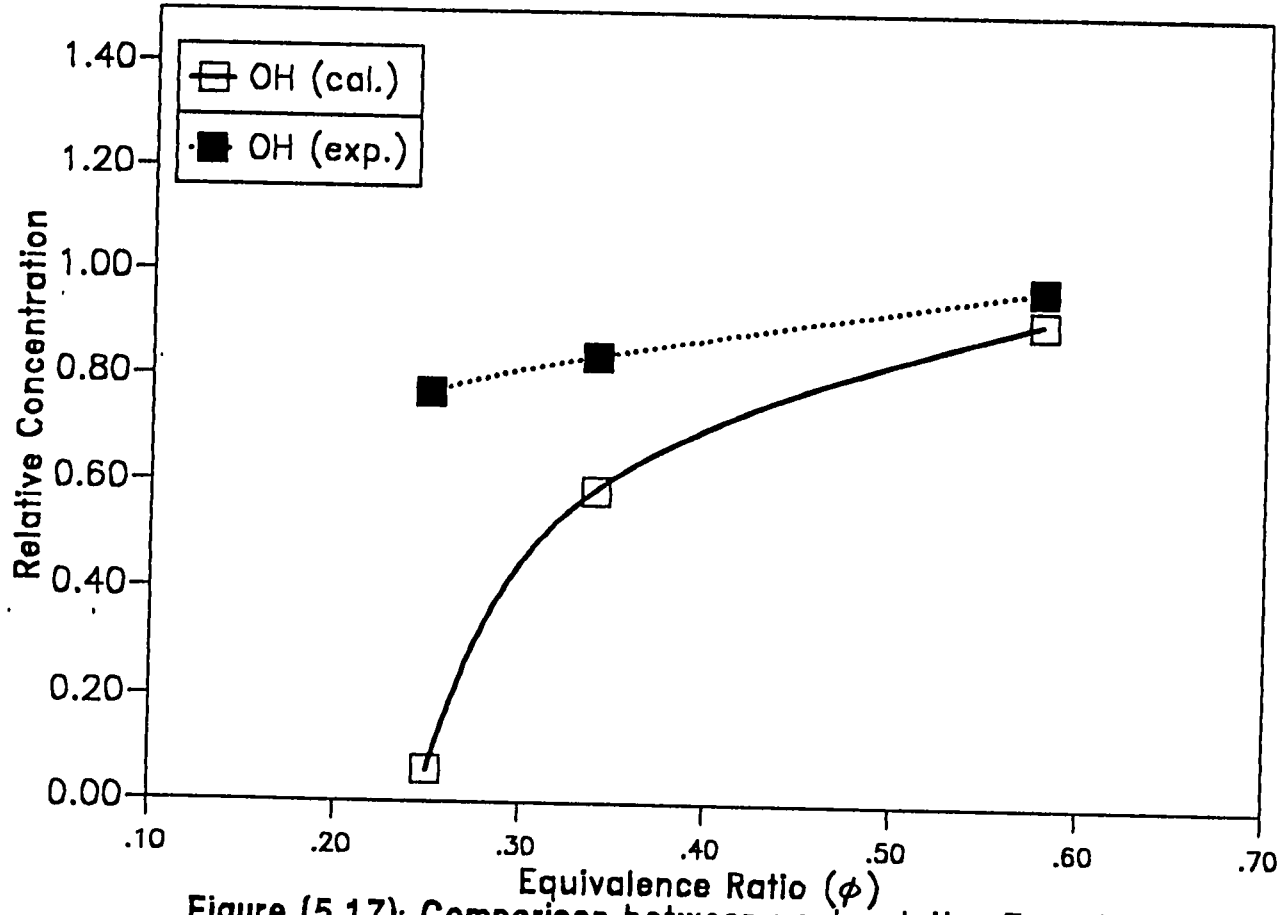

Figure (5.17): Comparison between peak relative Experimental and Calculated OH concentration versus equivalence ratio.

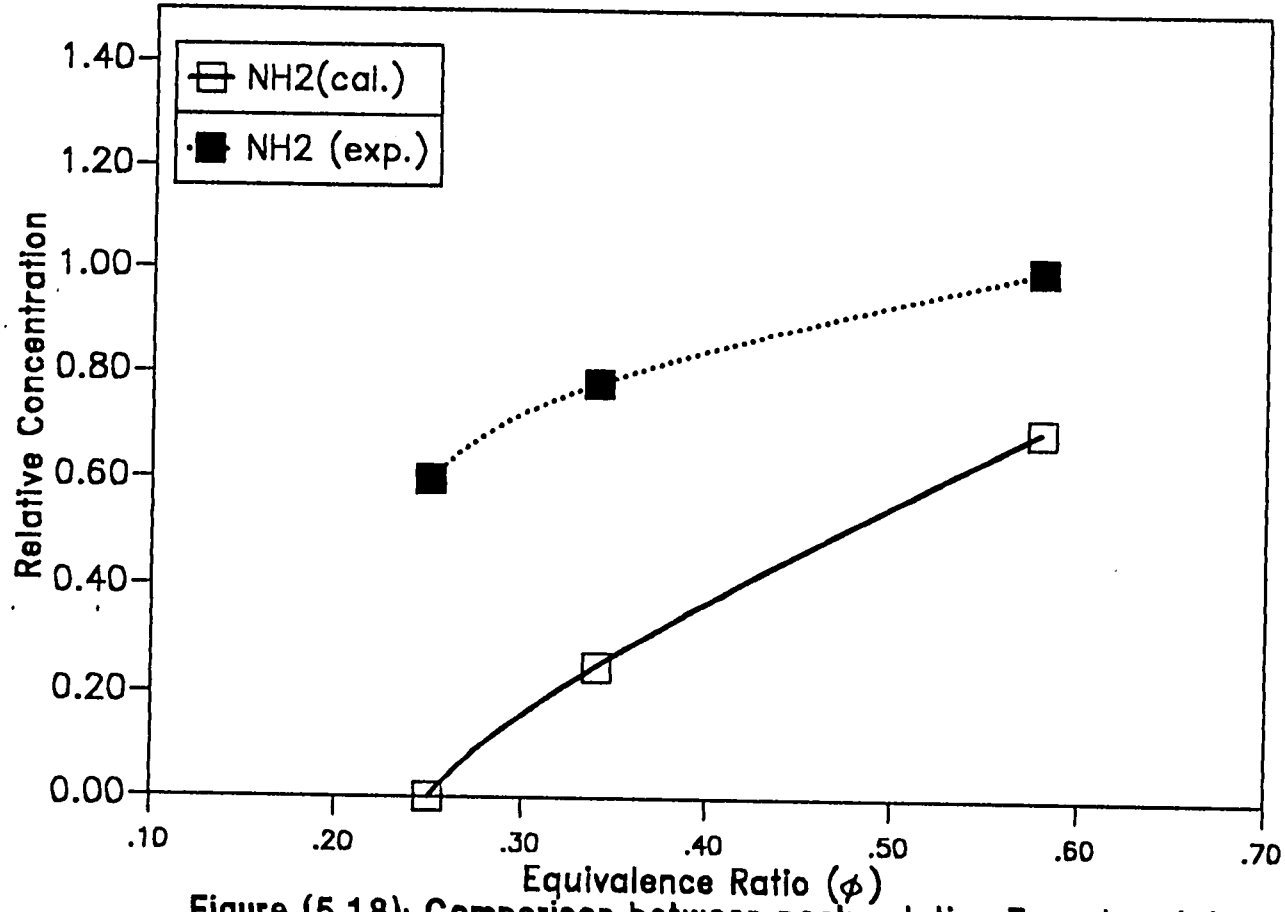

Figure (5.18): Comparison between peak relative Experimental and Calculated NH2 concentration versus equivalence ratio.

Figures (5.19), (5.20) and (5.21) shows the comparison between peak experimental and calculated NH , CN and CH concentrations respectively versus equivalence ratio. The dotted lines are the linear best fit to these points for both the experimental and calculated cases. It can be seen clearly that the peak concentration of all of these species increases with an increase in the equivalence ratio both for the experimental and calculated cases. This increase may be attributed to the higher temperatures that are encountered in high equivalence ratio flames. Therefore, the model predictions of peak concentration profiles of NH , CN and CH are in good qualitative agreement with the experimental profiles.

The quantitative and qualitative agreement of the model predictions with the stable and radical species profiles in is regarded good and indicates that the $CH_4 / NO_2 / O_2$ flames have been described accurately. The modelling simulation clearly predicts the general flame structure and species concentration profiles. Profiles of the same species in the other flames are not much different and show similar agreement between model and experiment.

5.8 Sensitivity Analysis :

Combustion modelling requires as input data sets of

(1) thermodynamic coefficients

(2) transport coefficients, and

(3) chemical reactions, including their rate coefficients.

Therefore, it is useful to be able to perform a sensitivity analysis, so as to systematically determine the effect of uncertain parameters on the solution of

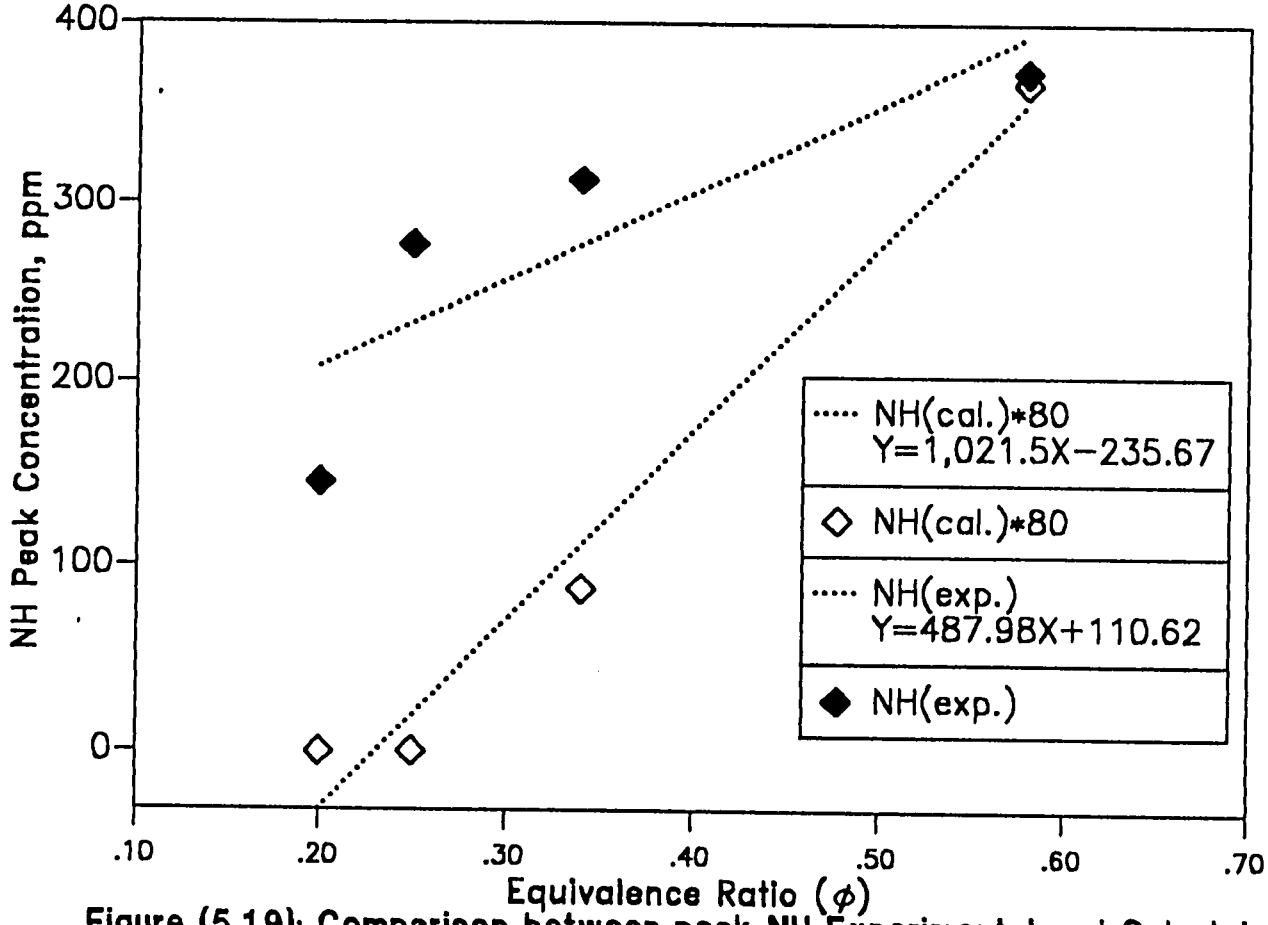

Figure (5.19): Comparison between peak NH Experimental and Calculated concentration versus equivalence ratio.

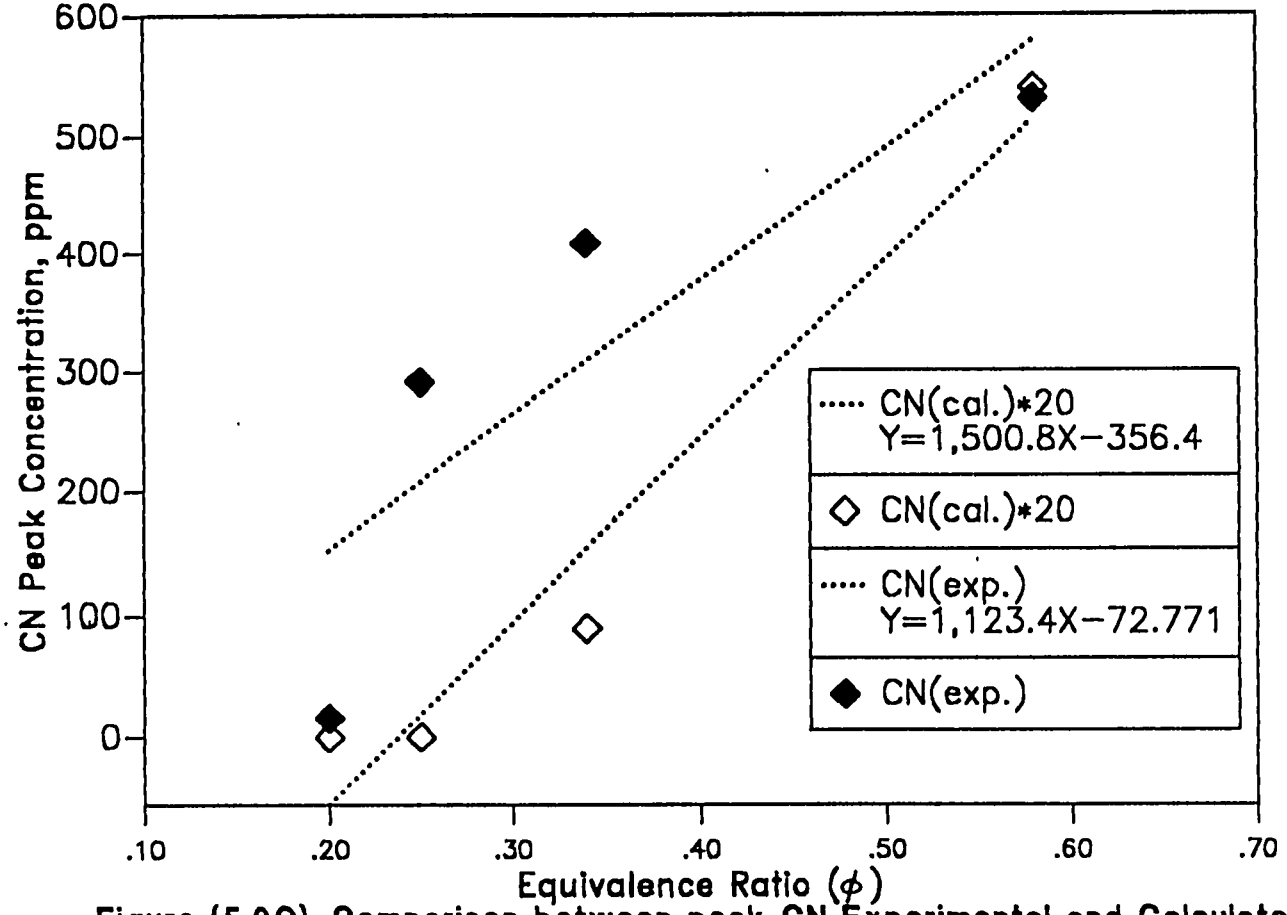

Figure (5.20): Comparison between peak CN Experimental and Calculated concentrations versus equivalence ratio

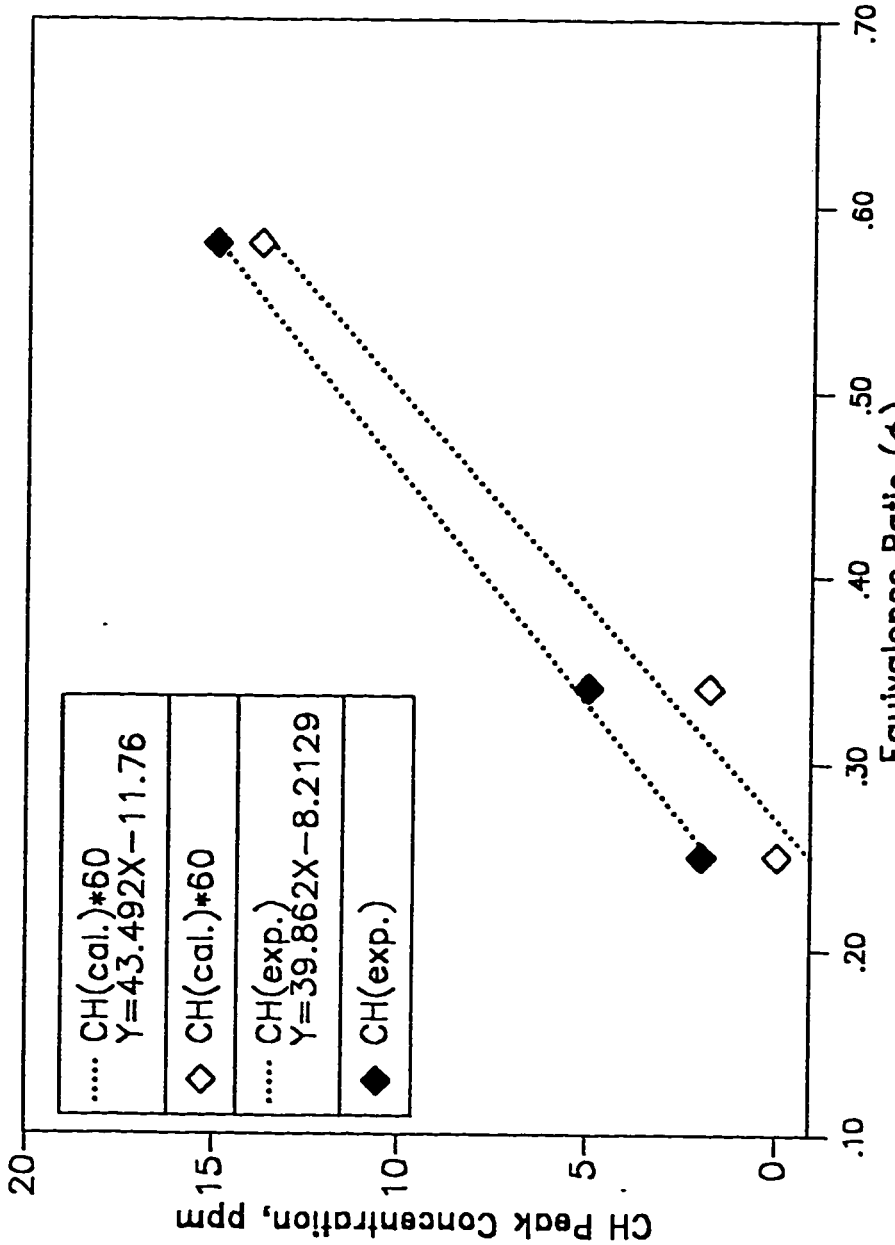

Figure (5.21): Comparison between peak CH Experimental and Calculated concentration versus equivalence ratio.

the model. If a system is very sensitive to a given parameter, more time and effort may be justified to determine a more accurate value for that parameter. On the other hand, an insensitive parameter requires less effort; and it may be possible to eliminate it and thus simplify a complex system. In addition, the sensitivity analysis is useful in understanding a complex mechanism, since it indicates which parts of the mechanism are important for a given problem.

Sensitivity analysis is a way to understand quantitatively how the solution to a model depends on parameters in the model. Once the Jacobian has been computed for the purpose of solving the boundary value problem, the sensitivity coefficients can be computed easily. The sensitivity analysis is often an invaluable tool in helping to interpret the results of a flame model.

Here the first order sensitivity coefficients of the solution profiles are considered with respect to the reaction rate coefficients. The boundary value problem can be stated in the following abstract notation

$$F(\theta,\alpha) = 0. \tag{5.1}$$

The idea that the approximate solution vectors θ are parameterized by some parameters α has been introduced here. In the present case, these α's will be the "A-factors" of the reaction rate coefficients. By differentiating Eqn.(5.1) with respect to α, a matrix equation for the sensitivity coefficients is obtained.

$$\frac{\partial F}{\partial \theta}\frac{\partial \theta}{\partial \alpha} + \frac{\partial F}{\partial \alpha} = 0 \tag{5.2}$$

The matrix $\partial F / \partial \theta$ is the Jacobian of the original system and $\partial F / \partial \alpha$ is the

matrix of partial derivatives of F with respect to the parameters. It is convenient to think of the $\partial F / \partial \alpha$ matrix column by column, with each column indicating the dependence of the residence of the residual vector F on the parameters. There are as many columns as there are parameters, i.e. reactions. The sensitivities coefficients are defined by $\partial \theta / \partial \alpha$. This matrix contains quantitative information on how each reaction rate affects the temperature and species profiles (and the flame speed) at each point in the flame. The sensitivity matrix has a structure similar to that of the $\partial F / \partial \alpha$ matrix. That is, each column shows the dependence of the solution vector on a particular reaction.

Some manipulation of the raw sensitivity coefficients makes them more useful. In the code, the normalized sensitivity coefficients in molar quantities are computed in the form of logarithmic derivatives, i.e.,

$$\frac{\alpha_i}{X_k}\frac{\partial X_k}{\partial \alpha_i} = \frac{\alpha_i}{Y_k}\frac{\partial Y_k}{\partial \alpha_i} - \alpha_i \overline{W} \sum_{j=1}^{K} \frac{1}{W_j}\frac{\partial Y_k}{\partial \alpha_i} \qquad (5.3)$$

where X_k are the mole fractions and $\overline{W}$ is the mean molecular weight.

5.9 Discussion

Results obtained from the flame modelling are discussed here in detail. To do this, a screening sensitivity analysis on the reaction mechanism for all the stable species and some of the important radical species will be performed. This analysis shows the pathways by which these species were produced and consumed in the flame. A schematic representation of the reaction mechanism for $CH_4 / NO_2 / O_2$ flames is presented at the end of this section.

5.9.1 CH_4 Reactions :

Methane is mainly decomposed through hydrogen abstraction. This occurs through reaction with other reactant gases, thermal decomposition, or through radical reactions. Methane-radical reactions include

$$CH_4 + H = CH_3 + H_2 \quad \text{(R1)}$$

$$CH_4 + OH = CH_3 + H_2O \quad \text{(R2)}$$

The thermal decomposition of methane yielding methyl radical occurs through reaction (3);

$$CH_4 + M = CH_3 + H + M \quad \text{(R3)}$$

The reactions with reactant gases are

$$CH_4 + O_2 = CH_3 + HO_2 \quad \text{(R6)}$$

$$CH_4 + NO_2 = CH_3 + HNO_2 \quad \text{(R5)}$$

The methane thermal decomposition plays a secondary role in flames because of radical diffusion. Reactions (1) and (2) are the most important reactions for methane destruction. From the sensitivity analysis it can be observed that reaction (1) contributes more than reaction (2) to methane consumption.

There are four possible paths for methyl consumption in the proposed mechanism. The first one forms CH_2 radical through the following reactions;

$$CH_3 + OH = CH_2 + H_2O \quad \text{(R12)}$$

$$CH_3 + H = CH_2 + H_2 \quad \text{(R13)}$$

$$CH_3 + M = CH_2 + H + M \quad \text{(R14)}$$

The second possible path for methyl depletion is to form formaldehyde intermediate through the following reactions;

$$CH_3 + O_2 = CH_2O + OH \quad \text{(R9)}$$

$$CH_3 + O = CH_2O + H \quad \text{(R10)}$$

$$CH_3 + O_2 = CH_2O + H + O \quad \text{(R11)}$$

$$CH_3 + OH = CH_2O + H_2 \quad \text{(R15)}$$

$$CH_3 + NO = CH_2O + NH \quad \text{(R17)}$$

The third path is to form CH_3O intermediate through the following reactions;

$$CH_3 + NO_2 = CH_3O + NO \quad \text{(R8)}$$

$$CH_3 + HO_2 = CH_3O + OH \quad \text{(R16)}$$

$$CH_3 + O_2 = CH_3O + O \quad \text{(R19)}$$

The CH_3O in turn forms formaldehyde intermediate through the following reactions;

$$CH_3O + O_2 = CH_2O + HO_2 \quad \text{(R44)}$$

$$CH_3O + M = CH_2O + H + M \quad \text{(R45)}$$

The fourth possible path forms hydrogen cyanide through the reaction;

$$CH_3 + NO = HCN + H_2O \qquad \text{(R18)}$$

The sensitivity analysis profiles for CH_4 are shown in Figures (5.22a) and (5.22b). These figures shows that methane has a long induction period before it starts to deplete. It can be seen again that the main reactions having negative sensitivity for methane formation include reactions (1) and (2). Reaction (55)

$$CO + OH = CO_2 + H$$

has high sensitivity for CH_4 consumption since it produces H atoms which augments the proceeding of reaction (1).

5.9.2 H_2O Reactions :

Water molecules are formed in the $CH_4 / NO_2 / O_2$ mechanism through the following reactions;

$$CH_4 + OH = CH_3 + H_2O \qquad \text{(R2)}$$

$$CH_3 + OH = CH_2 + H_2O \qquad \text{(R12)}$$

$$CH_2 + OH = HCO + H_2O \qquad \text{(R39)}$$

The production of H_2O depends entirely on the availability of OH radicals. The H_2O concentration grows steadily as methane is consumed and reaches a constant concentration when the fuel disappears.

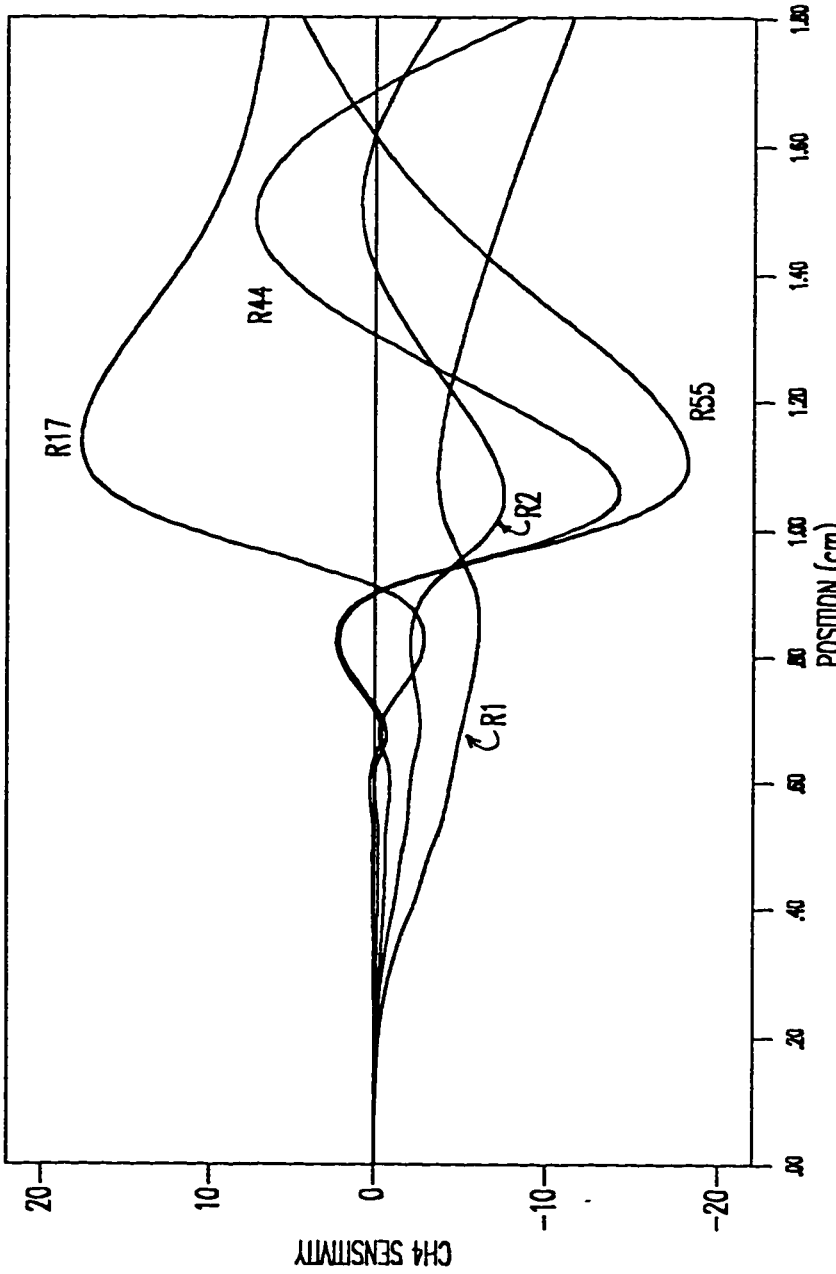

Figure 5.22a: Sensitivity Plot for CH4 for Flame 3, the Number Referred to the Reaction Number in Table (5.1).

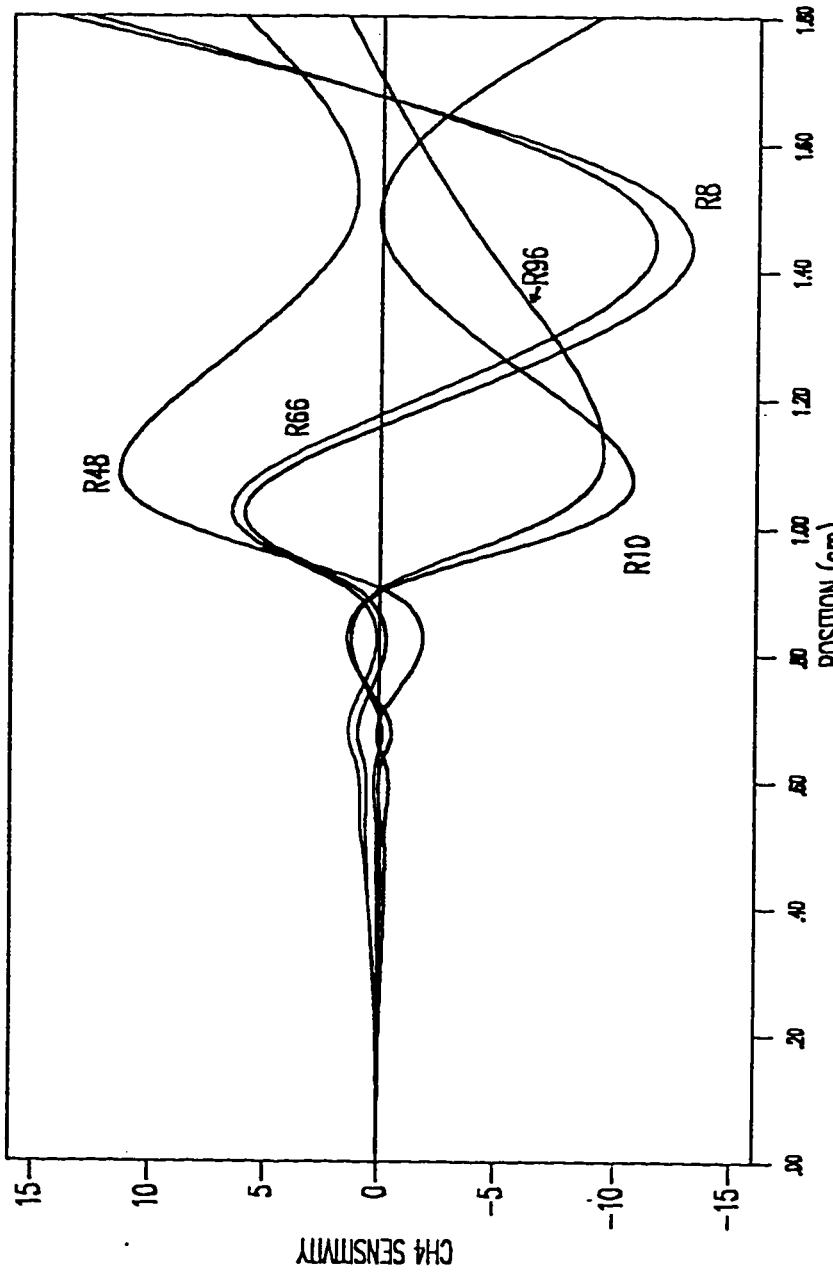

Figure 5.22b: Sensitivity Plot for CH4 for Flame 3, the Number Referred to the Reaction Number in Table (5.1).

The sensitivity analysis for the reaction rate of H_2O (Figures (5.23a) and (5.23b)) shows that the H_2O profile is primarily sensitive to the chain propagation reactions (17) (positive sensitivity) and (8) (negative sensitivity) which are, in fact, mirror images of each other. It can also be seen that reactions (66), (67) and (95) produces OH directly causing an increase in the H_2O production rate. Reaction (94) uses OH radicals and therefore it reduces the formation of H_2O in the flame. The sensitivity analysis reveals that reaction (2) is the major source of H_2O production.

5.9.3 CO and CO_2 Reactions :

In hydrocarbon flames, formation of carbon monoxide is due to the following set of reactions;

$$CH_3 + O = CH_2O + H \qquad \text{(R10)}$$

$$CH_3 + OH = CH_2O + H_2 \qquad \text{(R15)}$$

$$CH_2O + OH = HCO + H_2O \qquad \text{(R39)}$$

$$HCO + M = CO + H + M \qquad \text{(R50)}$$

The formaldehyde thermal decomposition is unimportant in flames, specially when formaldehyde is present as a flame intermediate. In contrast, HCO thermal decomposition dominates over HCO radical reactions as a CO production source.

Figures (5.24a), (5.24b) and (5.24c) show the sensitivity analysis for the CO

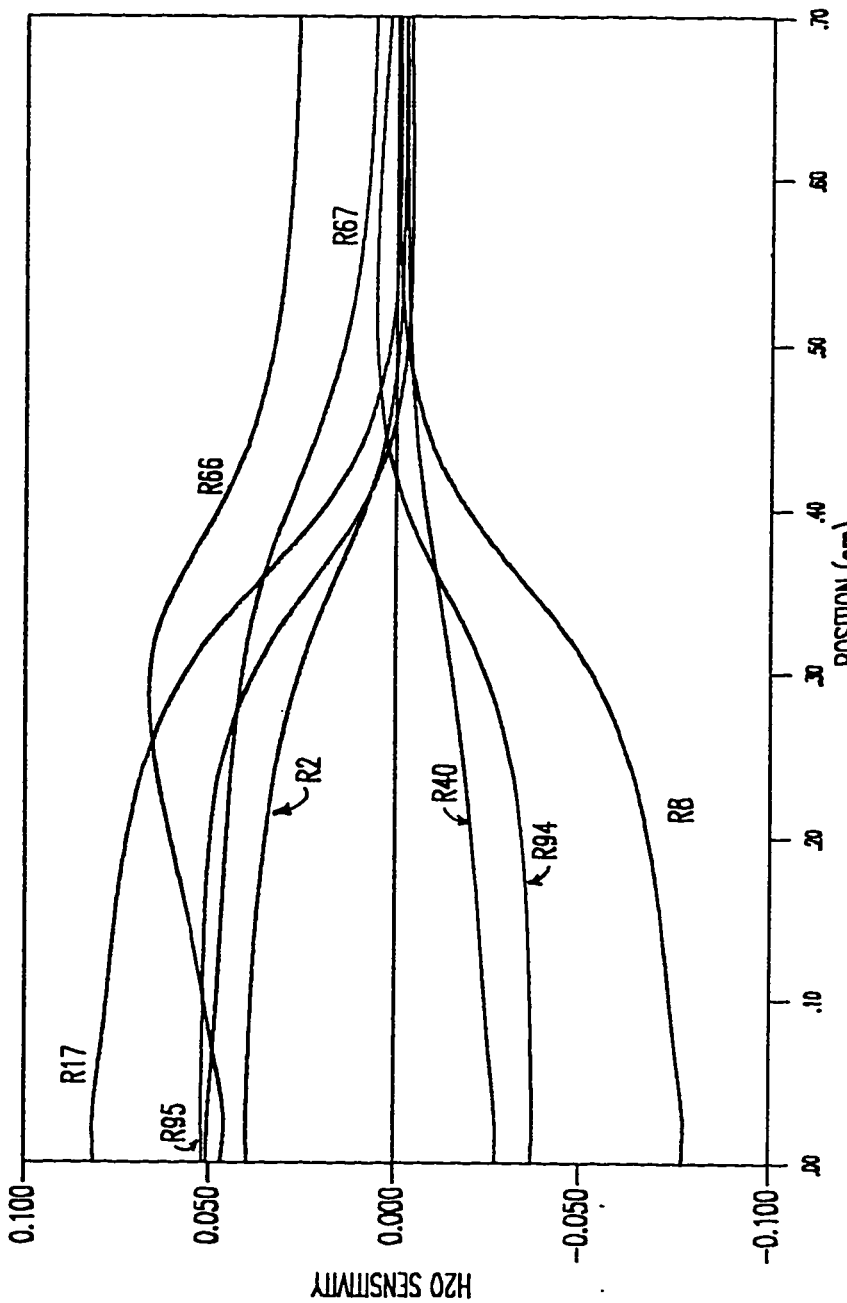

Figure 5.23a: Sensitivity Plot for H2O for Flame 3, the Number Referred to the Reaction Number in Table (5.1).

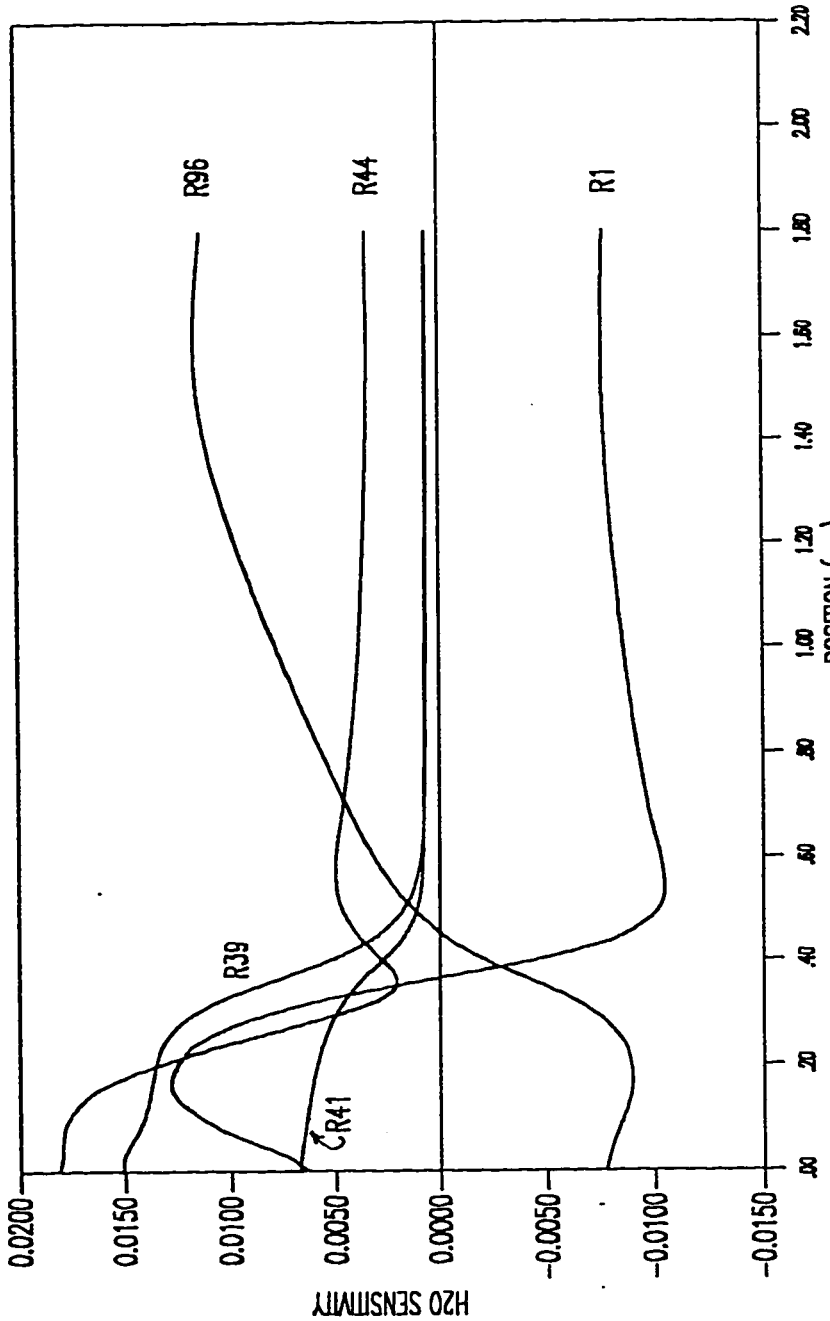

Figure 5.23b: Sensitivity Plot for H2O for Flame 3, the Number Referred to the Reaction Number in Table (5.1)

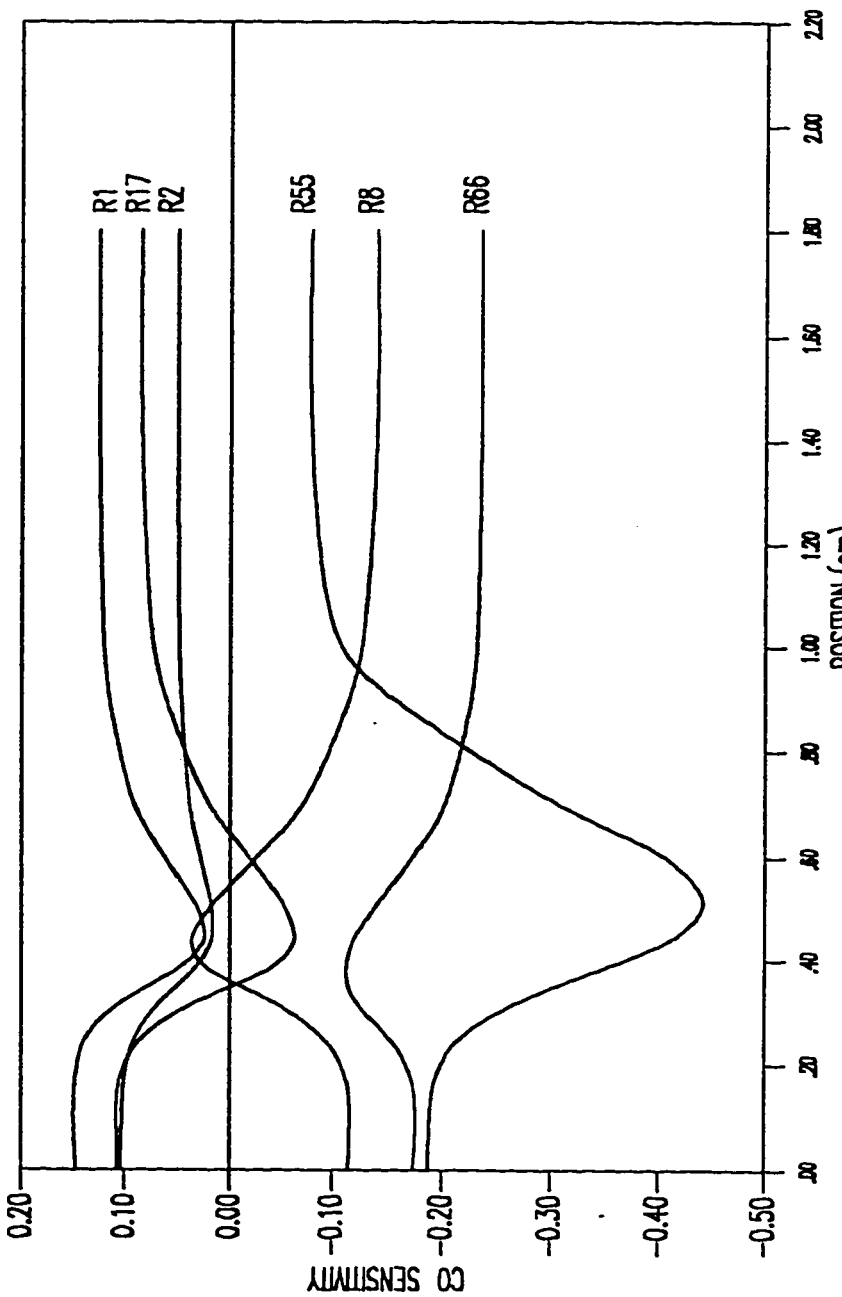

Figure 5.24a: Sensitivity Plot for CO for Flame 3, the Number Referred to the Reaction Number in Table(5.1).

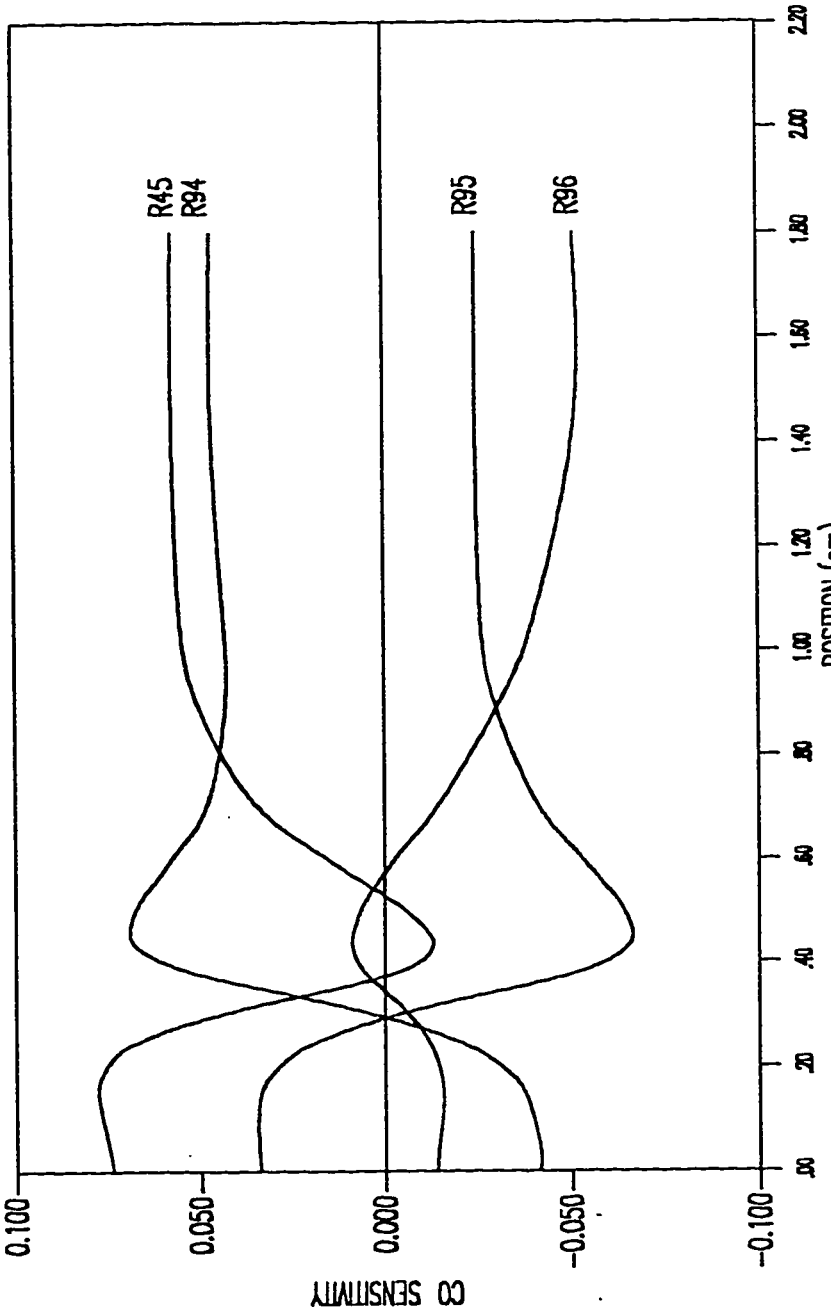

Figure 5.24b: Sensitivity Plot for CO for Flame 3, the Number Referred to the Reaction Number in Table (5.1)

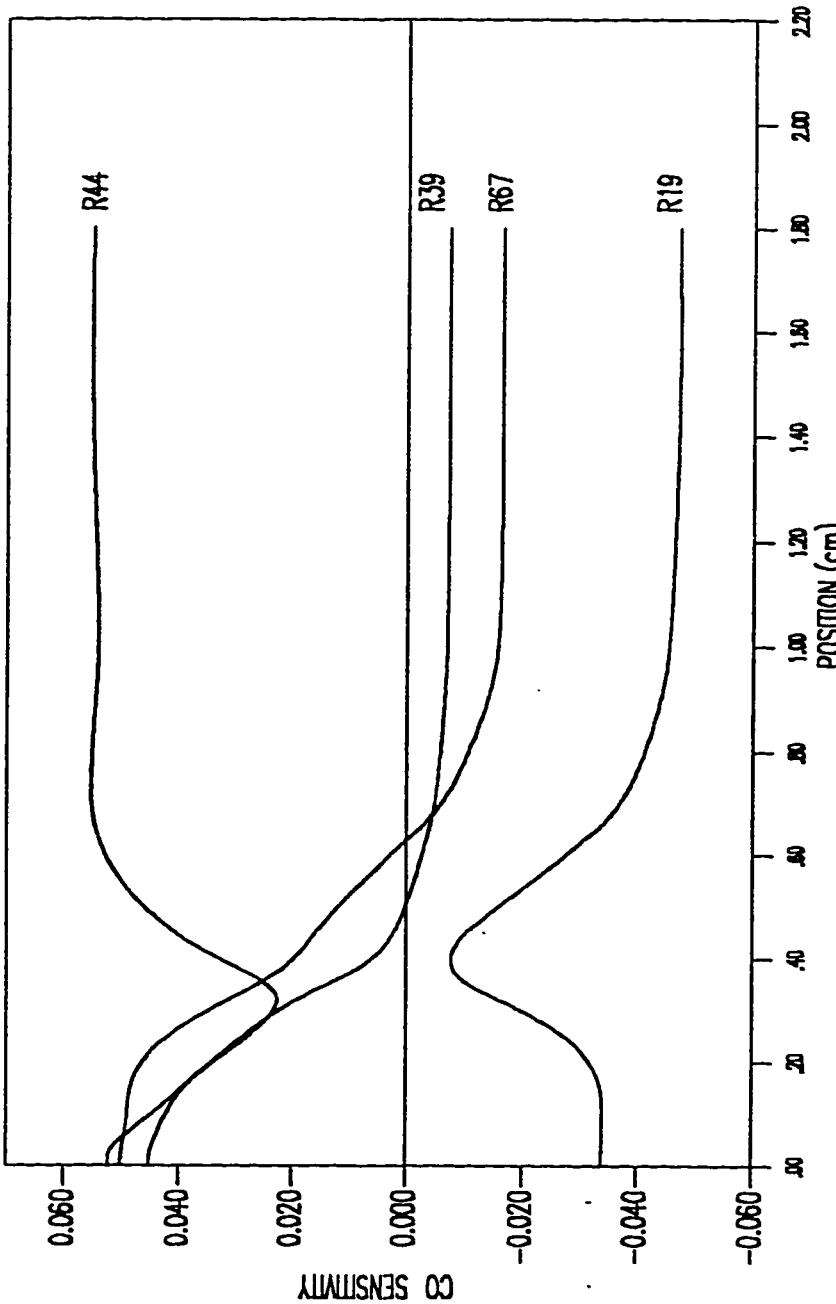

Figure 5.24c: Sensitivity Plot for CO for Flame 3, the Number Referred to the Reaction Number in Table (5.1)

molecule. Reactions (1), (2), and (17) have a positive sensitivity for CO production. Reactions (1) and (2) generates CH_3 radicals which form CO through the path shown in Figure (5.34) which is at the end of this chapter. Reaction (55) shows the highest negative sensitivity coefficient in controlling the CO reaction rate. In fact, any reaction which generates OH radical in the the mechanism (like reaction (66)) will boost reaction (55) and thus increase CO conversion to CO_2. Reaction (8) also shows negative sensitivity as it consumes CH_3 radical which in turn means that less CH_3 radicals will be available for reactions (1) and (2).

The oxidation mechanism for carbon monoxide is quite simple, consisting of;

$$CO + O + CO = CO_2 + CO \qquad \text{(R54)}$$

$$CO + OH = CO_2 + H \qquad \text{(R55)}$$

$$CO + HO_2 = CO_2 + OH \qquad \text{(R56)}$$

$$CO + O_2 = CO_2 + O \qquad \text{(R57)}$$

Most of the CO_2 that is produced results from reaction (55). The reaction of molecular oxygen with CH_2 radical is another possible path for CO_2 formation

$$CH_2 + O_2 = CO_2 + H_2 \qquad \text{(R25)}$$

$$CH_2 + O_2 = CO_2 + H + H \qquad \text{(R26)}$$

For CO_2 , the sensitivity analysis profiles are shown in Figures (5.25a),

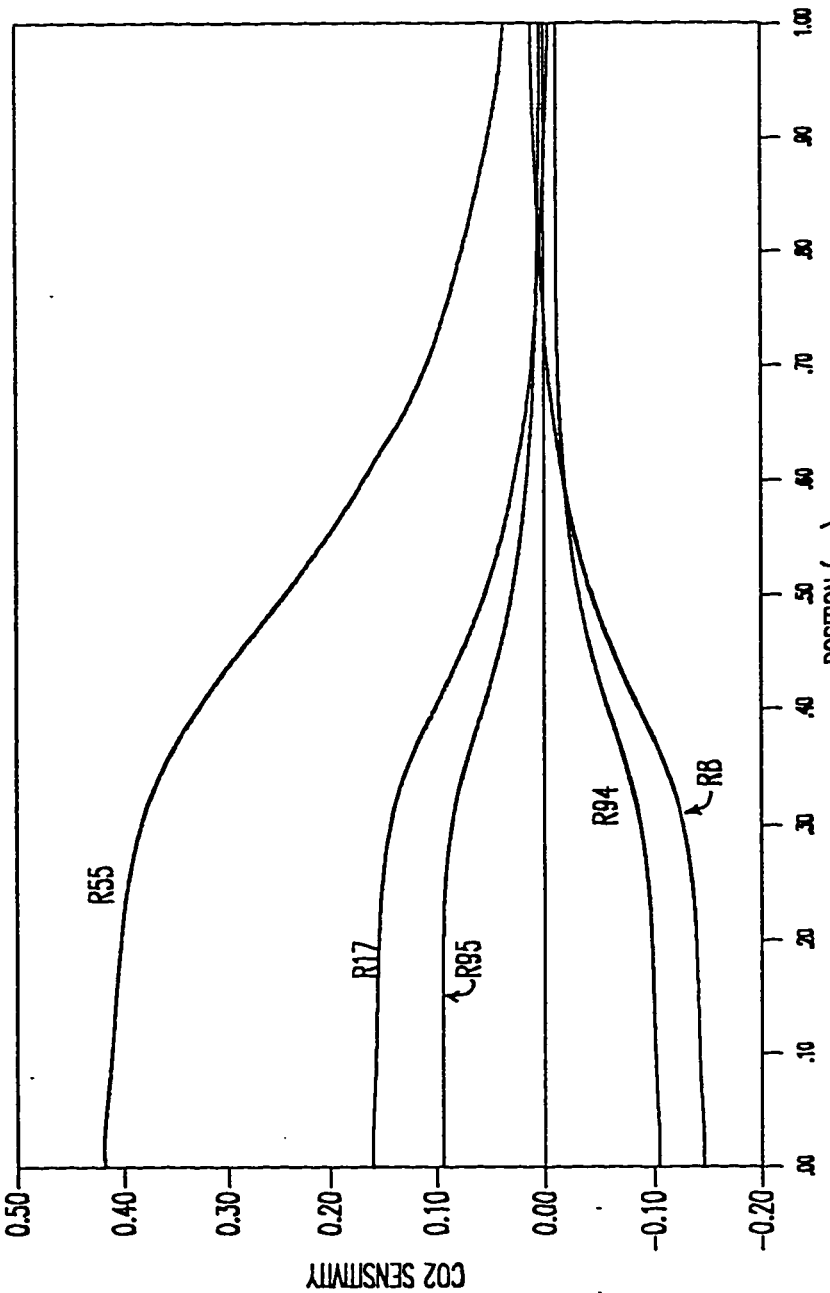

Figure 5.25a: Sensitivity Plot for CO2 for Flame 3, the Number Referred to the Reaction Number in Table (5.1)

(5.25b) and (5.25c). Again reaction (17) has a positive contribution to CO_2 formation. Also reaction (55) shows a positive sensitivity coefficient which supports the fact that this reaction is the main path for CO_2 formation. Reaction (95)

$$HNO_2 + M = OH + NO + M$$

increases the CO conversion to CO_2 by forming OH radical. This reaction seems to be an important source of OH formation especially in the early stages of the flame where the CH concentration is high. Reaction (94) consumes OH radical and therefore has a negative contribution to CO_2 production. Reaction (8) has a negative effect on CO_2 production as it competes with reaction (17) for CH_3 radical, thereby reducing the contribution of reaction (17). The contributions of reactions (8) and (17) and also of reaction (94) and (95) are almost mirror images of each other.

5.9.4 *CH* Reactions :

In methane flames, methyl radical (CH) is known to be formed by H abstraction from the methylene intermediate (CH_2) through the following general reactions

$$CH_2 + R = CH + HR$$

where R represents radical species mainly H or OH. The CH is a very highly reactive species and it is consumed in the flame by several reactions

$$CH + NO = NH + CO \qquad \text{(R31)}$$

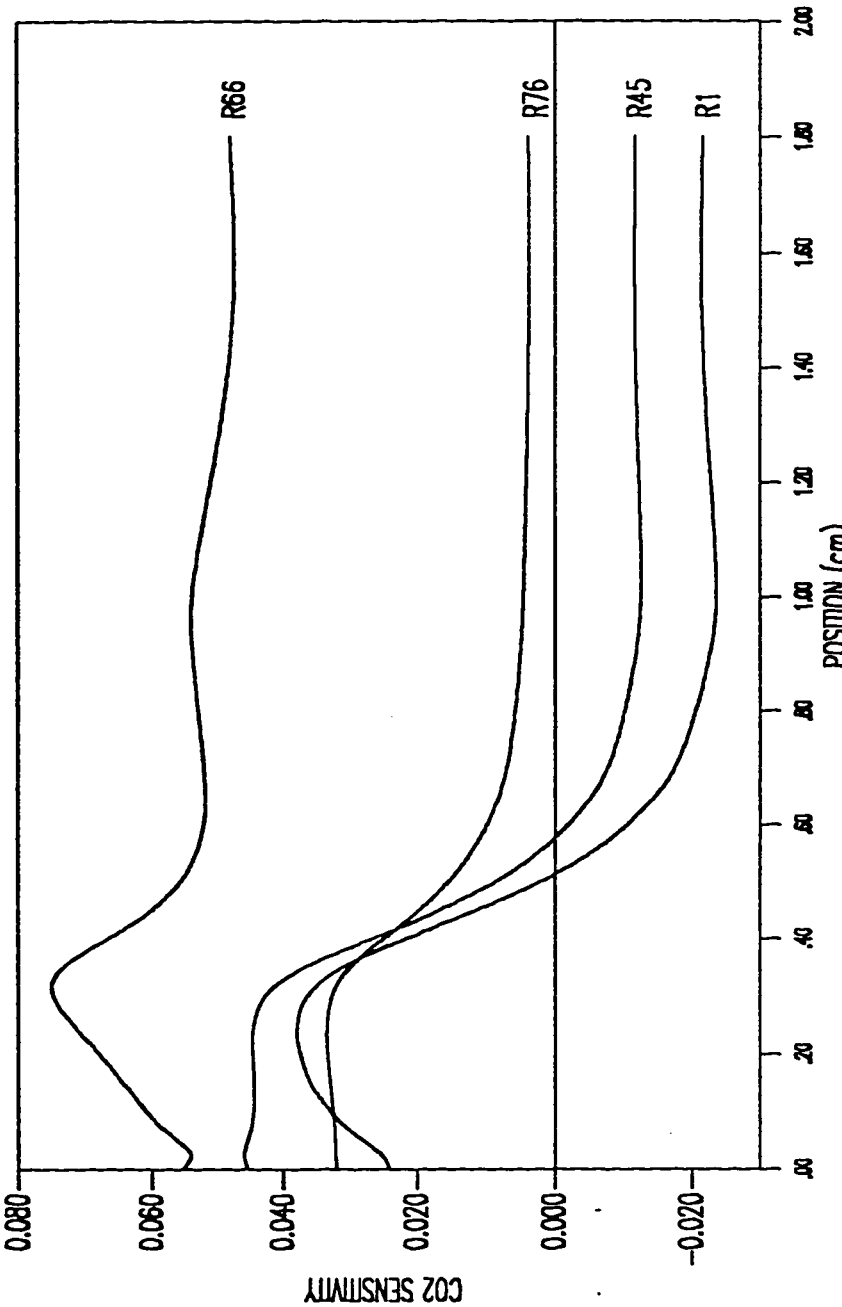

Figure 5.25b: Sensitivity Plot for CO2 for Flame 3, the Number Referred to the Reaction Number in Table (5.1)

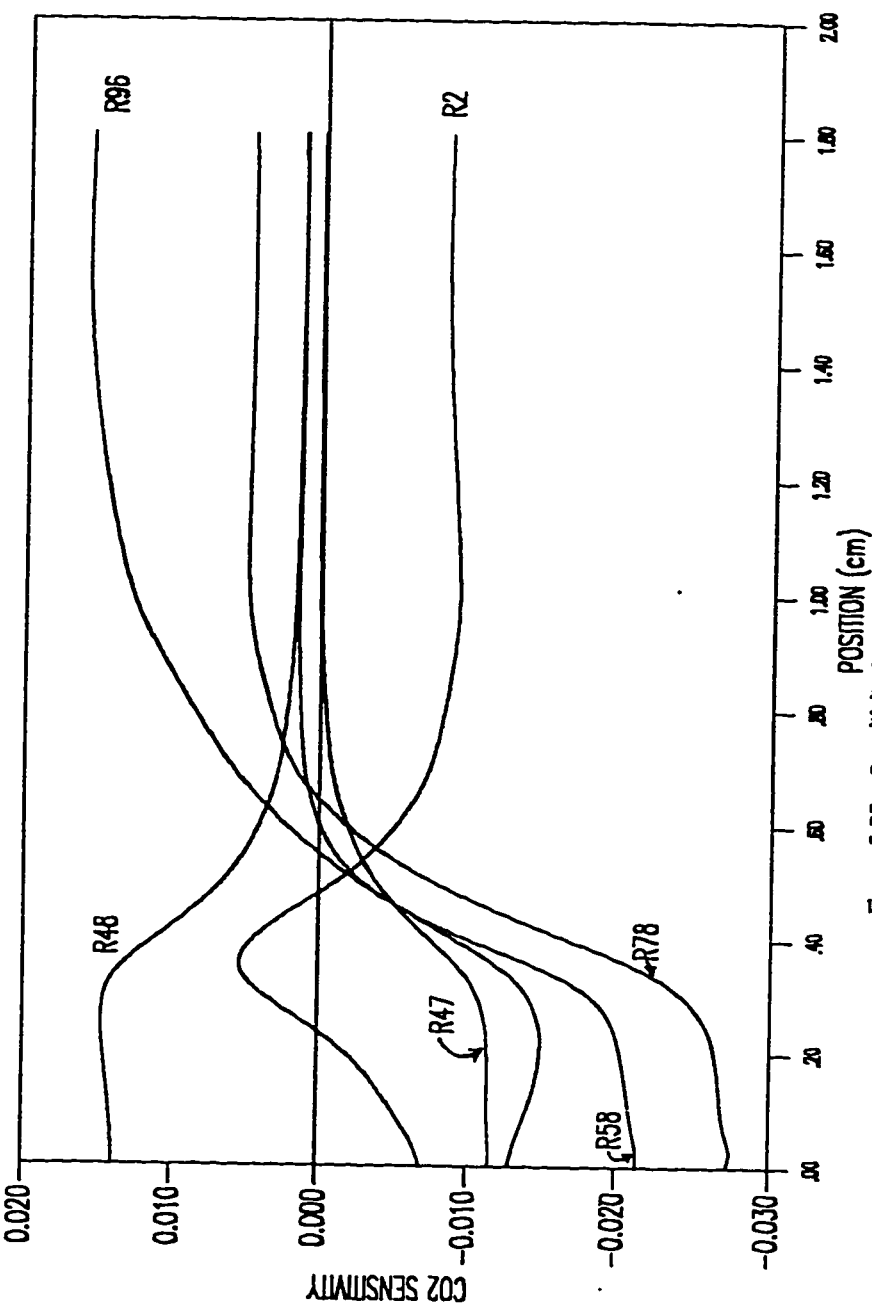

Figure 5.25c: Sensitivity Plot for CO2 for Flame 3, the Number Referred to the Reaction Number in Table (5.1)

$$CH + NO = HCN + O \qquad \text{(R32)}$$

$$CH + NO = CN + OH \qquad \text{(R33)}$$

$$CH + H_2O = CH_2O + H \qquad \text{(R34)}$$

$$CH + O_2 = OH + CO \qquad \text{(R35)}$$

$$CH + O = CO + H \qquad \text{(R36)}$$

Reactions (31), (35) and (36) are chain inhibition reactions while reactions (32), (33) and (34) are chain propagating reactions. Reaction (33) has a slightly higher reaction rate which makes it favorable over reaction (31). Since the *NO* molecule is known to be a very efficient radical scavenger, reaction (33) is believed to cause *NO* reduction especially in the early stages of the flame.

The sensitivity analysis profiles for *CH* reaction rate are plotted in Figures (5.26a), (5.26b) and (5.26c). Figure (5.26c) shows that reaction (21)

$$CH_2 + OH = CH + H_2O$$

is the main source of *CH* production. It also shows that reactions (33) and (35) are the main reactions through which *CH* reduction occurs. Reaction (17) competes with reaction (33) for the *NO* consumption and therefore has a positive contribution to *CH* formation. Reaction (8)

$$CH_3 + NO_2 = CH_3O + NO$$

on the other hand produces *NO* and therefore has a positive contribution to *CH* formation as it helps reaction (33) to proceed.

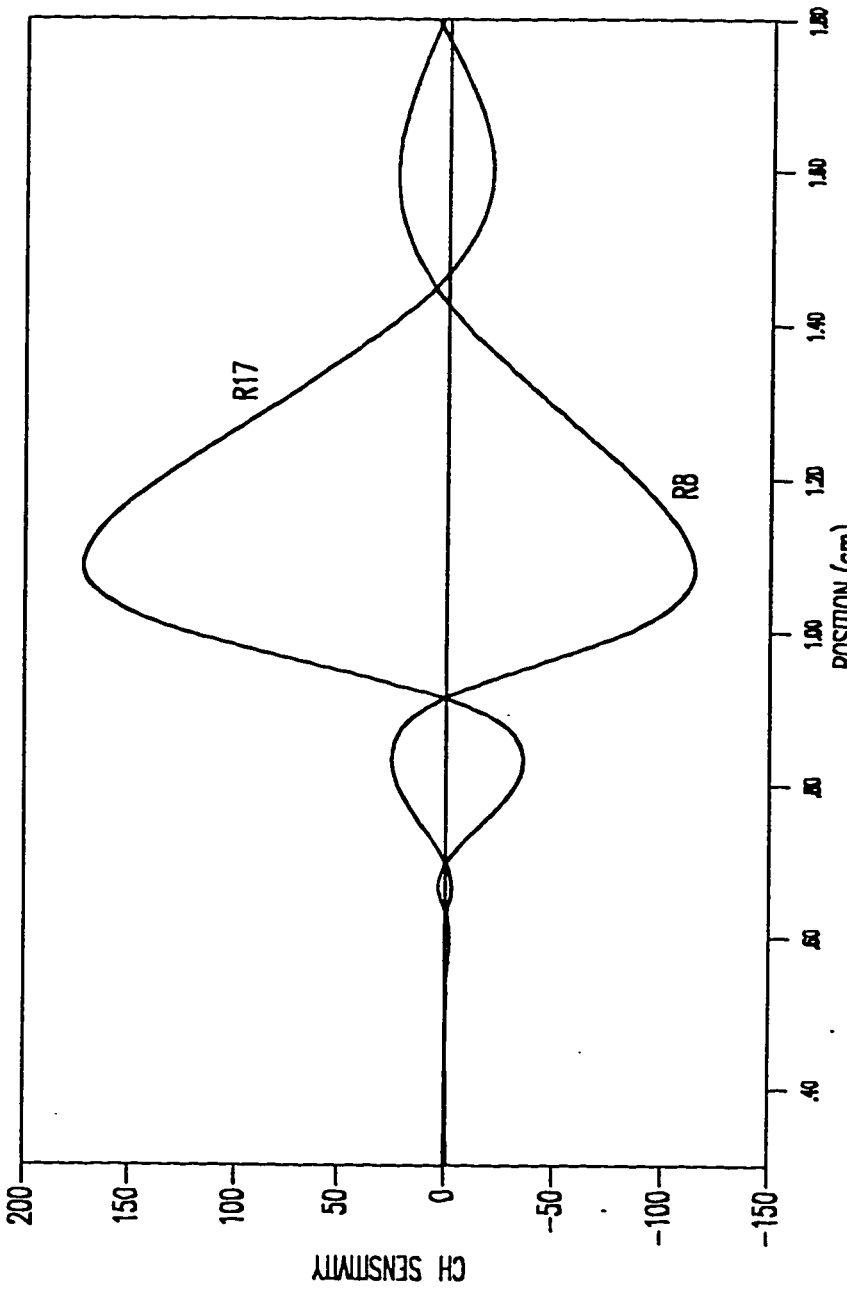

Figure 5.26a: Sensitivity Plot for CH for Flame 2, the Number Referred to the Reaction Number in Table (5.1).

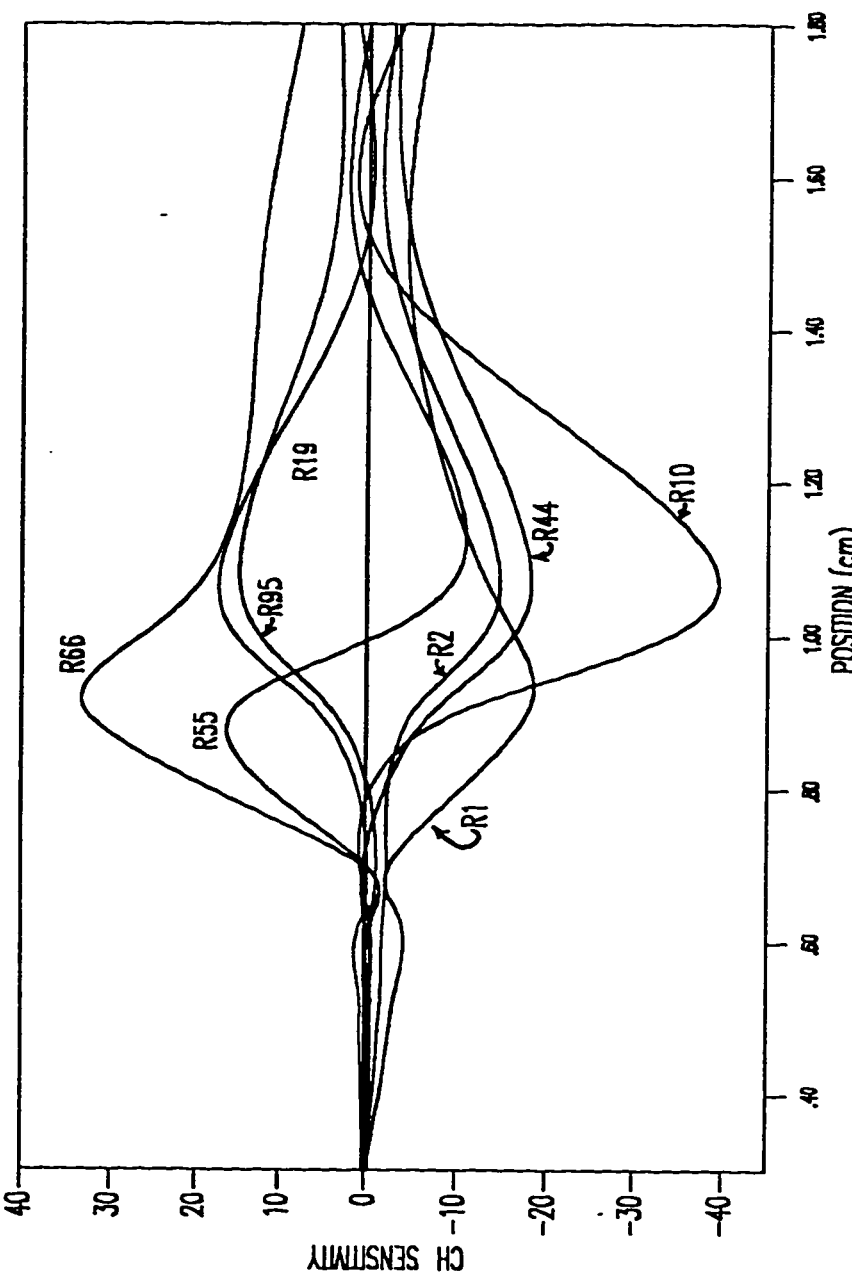

Figure 5.26b: Sensitivity Plot for CH for Flame 3, the Number Referred to the Reaction Number in Table (5.1)

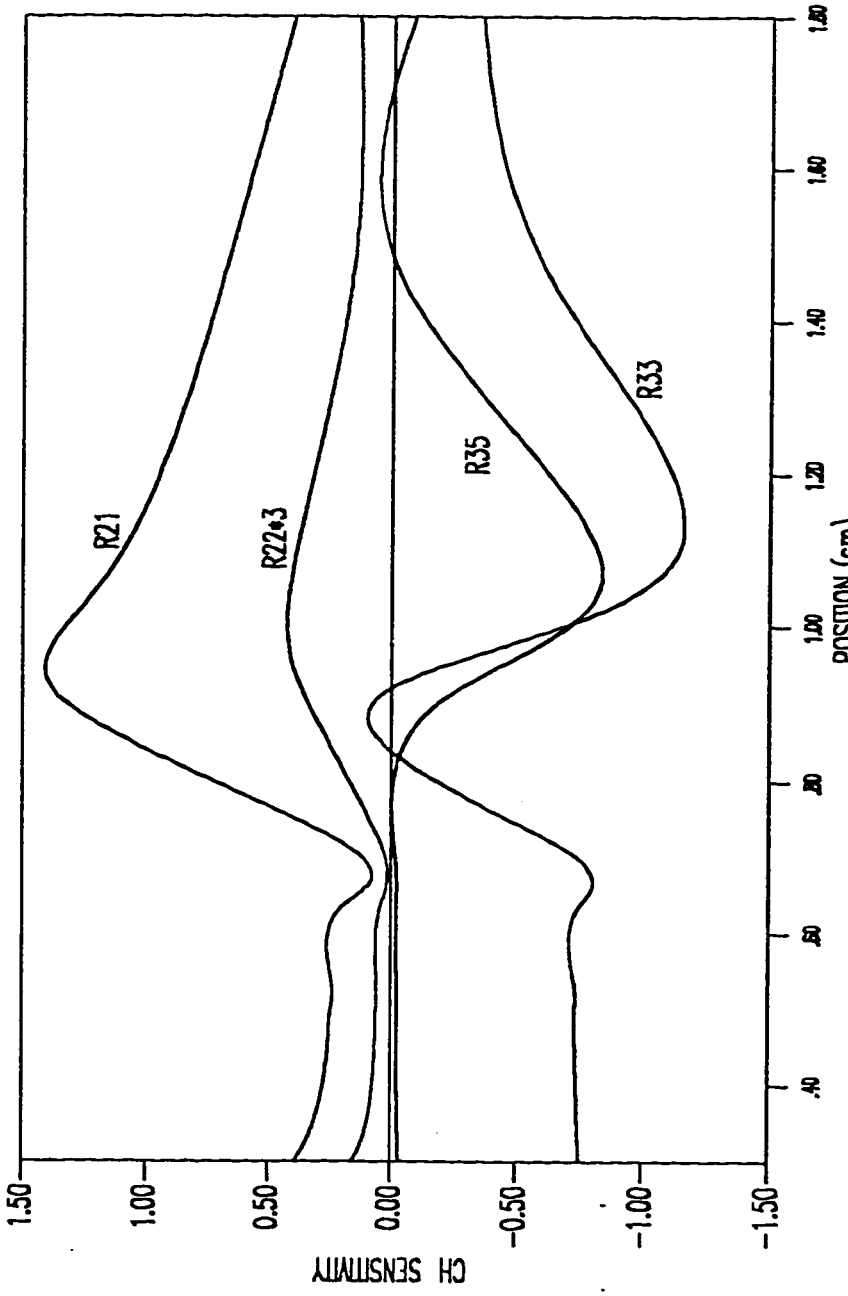

Figure 5.26c: Sensitivity Plot for CH for Flame 3, the Number Referred to the Reaction Number in Table (5.1).

5.9.5 *CN* Reactions :

The cyano radical (*CN*) is the first link between hydrocarbon and nitrogen species. In $CH_4 / NO_2 / O_2$ flames, *CN* is formed from *CH* reaction with *NO* as follows

$$CH + NO = CN + OH \qquad \text{(R33)}$$

The *CN* radical is consumed in the flame through the following reactions

$$CN + NO = N_2 + CO \qquad \text{(R86)}$$

$$CN + N_2O = NCO + N_2 \qquad \text{(R87)}$$

It is obvious from the above reactions that *CN* is consumed by chain propagation reactions.

Figures (5.27a), (5.27b) and (5.27c) shows the sensitivity analysis conducted on the reaction rate of *CN*. Reaction (86) seems to be the most important reaction for *CN* depletion, while reaction (8) produces *NO* which has a negative effect on *CN* formation according to reaction (86). Reaction (17) has a positive sensitivity for *CN* formation as it consumes *NO*. The high positive sensitivity coefficient of reaction (33) indicates the importance of this reaction as a major source of *CN* formation.

5.9.6 *NH* Reactions :

The imidogen (*NH*) radical was formed in the flame by the following three reactions

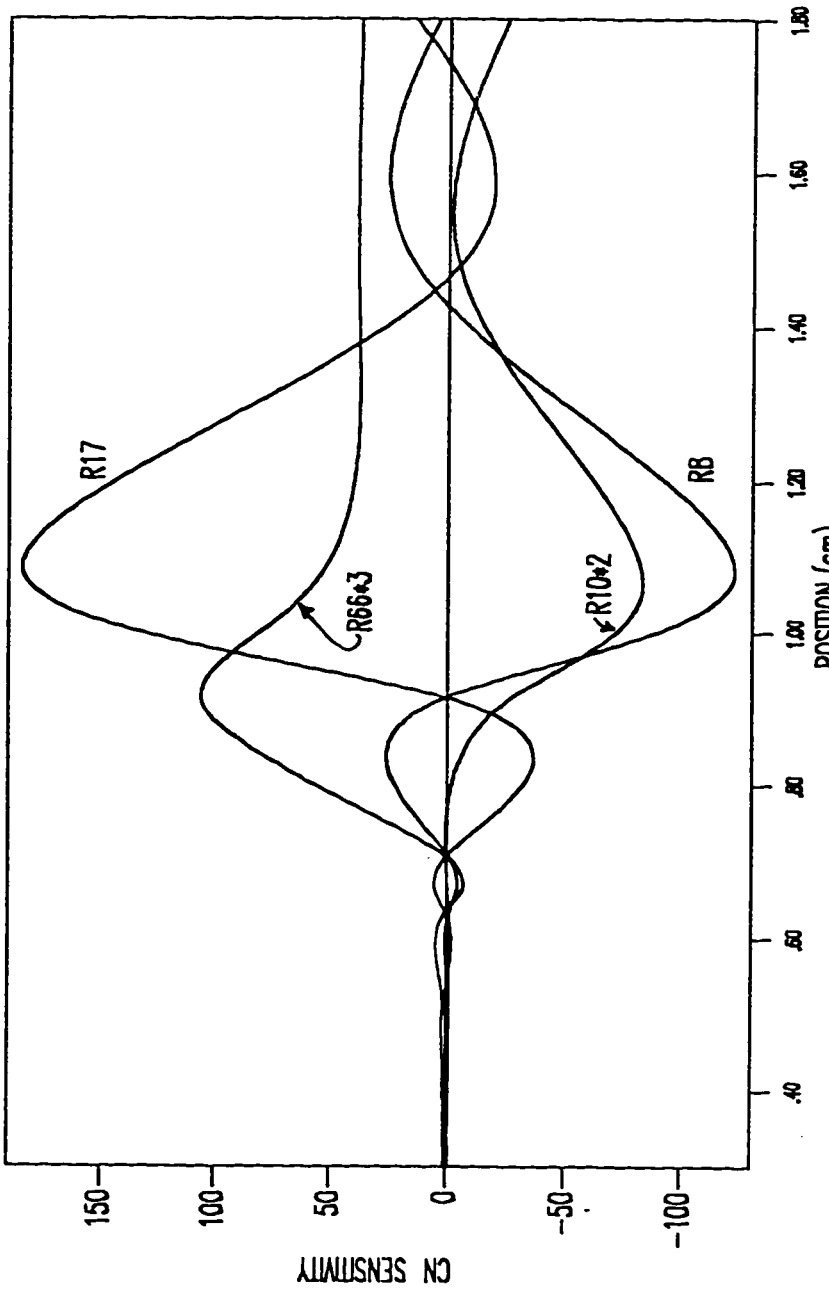

Figure 5.27a: Sensitivity Plot for CN for Flame 3, the Number Referred to the Reaction Number in Table (5.1)

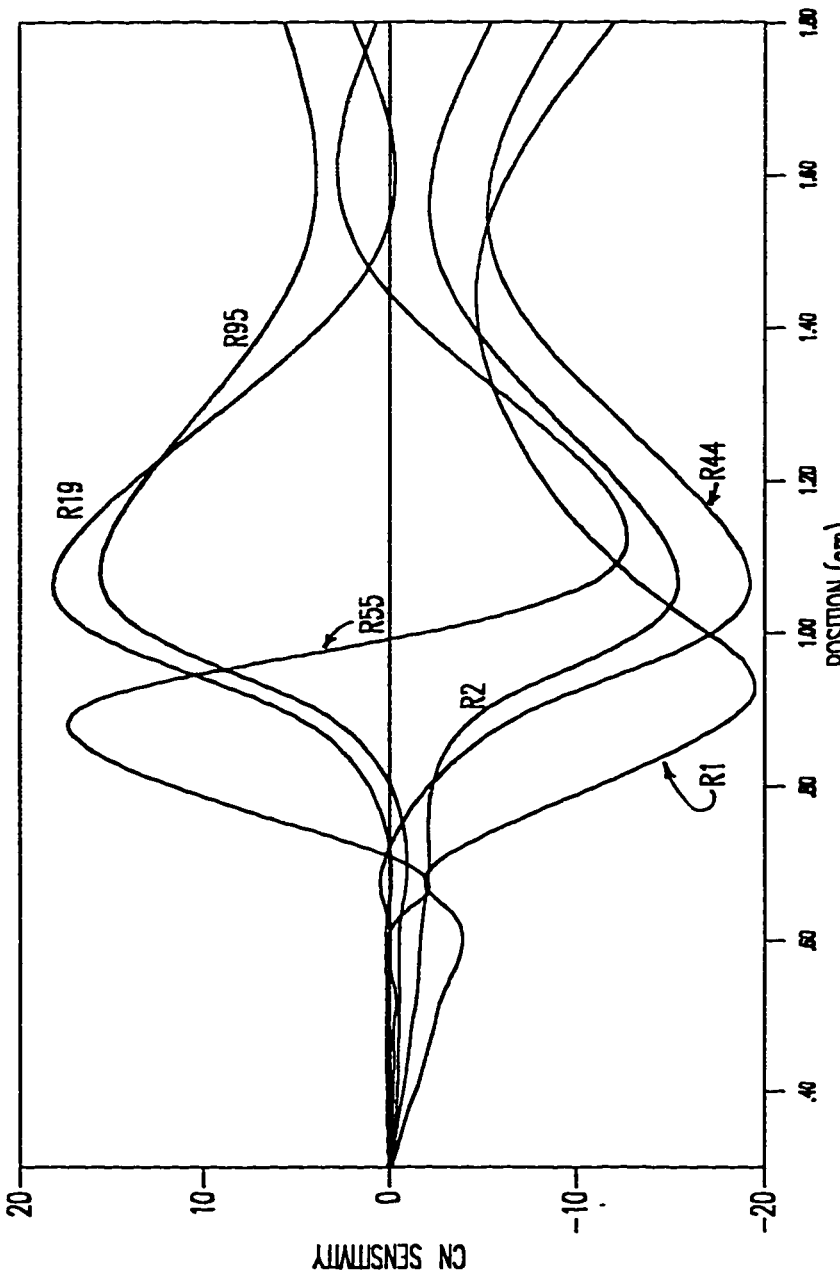

Figure 5.27b: Sensitivity Plot for CN for Flame 3, the Number Referred to the reaction Number in Table (5.1).

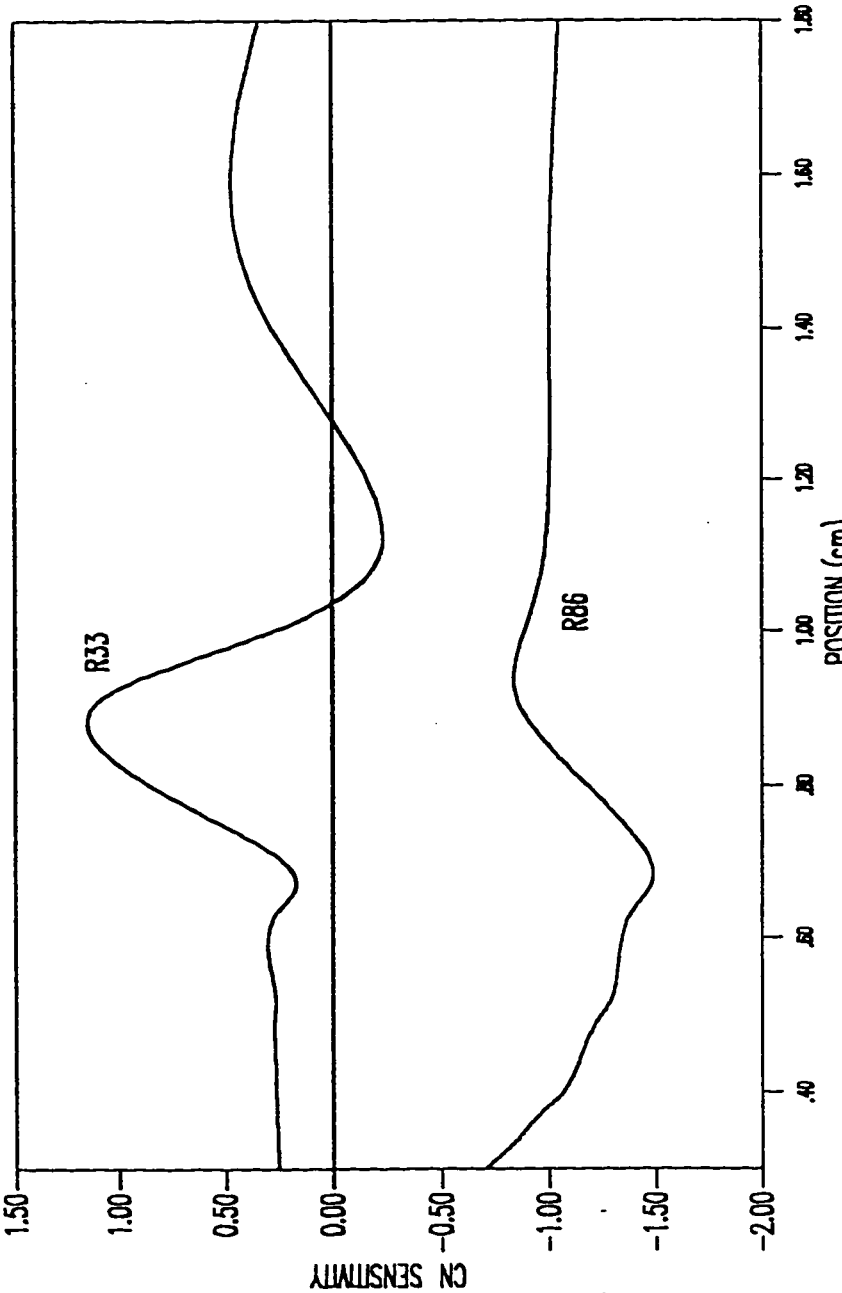

Figure 5.27c: Sensitivity Plot for CN for Flame 3, the Number Referred to the Reaction Number in Table (5.1).

$$CH_3 + NO = CH_2O + NH \quad \text{(R17)}$$

$$CH + NO = NH + CO \quad \text{(R31)}$$

$$NCO + H = NH + CO \quad \text{(R81)}$$

From the sensitivity analysis for *NH* (Figure 5.28a), it can be seen that the most important of the above set of reactions is reaction (17)

$$CH_3 + NO = CH_2O + NH.$$

Other major contributor to *NH* formation is believed to be reaction (81). Reaction (32) contributes positively towards *NH* formation as it directly generates *NCO* radical, which is needed for reaction (81).

The *NH* radical is consumed primarily through reaction (90)

$$NH + NO = N_2O + H.$$

Other important reactions for *NH* consumption include

$$NH + O_2 = HNO + O \quad \text{(R88)}$$

$$NH + O_2 = NO + OH \quad \text{(R89)}$$

$$NH + NO = N_2 + OH \quad \text{(R91)}$$

The sensitivity profiles for *NH* reaction rates are plotted in Figures (5.28a), (5.28b) and (5.28c). The *NH* radical has a positive contribution from reaction (17) as it is mainly produced through this reaction. Reaction (18)

$$CH_3 + NO = HCN + H_2O$$

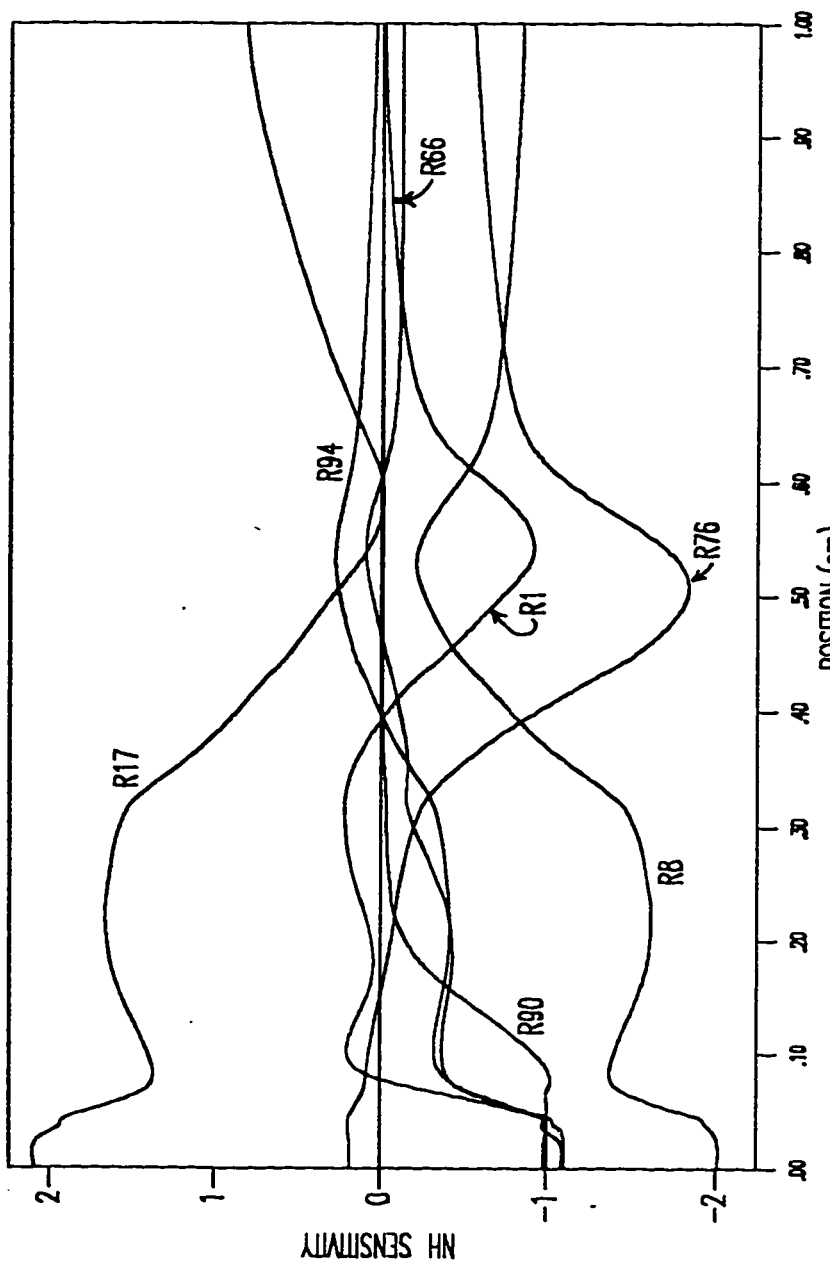

Figure 5.28a: Sensitivity Plot for NH for Flame 3, the Number Referred to the Reaction Number in Table (5.1)

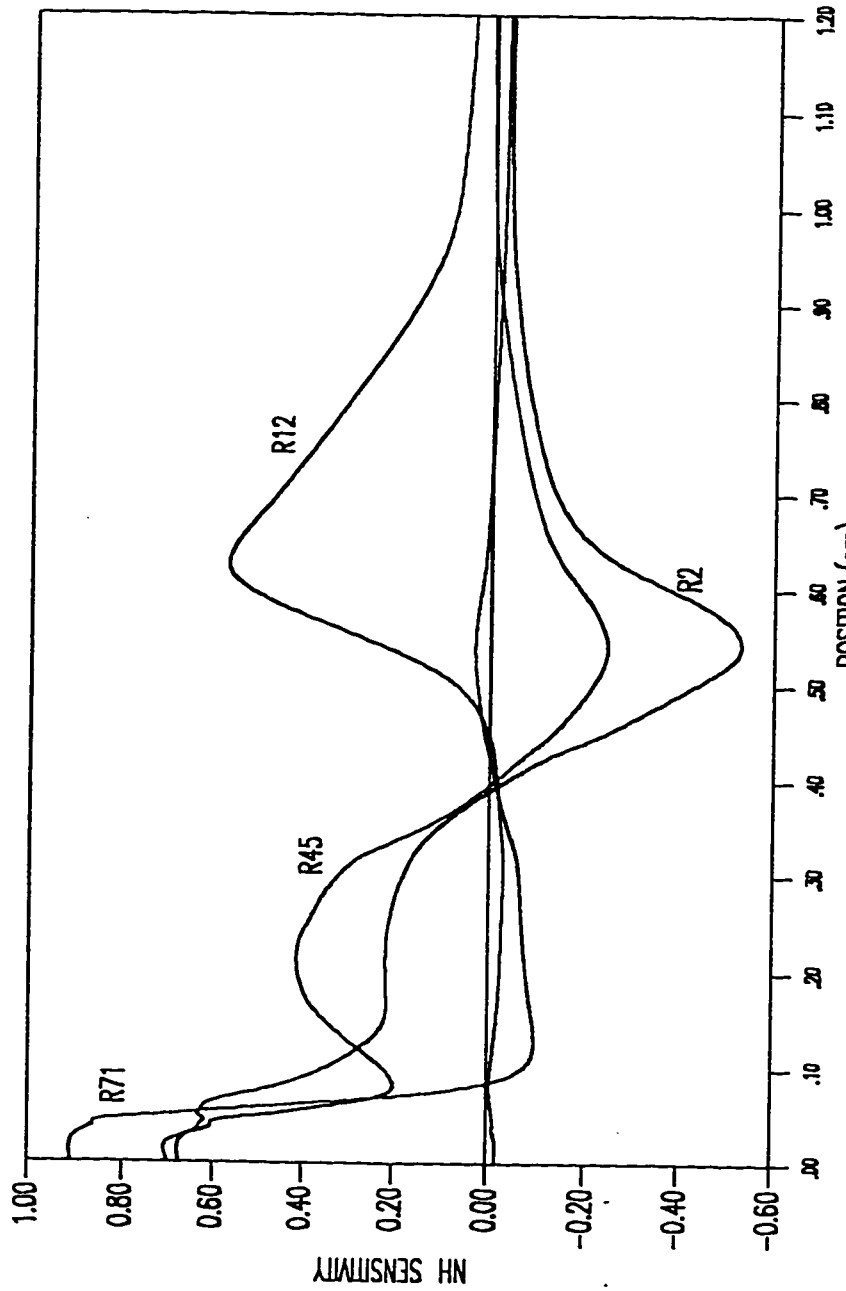

Figure 5.28b: Sensitivity Plot for NH for Flame 3, the Number Referred to the Reaction Number in Table (5.1)

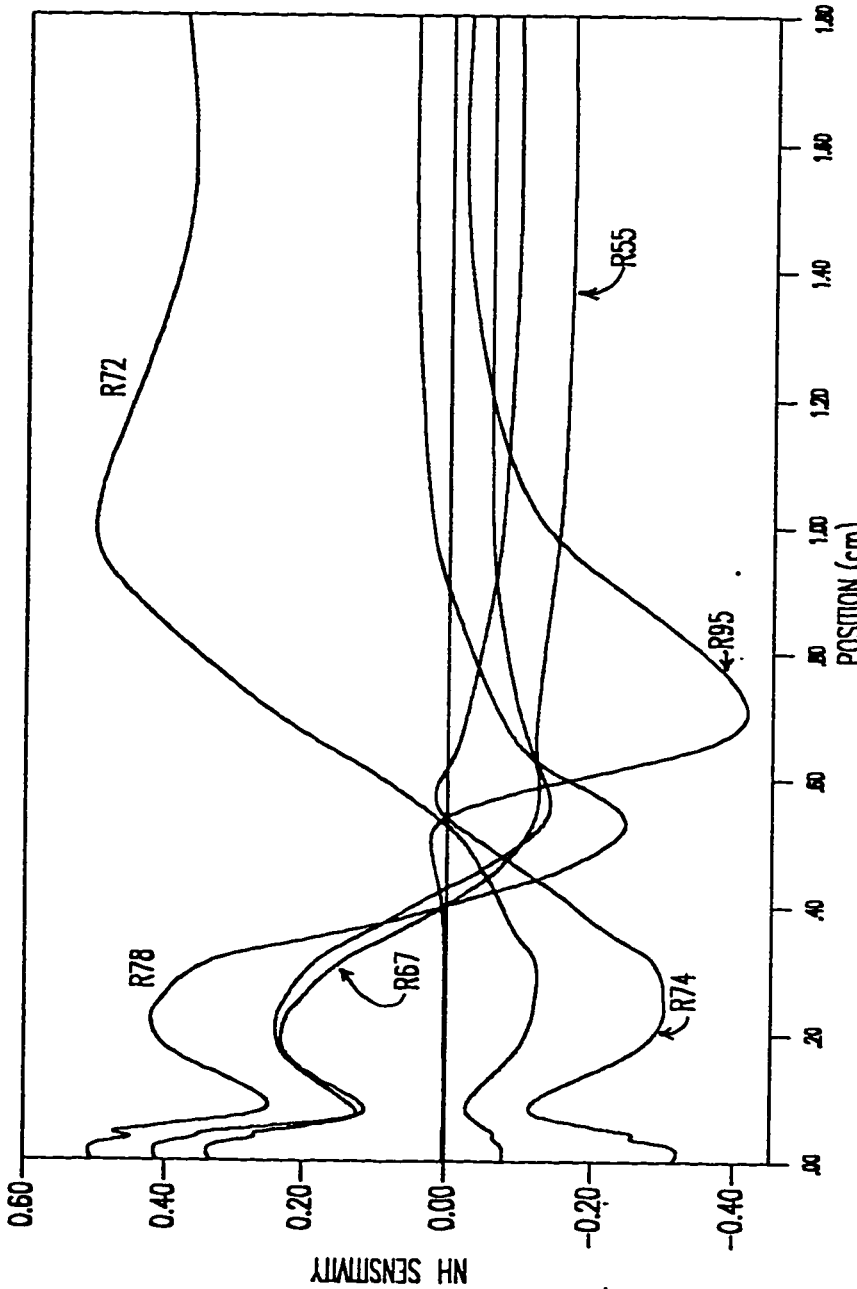

Figure 5.28c: Sensitivity Plot for NH for Flame 3, the Number Referred to the Reaction Number in Table (5.1)

competes with reaction (17), but the HCN radicals formed goes to reaction (72)

$$HCN + O = NCO + H$$

forming NCO radicals which in turn reacts with H radicals through reaction (81) to form more NH radicals.

Reactions (32)

$$CH + NO = HCN + O$$

and (33)

$$CH + NO = CN + OH$$

compete with reaction (31). However, reaction (32) follows similar path as described above for NH generation.

5.9.7 NH_2 Reactions :

Amidogen (NH_2) is formed in the flames by the following two reactions

$$HNCO + H = NH_2 + CO \qquad \text{(R84)}$$

$$NNH + NH = NH_2 + N_2 \qquad \text{(R100)}$$

A small amount of NH_2 formation is attributed to reaction (100), while the major contributor to NH_2 formation is believed to be due to reaction (84).

According to the proposed reaction mechanism, the NH_2 radical is consumed in the flames by the following chain branching reaction

$$NH_2 + NO = NNH + OH \qquad \text{(R85)}$$

The sensitivity analysis profiles for NH_2 are plotted in Figures (5.29a) and (5.29b). It shows that reaction (12) and (83) have the highest positive sensitivity for NH_2 formation. Reaction (12)

$$CH_3 + OH = CH_2 + H_2O$$

promotes reaction (20)

$$CH_2 + NO = HCN + OH.$$

The HCN produced reacts with oxygen atoms through reaction (72)

$$HCN + O = NCO + H$$

to form NCO radicals, which then reacts with hydrogen molecules through reaction (83)

$$NCO + H_2 = HNCO + H.$$

The products thus formed produces NH_2 directly through reaction (84). Reaction (66) also has positive sensitivity for NH_2 formation as it produces oxygen atoms which promotes reaction (72).

At approximately 5 mm away from the flame, reaction (72) shows negative sensitivity for NH_2 formation, which increases initially and then decreases. This may be attributed to the change in the direction of the reaction at higher temperatures. Reaction (8)

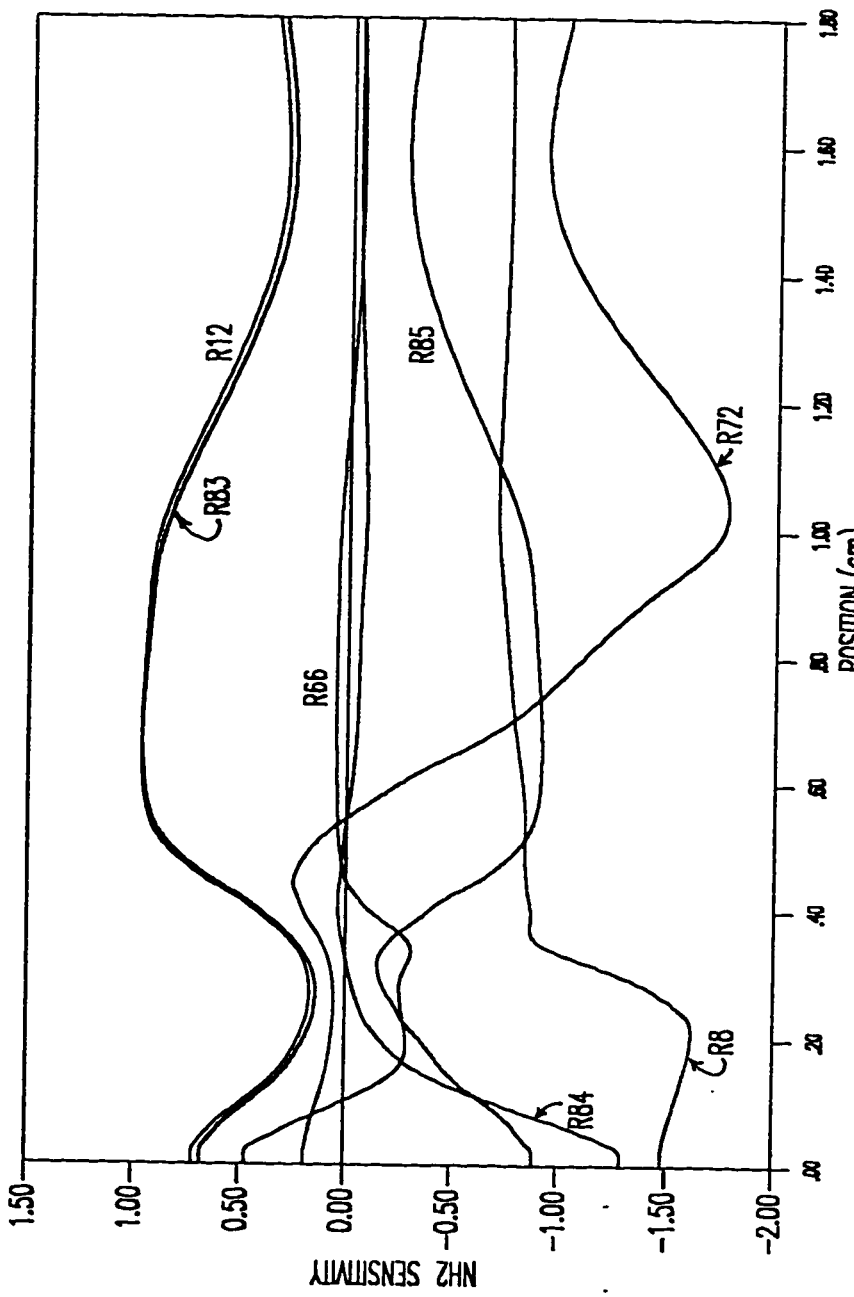

Figure 5.29a: Sensitivity Plot for NH2 for Flame 3, the Number Referred to the Reaction Number in Table (5.1).

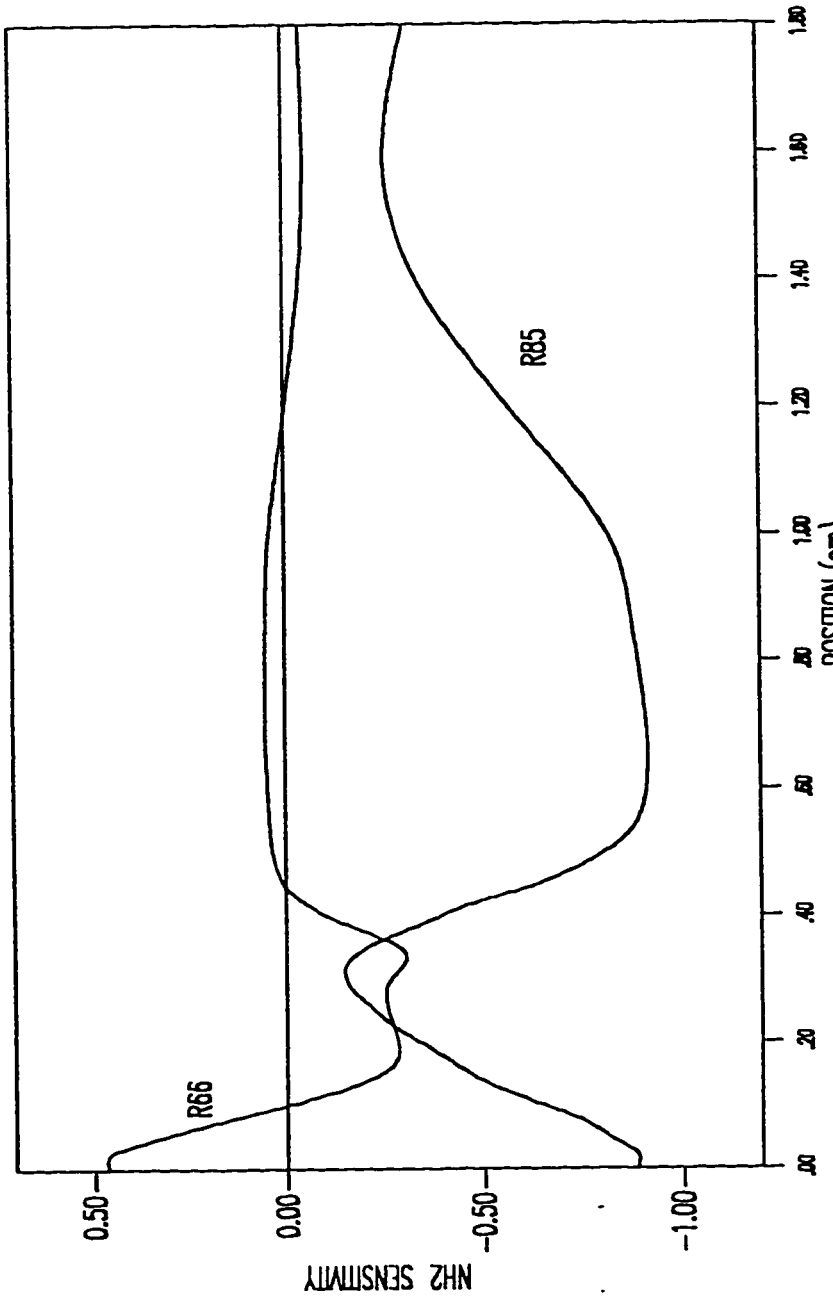

Figure 5.29b: Sensitivity Plot for NH2 for Flame 3, the Number Referred to the Reaction Number in Table (5.1).

$$CH_3 + NO_2 = CH_3O + NO$$

competes with reaction (18)

$$CH_3 + NO = HCN + H_2O$$

for the methyl radical and it therefore has a high negative sensitivity for NH_2 formation. Reaction (85) is a chain propagating reaction which causes direct reduction of NH_2 radical.

5.9.8 *OH* Reactions :

The hydroxyl (*OH*) radical is the most important radical species in the $CH_4 / NO_2 / O_2$ flames. It is responsible not only for *H* abstraction from CH_4 , but also for propagating the flame mechanism in general to its final products. The *OH* radical was found in abundance in the flames during experiments conducted by Al-Farayedhi [1], but only the relative concentrations were reported.

The sensitivity analysis pinpoints the main reactions responsible for *OH* formation in the flames which are

$$H + O_2 = OH + H_2 \qquad \text{(R66)}$$

$$HNO_2 + M = OH + NO + M \qquad \text{(R95)}$$

It also identifies the reactions through which the *OH* radical is consumed as

$$HNO_2 + OH = H_2O + NO_2 \qquad \text{(R94)}$$

$$CH_4 + OH = CH_3 + H_2O \qquad \text{(R2)}$$

$$CH_2O + OH = HCO + H_2O \quad \text{(R39)}$$

$$OH + OH = H_2O + O \quad \text{(R58)}$$

The sensitivity analysis for OH radical is shown in Figures (5.30a) and (5.30b). It can be seen that the reaction rate for OH radical is positively sensitive to reactions (17), (95) and (45) respectively. Of these, reaction (95) produces OH radical directly. Reaction (17)

$$CH_3 + NO = CH_2O + NH$$

and (45)

$$CH_3O + M = CH_2O + H + M$$

both are chain propagating reactions and both produces formaldehyde intermediate which reacts with NO_2 to form HNO_2 through reaction (37)

$$CH_2O + NO_2 = HCO + HNO_2$$

which then forms OH radical through thermal decomposition via reaction (95).

On the other hand, reactions (94), (8), (1) (2) and (39) display negative sensitivity for OH formation respectively. Again, reactions (94), (2) and (39) consume OH directly. Reaction (1)

$$CH_4 + H = CH_3 + H_2$$

competes for the hydrogen atom with reaction (66) which explains its negative sensitivity for OH formation. Reaction (8)

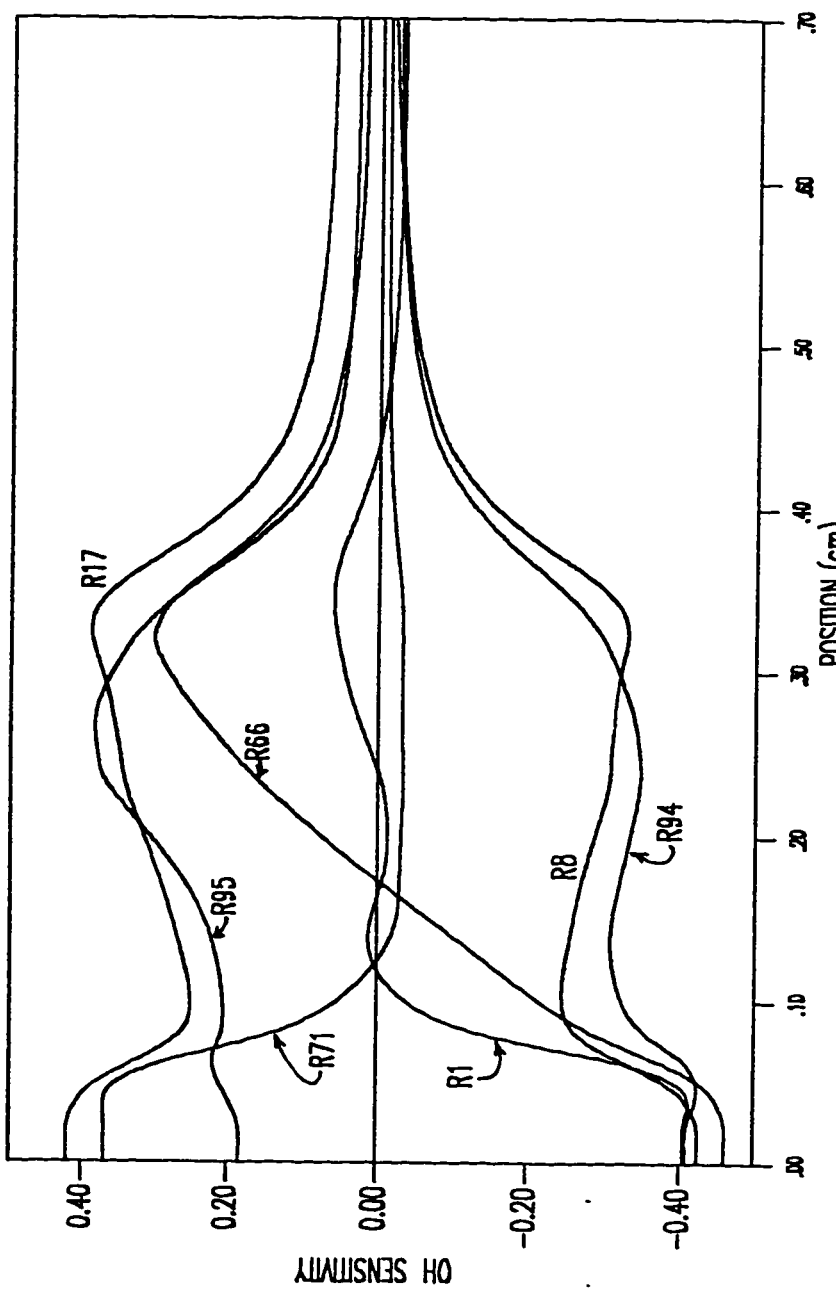

Figure 5.30a: Sensitivity Plot for OH for Flame 3, the Number Referred to the Reaction Number in Table (5.1).

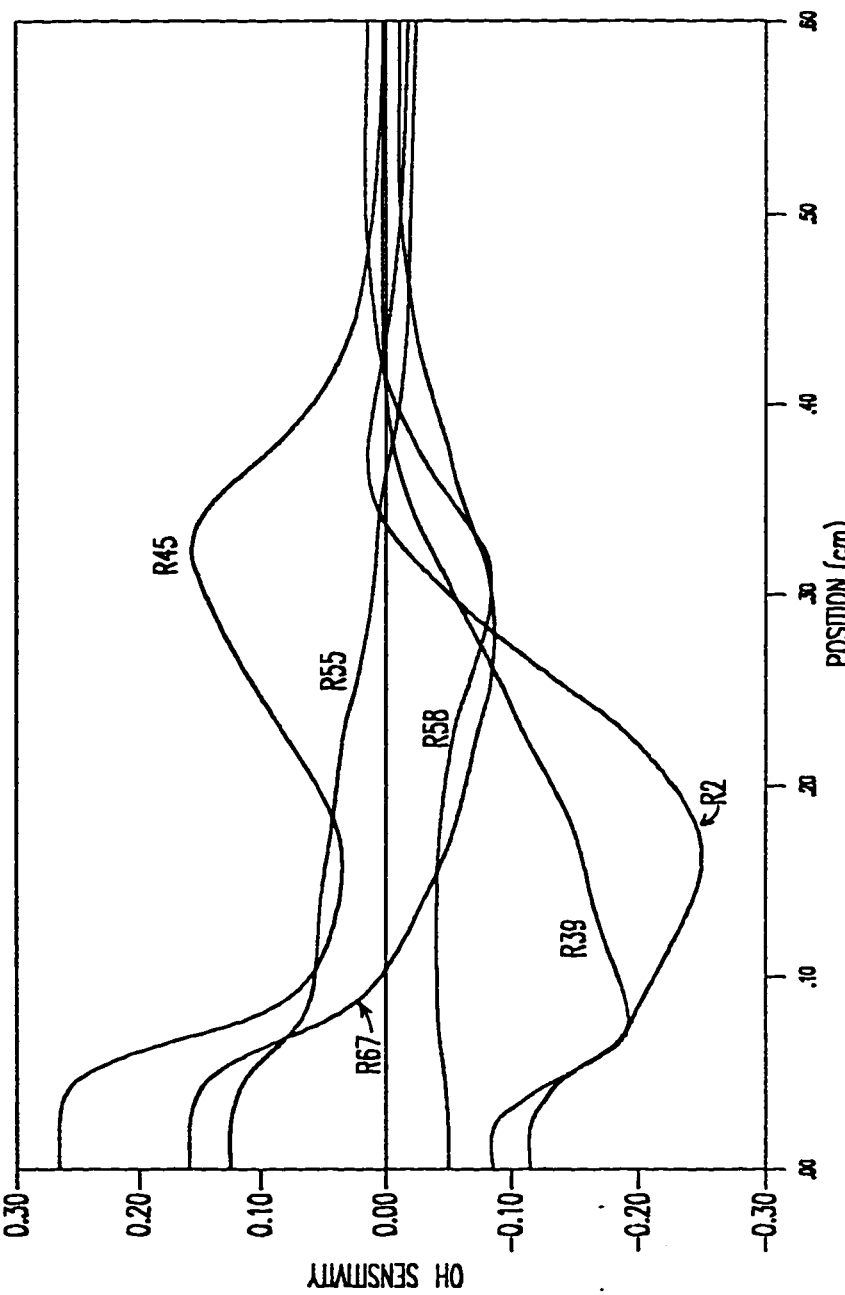

Figure 5.30b: Sensitivity Plot for OH for Flame 3, the Number Referred to the Reaction Number in Table (5.1).

$$CH_3 + NO_2 = CH_3O + NO$$

competes for the NO_2 with reaction (37) and therefore it shows negative sensitivity for OH formation.

5.9.9 NO_2 Reactions :

The recognition of air pollution as a problem of social concern has prompted a concentrated research effort on the kinetics of NO_x formation and decomposition.

The destruction of NO_2 in the flame can be attributed to the following reactions

$$NO_2 + CH_4 = HNO_2 + CH_3 \quad \text{(R5)}$$

$$NO_2 + CH_3 = NO + CH_3O \quad \text{(R8)}$$

$$NO_2 + CH_2O = HNO_2 + HCO \quad \text{(R37)}$$

$$NO_2 + HCO = HNO_2 + CO \quad \text{(R48)}$$

$$2NO + O_2 = 2NO_2 \quad \text{(R75)}$$

Nitrogen dioxide can also be formed in the flame via the following reactions

$$NO + HO_2 = NO_2 + OH \quad \text{(R62)}$$

$$NO + N_2O = N_2 + NO_2 \quad \text{(R74)}$$

$$HNO_2 + OH = H_2O + NO_2 \quad \text{(R94)}$$

Sensitivity analysis for the reaction rate of NO_2 is plotted in Figures (5.31a) and (5.31b). It reveals that reaction (8) accounts for most of the consumption of NO_2. Reaction (48) also consumes NO_2 more than the other remaining reactions. NO_2 is mainly regenerated through reactions (94) and (74). NO_2 destruction is most sensitive to the following reactions.

$$H + O_2 = OH + O, \qquad \text{(R66)}$$

$$HNO_2 + M = OH + NO + M \qquad \text{(R95)}$$

$$N_2O + M = N_2 + O + M. \qquad \text{(R76)}$$

5.9.10 *NO* Reactions :

Nitric oxide is a primary pollutant that arises from the oxidation of nitrogen compounds (fuel − *NO*) and nitrogen from the air (thermal − *NO*) during the combustion of fossil fuels. In both cases the end result is primarily the formation of *NO* because the residence time in most combustion units is too short for a significant amount of oxidation of *NO* to NO_2 to occur. High concentrations of *NO* are contained in car exhaust and in early plumes of power stations. The final *NO* emission, however, is a balance between the reactions that lead to its formation and those which promote its destruction. The latter are important since in practical systems they can be controlled.

Thermal dissociation of *NO* is significant only at very high temperatures and generally may be excluded from detailed kinetic modelling of *NO* in combustion flows. The reactions responsible for the formation of *NO* includes the following

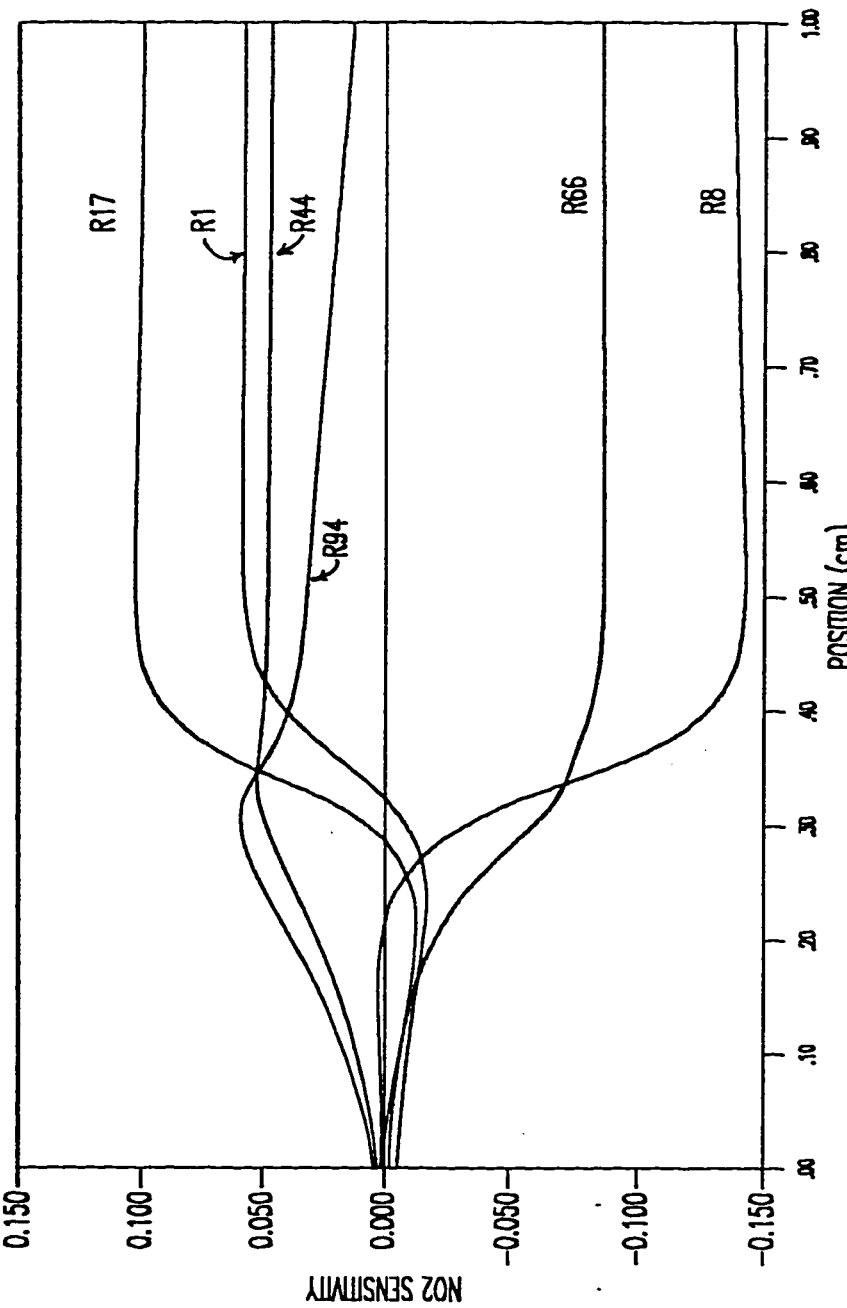

Figure 5.31a: Sensitivity Plot for NO2 for Flame 3, the Number Referred to the Reaction Number in Table (5.1).

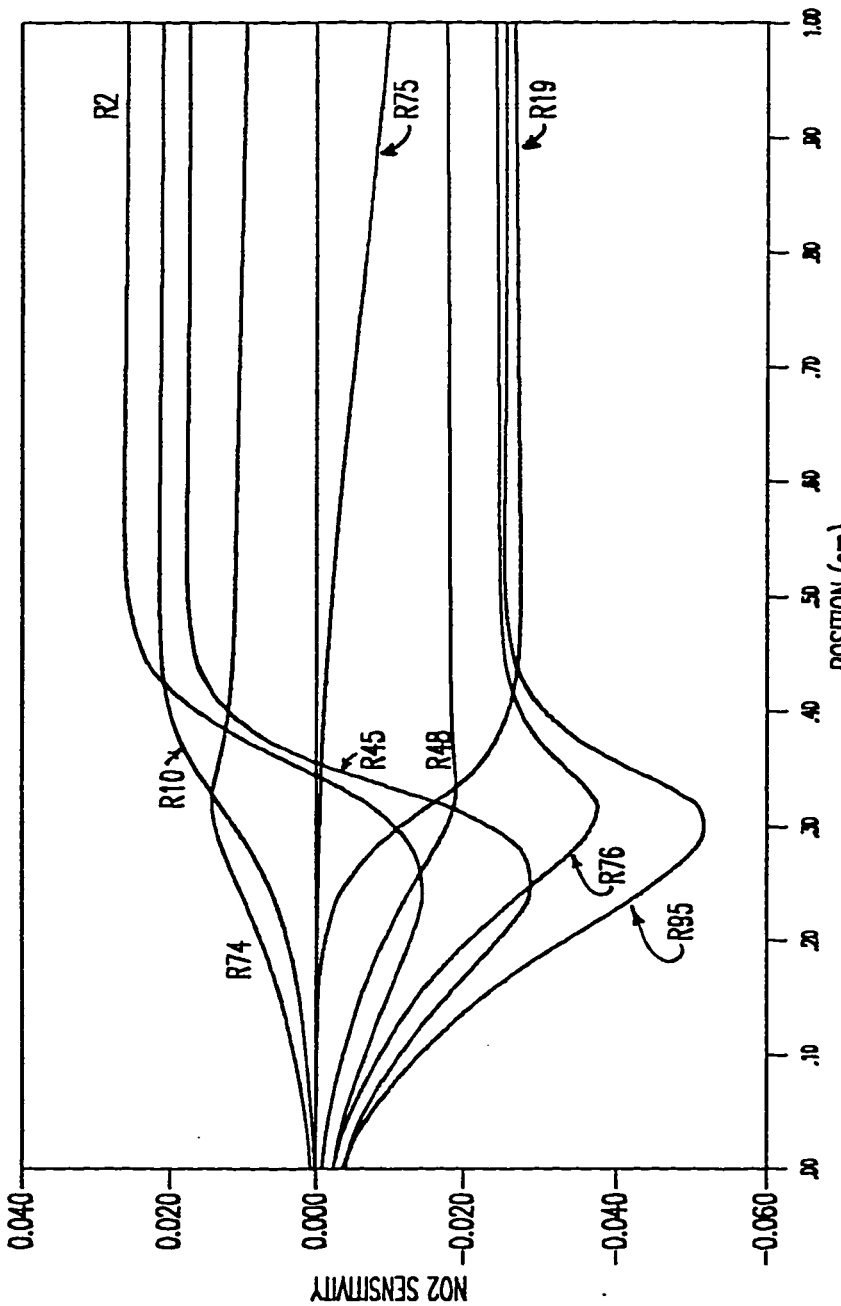

Figure 5.31b: Sensitivity Plot for NO2 for Flame 3, the Number Referred to the Reaction Number in Table (5.1).

$$CH_3 + NO_2 = CH_3O + NO \quad \text{(R8)}$$

$$HNO_2 + M = OH + NO + M \quad \text{(R95)}$$

$$HNO + M = H + NO + M \quad \text{(R96)}$$

$$HNO + O = NO + OH \quad \text{(R92)}$$

$$HNO + H = NO + H_2 \quad \text{(R93)}$$

$$N_2O + O = 2NO \quad \text{(R80)}$$

The consumption of *NO* takes place through the following reactions

$$CH_3 + NO = CH_2O + NH \quad \text{(R17)}$$

$$CH_3 + NO = HCN + H_2O \quad \text{(R18)}$$

$$CH_2 + NO = HCN + OH \quad \text{(R20)}$$

$$CH + NO = NH + CO \quad \text{(R31)}$$

$$CH + NO = CN + OH \quad \text{(R33)}$$

$$NCO + NO = N_2O + CO \quad \text{(R82)}$$

$$CN + NO = N_2 + CO \quad \text{(R86)}$$

The sensitivity analysis for *NO* is shown in Figures (5.32a), (5.32b) and (5.32c). It shows that reaction (8), which leads to the direct production of *NO*, has the highest positive sensitivity for *NO* formation. On the other hand, reaction (17), which reduces *NO* directly, contributes mostly towards *NO* destruction. These two reactions are, in fact, mirror images of each other as can be seen in Figure (5.32a).

Reaction (95) and (45)

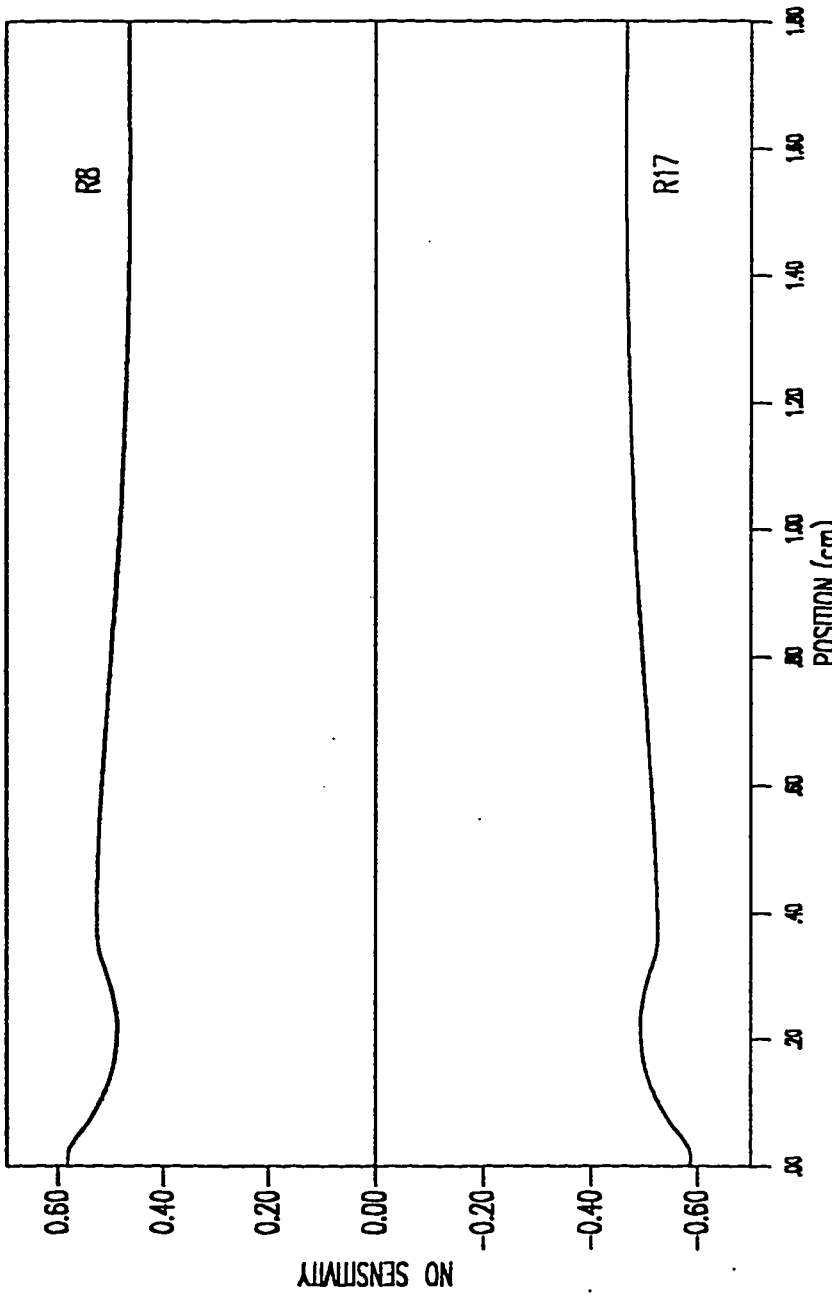

Figure 5.32a: Sensitivity Plot for NO for Flame 3, the Number Referred to the Reaction Number in Table (5.1).

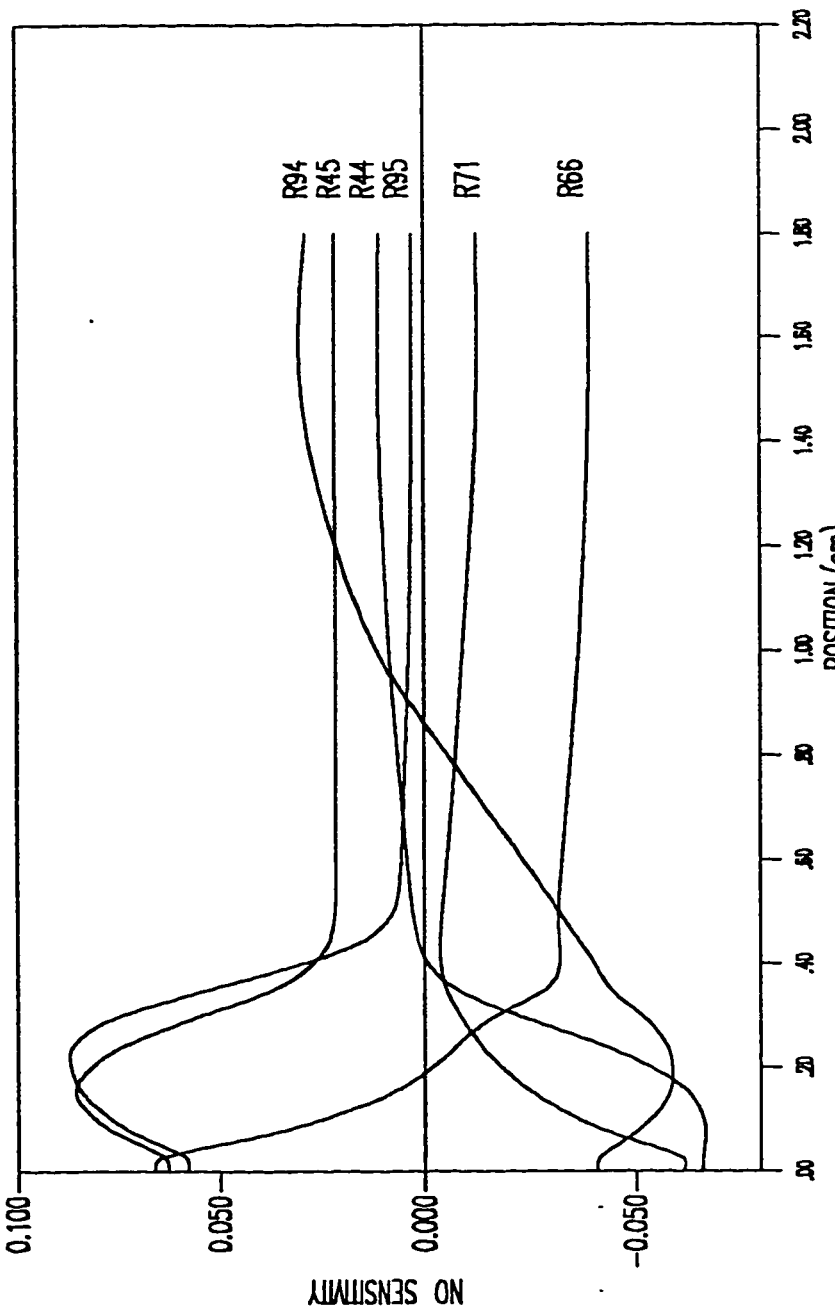

Figure 5.32b: Sensitivity Plot for NO for Flame 3, the Number Referred to the Reaction Number in Table (5.1).

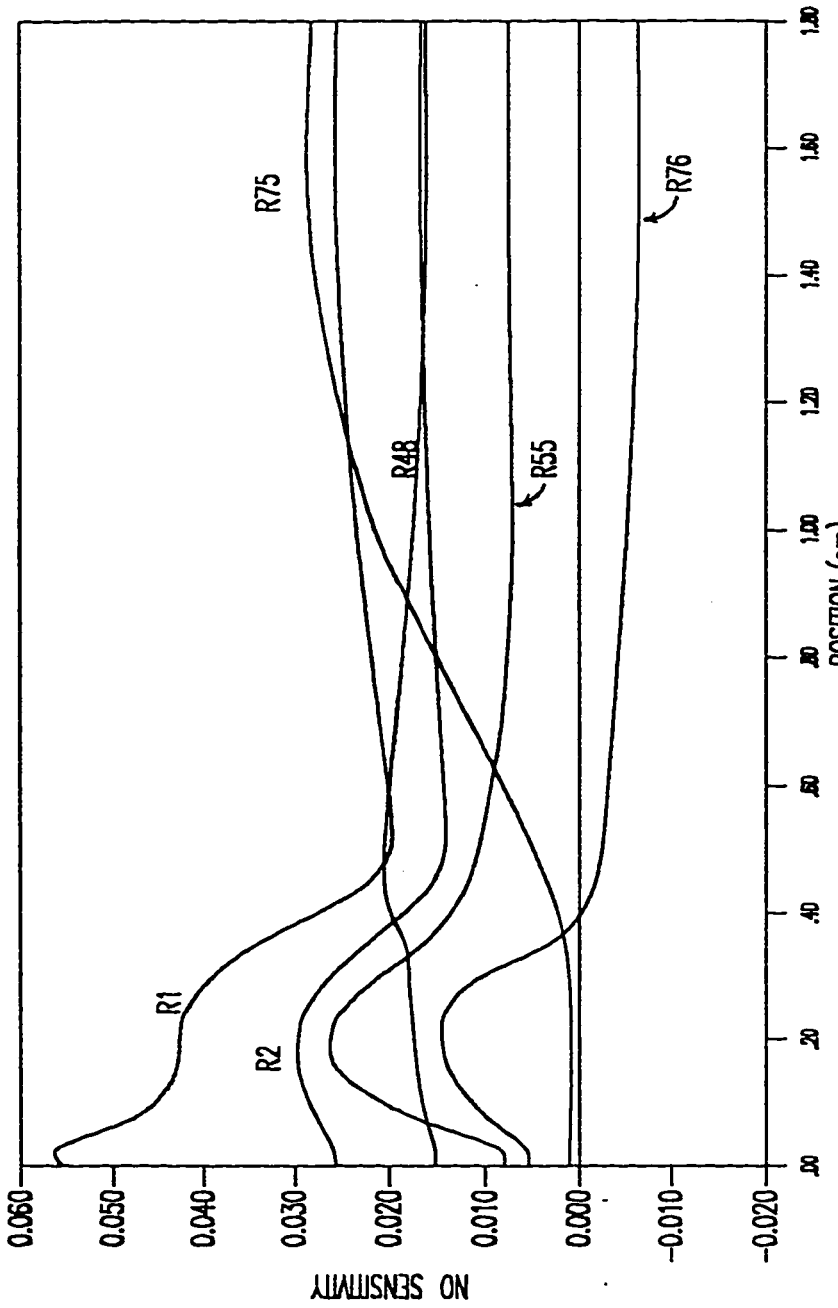

Figure 5.32c: Sensitivity Plot for NO for Flame 3, the Number Referred to the Reaction Number in Table (5.1).

$$CH_3O + M = CH_2O + H + M$$

also contribute positively towards *NO* formation. Of these, reaction (95) produces *NO* directly. Reactions (66)

$$H + O_2 = OH + O$$

and (71)

$$H + O_2 + M = HO_2 + M$$

show high sensitivity for *NO* destruction.

5.9.11 N_2 Reactions :

The nitrogen molecule is generated in the flame directly from N_2O through the following reactions

$$N_2O + NO = N_2 + NO_2 \quad \text{(R74)}$$

$$N_2O + M = N_2 + O + M \quad \text{(R76)}$$

$$N_2O + OH = N_2 + HO_2 \quad \text{(R77)}$$

$$N_2O + H = N_2 + OH \quad \text{(R78)}$$

$$N_2O + O = N_2 + O_2 \quad \text{(R79)}$$

$$N_2O + CN = N_2 + NCO \quad \text{(R87)}$$

A possible path for N_2 formation is suggested below

$$CH + NO = HCN + O \quad \text{(R32)}$$

$$HCN + O = NCO + H \quad \text{(R72)}$$

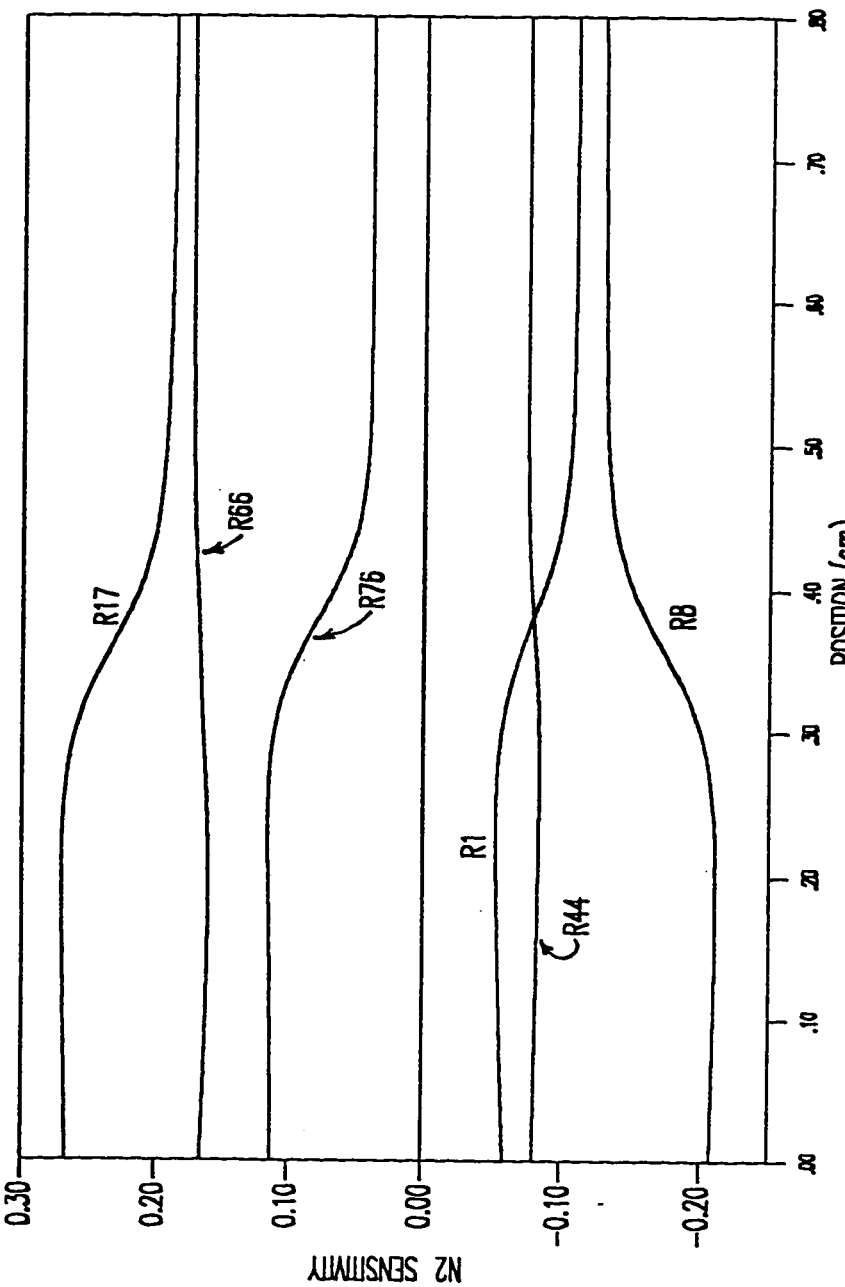

Figure 5.33a: Sensitivity Plot for N2 for Flame 3, the Number Referred to the Reaction Number in Table (5.1).

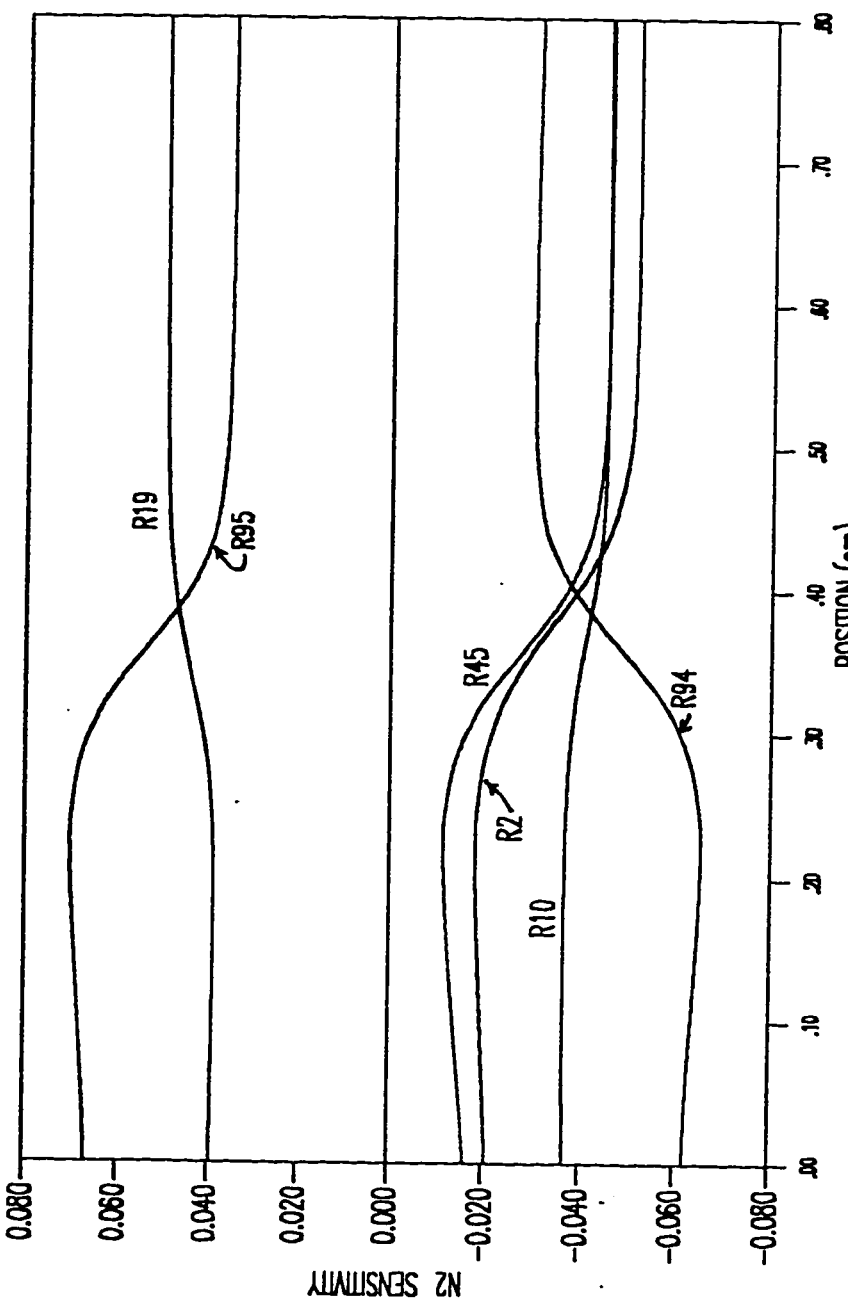

Figure 5.33b: Sensitivity Plot for N2 for Flame 3, the Number Referred to the Reaction Number in Table (5.1).

$$NCO + H = NH + CO \qquad \text{(R81)}$$

$$NH + NO = N_2 + OH \qquad \text{(R91)}$$

Reaction (76) which is the major source of N_2 production is a reaction of broad interest to kineticists as it plays an important role in various models of NO_x formation and decomposition; it forms the basis of increasingly used techniques for the controlled generation of O atoms in studies of elementary oxidation reactions.

The sensitivity analysis for N_2 is plotted in Figures (5.33a) and (5.33b). Figure (5.33a) shows that the N_2 molecule is formed mainly by reaction (76) i.e., from the dissociation of nitrous oxide. Reaction (17)

$$CH_3 + NO = CH_2 + NH$$

which is a chain branching reaction shows high positive sensitivity for N_2 formation. Reaction (8)

$$CH_3 + NO_2 = CH_3O + NO$$

competes with reaction (17) for CH_3 radical and so it displays high negative sensitivity towards the formation of N_2 molecule. These two reactions are mirror images of each other.

Figure (5.34) summarizes the schematic representation for the reaction mechanism for $CH_4 / NO_2 / O_2$ flames.

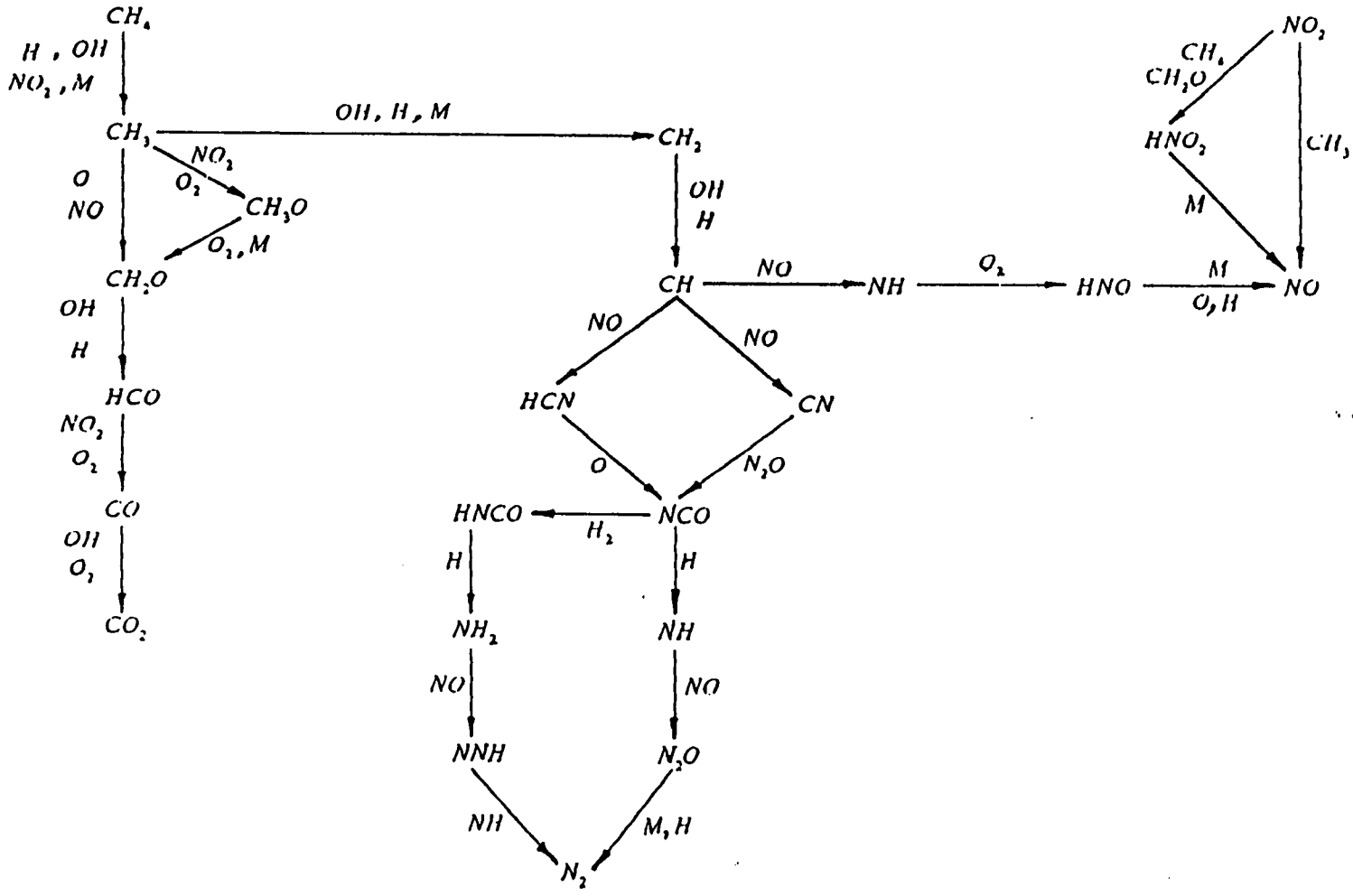

Figure 5.34: Schematic Representation for the Reaction Mechanism for $CH_4 / NO_2 / O_2$ Flames.

CHAPTER 6

CONCLUSIONS AND RECOMMENDATIONS

6.1 Conclusions :

The chemical kinetic mechanism modelling of five different $CH_4 / NO_2 / O_2$ flames was performed using the flame code. The experimental values of species and temperature profiles, mass flow rates, pressure etc. were obtained from previous work done by Al-Farayedhi [1] and Sadeqi [50]. All the flames were stabilized on a flat flame burner at a pressure of 50 torr, except for flame 1 which was stabilized at a pressure of 70 torr. Laser-Induced Fluorescence was used to detect and measure the intermediate species concentrations and temperature profiles in laminar, premixed, sub-atmospheric pressure, flat $CH_4 / NO_2 / O_2$ flames. The radical species detected were CH, CN, NH, OH and NH_2. All the flames studied are lean with equivalence ratios ranging from 0.20 to 0.92.

The chemical kinetic mechanism that was presented consisted of 101 reactions among 30 species, representing the most important reactions involved in this flame. This mechanism was used as input to the flame code to model the $CH_4 / NO_2 / O_2$ flames numerically. The flame code computed the concentration versus distance for all the species involved in the mechanism. The comparison between the calculated and experimental concentration profiles showed good overall agreement especially for the stable species. This excellent agreement

suggests the accuracy of the calculated profiles and the validity of the proposed mechanism to describe chemically the $CH_4 / NO_2 / O_2$ flames.

The formulation of this mechanism will be useful in understanding the nitrogen chemistry controlling the combustion of the gas phase in solid rocket propellants. The new information obtained in this work can be added to previous work on the structure of hydrocarbon flames supported by nitrogen oxides to understand completely the physics and chemistry of these flames.

6.2 Recommendations :

For future work, study of the structure of methane flames supported by nitric oxide (NO) and nitrous oxide (N_2O) should be carried out for understanding these flames to a much better extent. Future studies can also include HCN flames, since this intermediate is an important fuel in the gas phase of energetic material combustion.

Unless the concentration of all the species involved in the flame can be determined, a complete kinetic mechanism cannot be obtained for the flames. Therefore, for the experimental setup, the addition of a mass spectrometer to the species detection system is strongly recommended. This addition will enable the researcher to detect some important intermediates in the flames (e.g. NHO, CHO, and NCO) which cannot be detected by either the LIF system or the gas chromatograph.

NOMENCLATURE

a_{nk}	:	Coefficients to fits of thermodynamic data
A	:	Cross-sectional area of the stream tube encompassing the flame
A_i	:	Pre-exponential factor in the rate constant of i^{th} reaction
c_p	:	Constant pressure heat capacity of the mixture
c_{pk}	:	Specific heat at constant pressure of the k^{th} species
$\bar{c}_p$	:	Mass-weighted mean specific heat at constant pressure
C°_{pk}	:	Standard state specific heat at constant pressure of the k^{th} species
C_{pk}	:	Specific heat at constant pressure of the k^{th} species
$\bar{C}_p$	:	Molar-weighted mean specific heat at constant pressure
D_k	:	Mixture-averaged diffusion coefficient
D_{kj}	:	Binary diffusion coefficient
E_i	:	Activation energy in the rate constant of the i^{th} reaction
F	:	Residual vector
h_k	:	Specific enthalpy of the k^{th} species
H°_k	:	Standard state enthalpy of the k^{th} species
H_k	:	Enthalpy of the k^{th} species
i	:	Reaction index

I	:	Total number of reactions
J	:	Total number of grid points
k	:	Species index
K	:	Total number of species
k_{f_i}	:	Forward rate constant of the i^{th} reaction
k_{r_i}	:	Reverse rate constant of the i^{th} reaction
K_{c_i}	:	Equilibrium constant in concentration units for the i^{th} reaction
K_{p_i}	:	Equilibrium constant in pressure units for the i^{th} reaction
K_{T_k}	:	Thermal diffusion ratio units for the i^{th} reaction
M	:	Mass flow rate
N	:	Number of coefficients in polynomial fits to C°_p/R
P	:	Pressure
P_{atm}	:	Pressure of one standard atmosphere
ppm	:	Part per million
q_i	:	Rate of progress of the i^{th} reaction
R	:	Universal gas constant
R_c	:	Universal gas constant in the same units as the activation energy, E_i
S°_k	:	Standard state entropy of the k^{th} species
S_k	:	Entropy of the k^{th} species
$SLPM$	:	Standard liters per minute
T	:	Temperature

T_b : Specified burner temperature

u : Velocity of the fluid mixture

V_k : Diffusion velocity of the k^{th} species

V_{od} : Ordinary diffusion velocity of the k^{th} species

V_{td} : Thermal diffusion velocity of the k^{th} species

V_c : Correction velocity of the k^{th} species

$\overline{W}$: Mean molecular weight

X_k : Mole fraction of the k^{th} species

$[X_k]$: Molar concentration of the k^{th} species

Y_k : Mass fraction of the k^{th} species

Greek Symbols

α : A-factors of the reaction rate coefficients i^{th} reaction

β_i : Temperature exponent in the rate constant of the i^{th} reaction

ε : Mass flux fraction of the k^{th} species

φ : Equivalence ratio

ρ : Mass density

ν_{ki} : Stoichiometric coefficients of the k^{th} species in the i^{th} reaction, $\nu_{ki} = \nu''_{ki} - \nu'_{ki}$

ν'_{ki} : Stoichiometric coefficients of the k^{th} reactant species in the i^{th} reaction

ν''_{ki} : Stoichiometric coefficients of the k^{th} product species in the i^{th} reaction

$\dot{\omega}_k$	:	Chemical production rate of the k^{th} species
λ	:	Thermal conductivity of the mixture.
θ	:	Solution Vector

Superscripts

$+$	:	Excited State
o	:	Standard state one atmosphere

LIST OF REFERENCES

[1] Al-Farayedhi, A. A., "Laser-Induced Fluorescence Measurements of CH, CN, NH, OH, and NH_2 Intermediates in $CH_4 / NO_2 / O_2$ and $CH_2O / NO_2 / O_2$ Flames," Ph.D. Thesis, Mechanical Engineering, University of Colorado, Boulder, 1987.

[2] Ashmore, P. G., Thesis, University of Cambridge, 1949.

[3] Ashmore, P. G., and Preston, K. F., Combustion and Flame, 11:125, 1967.

[4] Atkinson,R. and Pitts, J.N., J. Chem. Phys., 68:3581, 1978.

[5] Badr, M. A. H., "Laser-Induced Fluorescence Measurements of Radical Species in Flames of Methane-Nitrous Oxide and Formaldehyde-Nitrous Oxide," Ph.D. Thesis, Mechanical Engineering, University of Colorado, Boulder, 1989.

[6] Barnard, J. A., and Bradley, J. N., "Flame and Combustion," Second Edition, Chapman and Hall, New York, 1985.

[7] Baulch, D., Drysdale, D.D. and Horne, D.G., "Evaluated Kinetic Data for High Temperature Reactions," Vol. 2, "Homogeneous Gas Phase Reactions in the $H_2 / N_2 / O_2$ System," Butterworths, London, 1973.

[8] Bittker, D., and Scullin, V., NASA Tech Note TND-6586, 1972.

[9] Bowman, C.T., 15th Symposia (International) on Combustion, p.869,

1975a.

[10] Branch, M. C., "Chemical Kinetics of Gas Phase Decomposition Products of Nitramine Propellants, "Proceedings of the Twenty First JANAF Combustion Meeting, Vol. 1, CPIA pub. No. 421, pp. 409-415, 1984.

[11] Branch, M. C., Al-Farayedhi, A. A., Sadeqi, M., "Laser-Induced Fluorescence Measurements of the Structure of $CH_4 / NO_2 / O_2$ Flames," Proceedings of the Second ASME/JSME Thermal Engineering Conference, Vol. 1, pp. 181-196, 1987.

[12] Burcat, A., Combustion and Flame 28:319, 1977.

[13] Butler, J. D., "Air Pollution Chemistry", Academic Press., New York, 1979.

[14] Chapman, S. and Cowling, T.G., "The Mathematical Theory of Non-Uniform Gases," Third Edition, Cambridge University Press, Cambridge. Combustion and Flame 50:323-340, 1983.

[15] Clark, T.C. and Dove, J.E., Can. J. Chem., 51:2147, 1973a.

[16] Coffee, T. P., and Heimerl, J.M., "A Transport Algorithm for Premixed, Laminar, Steady State Flames," Combustion and Flame 43:273, 1981.

[17] Coffee, T. P., and Heimerl, J.M., "Transport Algorithm for Methane Flames," Combustion Science and Technology 34:31, 1983.

[18] Coffee, T. P., and Heimerl, J.M., "Sensitivity Analysis for Premixed,

Laminar, Steady State Flames," Combustion and Flame 50:323-340, 1983.

[19] Curtiss, C.F. and Hirschfelder, J.O., "Transport Properties of Multicomponent Gas Mixtures," J. Chem. Phys., 17, p. 550, 1949.

[20] Dabora, E. K., "Effect of NO_2 on the Ignition Delay of CH_4– Air Mixtures," Combustion and Flame 24:181-184, 1975.

[21] Dean, A.M., Johnson, R.L. and Steiner, D.C., Combustion and Flame, 37:41, 1980.

[22] Dorko, E. A. et al., "Shock Tube Investigation of Ignition in Methane-Oxygen-Nitrogen Dioxide-Argon Mixtures," Combustion and Flame 24:173-180, 1975.

[23] Elsom, D., "Atmospheric Pollution," Basil Blackwell Inc., Oxford, OX41JF, U.K., 1987.

[24] Ernst, J, Wagner, H.Gg. and Zellner, R., Ber. Bunsenges. Phys. Chem., 82:409, 1978.

[25] Fifer, R. A., "Modern Developments in Shock Tube Research," Proceedings of Tenth Shock Tube Symposium (Goro Kamimoto, ed.), Shock Tube Research Society, Japan, International, p. 613., 1975.

[26] Frenklach, M., "Modeling," Combustion Chemistry (W. C. Gardinar, Jr., ed.), Springer-Verlag, New York, 1984.

[27] Fujii, N., Kakuda, T., akcishi, N. and Miyama, H., "Kinetics of the High Temperature Reaction of CO with N_2O," J. Physical Chemistry, Vol. 91, pp. 2144-2148, 1987.

[28] Gardiner, W. C., Jr., "Introduction to Combustion Modeling," Combustion Chemistry (W. C. Gardinar, Jr., ed.), Springer-Verlag, New York, 1984.

[29] Glassman, I. "Combustion," Academic Press, Inc., New York, 1977.

[30] Hanson, R. K. and Salimian, S., "Survey of Rate Constants in the N/H/O System," Combustion Chemistry (W. C. Gardinar, Jr., ed.), Springer-Verlag, New York, 1984.

[31] Jachimowski, C.J. Combustion and Flame, 23:233, 1974.

[32] Kanury, A. M., "Introduction to Combustion Phenomenon," Chapter 4, Gordon and Breach Science Publishers, New York, 1975.

[33] Kee, R. J., Miller, J. A. and Jefferson, T. H., "CHEMKIN: A General-Porpose, Problem-Independent, Transportable, Fortran Chemical Kinetics Code Package," Sandia National Laboratories Report SAND80-8003, 1980.

[34] Kee, R. J., Warnatz, J., and Miller, J. A., "A Fortran Computer Program Package for the Evaluatuin of Gas-Phase Viscosities, Conductivities, and Diffusion Coefficients," Sandia National Laboratories Report SAND83-8209, 1983.

[35] Kee, R. J., Grcar, J. F. Smooke, M. D. and Miller, J. A., "A Fortran Program for Modeling Steady Laminar One-Dimensional Premixed Flames," Sandia National Laboratories Report SAND85-8240, 1985.

[36] Kee, R. J., Rupley, F. M. and Miller, J. A., "The Chemical Thermodynamics Data Base," Sandia National Laboratories Report SAND87-8215, 1987.

[37] Kubota, N., "Physicochemical Processes of HMX Propellant Combustion," Nineteenth Symposium (International) on Combustion, 777-785, The Combustion Institute, 1982.

[38] Kuo, K. K., "Principles of Combustion," John Wiley and Sons, New York, 1986.

[39] Laidler, K. J., "Introduction to Combustion Phenomenon," 2nd ed., McGraw-Hill Book Co., New York, 1975.

[40] Lee, Q.N. and Vanpee, M., "Free Radical Concentration Measurement in Nitric Oxide / Acetylene Flames," Combustion and Flame, 62:193-210, 1985.

[41] Mathur, S., Tondon, P.K., AND Saxena, S.C., "Thermal Conductivity of Binary Ternary and Quaternary Mixtures of Rare Gases," Mol. Phys., 12, p. 569, 1967.

[42] Miller, E. and Setzer, H.J. "Burning Structure and Stability of n-Butane Nitrogen Dioxide Flame in Air," Sixth Symposium (International) on Combustion, 164, The Combustion Institute, 1957.

[43] Miller, J. A., Bowman, C. T., "Mechanism and Modelling of Nitrogen Chemistry in Combustion," Fall Meeting, Western States Section, The Combustion Institute, Paper WSS / CI 88-63, 1988.

[44] Myerson, A. L., Taylor, F.R. and Faunce, B.G., "Ignition Limit and Product of the Multistage Flames of Propane Nitrogen Dioxide Mixtures," Sixth Symposium (International) on Combustion, 154, The Combustion Institute, 1957.

[45] Norwich, R. G. W., and Wallace, J., Journal of Proceedings of Royal Society, A145:307 ,1934.

[46] Parker, W.G. and Wolfhard, H.G., "Some Characteristics of Flames Supported by NO and NO_2," Fourth Symposium (International) on Combustion, 420-428, The Combustion Institute, 1953.

[47] Parr, T. and Hanson-Parr, D., "Species and Temperature Profiles in Ignition and Deflagration of HMX," Spring Meeting, Western States Section, The Combustion Institute, Paper No. 87-8, 1987.

[48] Perry, R.A., "NO Reduction Using Sublimation of Cyanuric Acid," U.S. Patent 4, 731, 231, 1988.

[49] Philips, L.F., "Numerical Study of the Breakdown of Cyanogen in an $H_2 / N_2 / O_2$ Flame," Combustion and Flame, 26:397, 1976.

[50] Sadeqi, M. "Structure of Multiple Luminous Zones of Flames of Methane and Formaldehyde with Nitrogen Dioxide and Oxygen," Ph.D.

Thesis, Mechanical Engineering, University of Colorado, Boulder, 1987.

[51] Siebers, D.L. and Caton, J.A., "Reduction of Nitrogen Oxides by *RAPRENO*$_x$ Process," Sandia National Laboratories Report, SAND 88-8713B, March, 1988.

[52] Simonaitis, R. and Heicklen, J., International Journal of Chemical Kinetics, 5:231, 1973.

[53] Skinner, G.B., Sweet, R.C. and Davis, S.K. Journal of Physical Chemistry, 75:1, 1971.

[54] Slack, M. W., Combustion and Flame 30:325-326, 1977.

[55] Slack, M. W., and Grillo, A. R., "Shock Tube Investigation of Methane-Oxygen Ignition Sensitized by NO_2," Combustion and Flame 44:155-172 , 1981.

[56] Sloane, T. M., "Ignition and Flame Propagation Modeling With an Improved Methane Oxidation Mechanism," Combustion Science and Technology, Vol. 63. pp. 287-313, 1989.

[57] Smith, O. I. and Thorne, L.R., "The Structure of Cyanogen-Nitrigen Dioxide Premixed Flames," Fall Meeting, Western State Section, The Combustion Institute, Paper No. 86-34, 1986.

[58] Strehlow, R. A., "Fundamentals of Combustion," Robert E. Kreiger Publishing Co., Huntington, New York, 1979.

[59] Thomas, J. H., "Gas Phase Reaction of Nitrogen Dioxide Part 1: Oxidation of Acetylene," Trans. Faraday Soc., 48, 1142, 1952.

[60] Thomas, J. H., "Gas Phase Reaction of Nitrogen Dioxide Part 2: The Oxidation of Glyoxal," Trans. Faraday Soc., 49, 630, 1953.

[61] Thorne, L. R., Branch, M. C., Chandler, D. W., Kee, R. J., and Miller, J. A., "Hydrocarbon / Nitric Oxide Interactions in Low-Pressure Flames," Spring Meeting, Western States Section, The Combustion Institute, WSS / CI 86-29, 1986.

[62] Tsatsaronis, G., "Prediction of Propagating Laminar Flames in Methane, Oxygen, Nitrogen Mixtures," Combustion and Flame, Vol. 33, pp. 217-239, 1978.

[63] Vandooren, J., Oldenhove de Guertechin, L., and Van Tiggelen, P. J., "Kinetics in a Lean Formaldehyde Flame," Combustion and Flame, Vol. 64, pp. 127-139, 1986.

[64] Warnatz, J., "Rate Coefficients in the C/H/O System," Combustion Chemistry (W. C. Gardinar, Jr., ed.), Springer-Verlag, New York, 1984.

[65] Wharton, W.W., Violett, T.D. and Miller, E., "Spectroscopic Investigation of n-Butane- NO_2 Flames," Sixth Symposium (International) on Combustion, 173-177, The Combustion Institute, 1957.

[66] Westbrook., C. K., and Dryer, F. L., "Chemical Kinetics Modeling of Hydrocarbon Combustion," Progress in Energy and Combustion Science,

Vol. 10, pp. 1-57, 1984.

[67] Wolfhard, H.G. and Parker, W.G., "Spectra and Combustion Mechanism of Flames Supported by Oxides of Nitrogen," Fifth Symposium (International) on Combustion, Reinhold Publishing Corp., New York, pp. 718-728, 1955.